EMBRY-RIDDLE
Aeronautical University
SCHOLARLY COMMONS

Dissertations and Theses

3-19-2018

Nonlinear Control of Underactuated and Constrained Systems

Derek Hoffman

Follow this and additional works at: https://commons.erau.edu/edt

 Part of the Aerodynamics and Fluid Mechanics Commons

Scholarly Commons Citation
Hoffman, Derek, "Nonlinear Control of Underactuated and Constrained Systems" (2018). *Dissertations and Theses*. 383.
https://commons.erau.edu/edt/383

This Dissertation - Open Access is brought to you for free and open access by Scholarly Commons. It has been accepted for inclusion in Dissertations and Theses by an authorized administrator of Scholarly Commons. For more information, please contact commons@erau.edu.

NONLINEAR CONTROL OF UNDERACTUATED AND CONSTRAINED SYSTEMS

By

Derek Hoffman

A Dissertation submitted in Partial Fulfillment of the Requirements for the Degree

of

Doctor of Philosophy in Engineering Physics

Embry-Riddle Aeronautical University

Department of Physical Sciences

Daytona Beach, FL 32114

March 19th, 2018

Copyright by Derek Hoffman 2018

All Rights Reserved

NONLINEAR CONTROL OF UNDERACTUATED AND CONSTRAINED SYSTEMS

By Derek Hoffman

This dissertation was prepared with the guidance of the candidate's dissertation committee chair, Dr. Mahmut Reyhanoglu, Department of Physical Sciences, and has been approved by the members of his dissertation committee. It was submitted to the Department of Physical Sciences and was accepted in partial fulfillment of the requirements for the

Degree of

Doctor of Philosophy in Engineering Physics

DISSERTATION COMMITTEE:

M. Reyhanoglu
Dr. Mahmut Reyhanoglu, Chair

Dr. William MacKunis, Member

Dr. Yiechiel Crispin, Member

Dr. Anthony Reynolds, Member

Dr. Matthew Zettergren, EP Graduate Program Coordinator

Dr. Terry Oswalt, Department Chair, Physical Sciences

Dr. Michael Hickey, Dean of Research and Graduate Studies

3/19/2018
Date

Acknowledgments

The author would like to recognize his advisor, Dr. Mahmut Reyhanoglu, for the mentorship, opportunity, and support provided through the graduate program, and for demonstrated passion towards the fulfillment of research and this dissertation.

Further, the author would like to give thanks for the joint effort of his colleagues, most notably Muhammad Rehan and Dr. William MacKunis, on the collaborative publications seen in this document. In particular, Mr. Rehan's invaluable help troubleshooting "that blasted quadrotor" was monumental to the success of the provided experimental data, and Dr. MacKunis's experience on control law formulation frequently facilitated stability analysis.

On a more personal note, the author wishes to express gratitude towards his family and their encouragement far before "dissertation" was a word in his vocabulary. Much thanks to Eric and Marité Hoffman for their parental supervision and the occasional feeding since birth. Equally important in the author's view is the care and devotion from his grandparents, Julio Cesar and Maria Ester "Teté" Durand, who time and again have shown that familial love is independent of distance.

Certainly not to be omitted is the support of friends and family not listed, who have contributed varying efforts toward the culmination of this dissertation, direct or otherwise. The author would be remiss to recognize the multitude of factors that have brought him to this moment.

Contents

Acknowledgements vii

Abstract viii

1 Introduction 1

2 Mathematical Background 4

2.1 Differentiability and Manifolds 4

2.2 Generalized Coordinates and Lagrange's Equations of Motion 6

2.2.1 The Lagrangian Function 7

2.2.2 Hamilton's Principle 8

3 Manifold Constraint Formulation 11

4 Constraint Embedding Formulation 14

5 Examples: Local Coordinate Underactuated Systems 17

5.1 Robotic Manipulators 17

5.1.1 Hybrid Robotic Manipulator Cantilevered and Subjected to Single Torque 21

5.1.2 Modeling and Control of a Two-Torque Hybrid Robotic Manipulator 29

5.1.3 Finite-Time Control of a Compliant Base Robot Manipulator 41
5.2 Robust Quaternion-based Nonlinear Tracking Control of a Quadrotor Attitude Test Bed . . . 51
5.2.1 Dynamic Model Formulation . . . 53
5.2.2 Kinematic Model Formulation . . . 56
5.2.3 Control Objective . . . 56
5.2.4 Control Development . . . 58
5.2.5 Stability Analysis . . . 63
5.2.6 Numerical Simulation Results . . . 65
5.2.7 Experimental Results . . . 70

6 Examples: Global Coordinate Underactuated Systems 75
6.1 Hybrid Robotic Manipulator Cantilevered and Subjected to Single Torque Revisited . . . 77
6.1.1 Model Formulation . . . 77
6.1.2 Stability Analysis . . . 85
6.1.3 Simulations . . . 87
6.2 Modeling and Control of a Two-Torque Hybrid Robotic Manipulator Revisited . . . 90
6.2.1 Model Formulation . . . 91
6.2.2 Tracking Error . . . 95
6.2.3 Stability Analysis . . . 95
6.2.4 Simulations . . . 98
6.3 Geometric Tracking Control of a 3D Revolute Joint Robot . . . 101
6.3.1 Model Formulation . . . 101
6.3.2 Tracking Error . . . 104

6.3.3 Stability Analysis 105
6.3.4 Simulations 109
6.4 Robust Quaternion-based Nonlinear Tracking Control of a Quadrotor Attitude Test Bed Revisited 112
6.4.1 Dynamic Model Formulation 113
6.4.2 Kinematic Model Formulation 114
6.4.3 Control Objective 115
6.4.4 Control Development 118
6.4.5 Stability Analysis 122
6.4.6 Numerical Simulation Results 125
6.4.7 Experimental Results 129

7 Examples: Constraint Embedding of Unactuated Degrees of Freedom 131

7.1 Planar Rigid Body with Unactuated Sliding Mass 132
7.1.1 Model Formulation 132
7.1.2 Controller Design 135
7.1.3 Simulations 140
7.2 PPR Robot with Unactuated Arm Oscillation 146
7.2.1 Model Formulation 146
7.2.2 Controller Design 150
7.2.3 Simulations 151

8 Conclusions and Future Research 156

Abstract

It is the purpose of this document to elaborate on the control of systems that are underactuated or otherwise constrained. To do so, local- and global-coordinate formulations are implemented to generate well-defined system dynamics for a multitude of scenarios. These dynamics are shown to lie on manifolds defined by mathematical restrictions, allowing for singularity-free modeling for global considerations. Feedback controllers by extension share these benefits, facilitating singularity-free control algorithms as a result. Further, unactuated degrees of freedom can be treated as additional constraints, resulting in an embedded manifold upon the original dynamics. A transformation between a provided set of dynamical equations containing one or more unactuated degrees of freedom to a new set of coupled dynamics avoiding their perturbation will be shown. The necessary background is included with procedures outlining the solution of similarly-structured classes of systems. For complete insight, a Lagrangian formulation of the dynamical equations of motion is elaborated on, although differential geometric techniques do not demand restrictions on the dynamical methods applied. Examples are provided to demonstrate the proposed techniques. Appropriate controllers are then designed and proven to be effective at obtaining the control objective, initially through mathematical rigor. Following such proofs, simulational and experimental benchmark systems are given with corresponding MATLAB/Simulink plots for numerical analysis.

List of Figures

5.1 Schematic model of a one-torque hybrid robot manipulator. 21

5.2 Time behavior of rigid member angle and angular velocity. 28

5.3 Time behavior of vibrational deflection and velocity. 28

5.4 Time behavior of angular acceleration (u). 29

5.5 Schematic model of a two-torque hybrid robot manipulator. 30

5.6 Finite-time system block diagram. 36

5.7 Angular position time behavior 39

5.8 Vibration deflection time behavior. 40

5.9 Torques for each hub. 41

5.10 Schematic of the compliant base robotic manipulator. 42

5.11 Block diagram representation of the simplified system. 46

5.12 Time behavior of θ_i. 49

5.13 Time behavior of $\dot{\theta}_i$. 50

5.14 Time behavior of $x, \dot{x}$. 50

5.15 Time behavior of u_i. 51

5.16 Angular position behavior of pitch tracking. 67

5.17 Voltage requirements of pitch tracking. 68

5.18 Angular position behavior of roll tracking. 69

5.19 Voltage requirements of roll tracking. 70

5.20 Pitch tracking behavior of Quanser test bed. 71
5.21 Voltage requirements of Quanser test bed pitch tracking. 72
5.22 Roll tracking behavior of Quanser test bed. 73
5.23 Voltage requirements of Quanser test bed roll tracking. 74

6.1 Schematic model of a one-torque hybrid robot manipulator, global configuration. 77
6.2 Time behavior of error function Θ. 88
6.3 Time behavior of configuration error e_x. 89
6.4 Time behavior of angular velocity error e_v. 89
6.5 Time behavior of required torque. 90
6.6 Hybrid robotic manipulator schematic, two torque configuration. . . . 91
6.7 Time behavior of error functions Θ_i. 99
6.8 Time behavior of configuration errors e_{q_i}. 99
6.9 Time behavior of angular velocity errors e_{ω_i}. 100
6.10 Time behavior of control torques. 100
6.11 Schematic model of a three-dimensional revolute joint robot. 101
6.12 Time behavior of error function Θ. 110
6.13 Time behavior of configuration error e_q. 111
6.14 Time behavior of angular velocity error e_ω. 111
6.15 Time behavior of control torque τ. 112
6.16 Configuration Error of Differential Geometric Controller. 127
6.17 Configuration Error of Quaternion Controller. 127
6.18 Applied Voltage Input of Differential Geometric Controller. 128
6.19 Applied Voltage Input of Quaternion Controller. 128
6.20 Experimental Configuration Error of Differential Geometric Controller. 130

6.21 Experimental Applied Voltage Input of Differential Geometric Controller. 130

7.1 Planar Robot with Sliding Mass Schematic. 132

7.2 Planar robot angular behavior. 142

7.3 Planar robot vertical behavior. 142

7.4 Planar robot horizontal behavior. 143

7.5 Planar robot horizontal actuation effort. 143

7.6 Planar robot vertical actuation effort. 144

7.7 Planar robot torque actuation. 144

7.8 Planar robot sliding mass behavior. 145

7.9 Prismatic-Prismatic-Revolute Robot Schematic. 146

7.10 PPR angular behavior. 152

7.11 PPR vertical behavior. 152

7.12 PPR horizontal behavior. 153

7.13 PPR horizontal actuation effort. 153

7.14 PPR vertical actuation effort. 154

7.15 PPR torque actuation. 154

7.16 PPR end effector behavior. 155

List of Tables

5.1 Physical parameters of the one-torque hybrid robot manipulator. . . . 27

5.2 Physical parameters of the two-torque hybrid robot manipulator. . . . 38

5.3 Physical parameters of the compliant base robot manipulator. 48

5.4 Physical parameters of the quadrotor attitude test bed. 66

6.1 Physical parameters of the revolute robot. 109

7.1 Physical parameters of the planar robot with sliding mass. 141

7.2 Physical parameters of the PPR robot. 151

Chapter 1

Introduction

Considerations of real-life challenges naturally come with nonlinear factors. A noteworthy example is the case where control actuation indirectly acts on one or more of a given system's degrees of freedom (DOFs). Even more troublesome is the presence of DOFs that are not actuated whatsoever, necessitating care in the control design.

Within the topic of robotics and aerospace applications, the provided control actuation inputs are often less than the given system's degrees of freedom. By definition, these systems are referred to as underactuated (Tedrake, 2009). Due to the variety of physical scenarios that can lead to underactuation, an equally numerous array of methods may be used to attain the control objective. Seen in Barbazza et al (2017) is the use of a differential flatness framework on a planar, cable-driven micro-macro robot to achieve point-to-point maneuvers, in conjunction with multiobjective optimization framework for the combined minimization of maneuver time and control actuation. A swarm of surface vessels operating in uncertain environment disturbances in Mirzaei et al (2017) make use of dynamical coupling to direct the 3 degrees of freedom presented with the 2 control inputs provided. Vertical Take-Off and Landing (VTOL) aerial vehicles plagued with underactuation in Naldi et al (2017) obtain

required control objectives via an inner-outer control loop technique, applying attitude output as a positional virtual input. On-course and radial thrust failure for a hovering spacecraft along a circular orbit is considered by Huang and Yan (2016). Motion control of an underactuated, wheeled, inverted pendulum setup is attained in Yang et al (2014) through neural-network application. The list of further examples is non-exhaustive, yet each takes advantage of either coupling in the dynamical formulation, or foresight for an in-depth control law. Nevertheless, creativity is a requisite for control success in underactuated systems.

Although fully actuated systems do not rely on dynamical couplings to obtain actuation, effective control and stability demands thorough insight. This is especially true in the frequent case where additional constraints are applied. A case in point is Roy et al (2017), where a class of uncertain Euler-Lagrange systems are demonstrated to be controllable by a three-part adaptive, robust, time-delay algorithm. For the scope of the following investigation, the topic of entirely unactuated degrees of freedom are of high merit. A planar rigid body experiencing a sliding internal mass in Reyhanoglu et al (1998) is controlled via a discontinuous feedback technique. Through considering two unactuated DOFs of a three-link biped walker as two passive links, Morales and de La Hera (2012) make use of symmetric periodic gaits to achieve the control objective. In short, perturbation of unactuated degrees of freedom may be avoided by mapping additional conditions to the system, modifying the dynamics in the process.

For the purpose of base-value intuition, local coordinates are applied and used for the vast majority of control designs and dynamical formulations. One such example is the quaternion, a rotation about a described axis in order to avoid singularities in other conventional notations. Even with such ingenuity, local considerations will lead to both mathematical and processing ambiguities, ultimately resulting in singularities

regardless (see Mahew et al (2011a, 2011b) for further details). In contrast, differentiable manifolds defined as embedded in finite-dimensional vector spaces lead to more concise derivations, as well as the benefit of global considerations (Lee et al., 2017). In turn, controllers defined through these means are singularity-free, with the ability to directly apply additional system constraints. Unactuated degrees of freedom are no exception, and in fact lend themselves readily to this method. Through integral manifold considerations, a class of nonlinear singularly perturbed systems in Sharkey and O'Reilly (2003) are guided to a desired trajectory by observing it as a separate manifold. Attitude control of multiple rigid bodies is seen in Weng et al (2013), by regarding assigned auxiliary variables to the bodies residing in Special Orthogonal Group-3 (SO(3)). Higher-order sliding manifolds are applied in Cavallo and Natale (2003) to obtain output feedback control for multi-input, multi-output dynamics. Control of higher-order chaotic systems is obtained with invariant manifolds in Yu et al (2001). Increased performance in the speed regulation of an aero-engine follows from the work seen in Shi et al (2017) to develop a switched equilibrium manifold expansion, solving the dynamically-inherent switching control challenge. By identifying a mapping between the current system and a desired trajectory, manifolds can be used to devise innovative control paradigms. This in turn yields improved closed-loop system performance.

In light of such literature, the following document encompasses the following: 1) propositions and expansions upon general procedures and formulations for constraint embedding and identification, 2) provision of insight on the resulting modified dynamics, 3) design of innovative control paradigms through frequently used methods such as (but not limited to) Lyapunov Stability Analysis, 4) identification of controller effectiveness through simulation and experimental results, and 5) conclusions on the presented research, along with suggestive points for future work.

Chapter 2

Mathematical Background

Derivations and mathematical foundation provided in this chapter is self-contained for the remaining content. The following sections provide basic insight into differential geometric methods and Lagrangian formulation. Additional material can be viewed in (Crampin and Pirani, 1986), (Goldstein et al., 2011), (Lee et al., 2017), (Nijmeijer and van der Schaft, 1990).

2.1 Differentiability and Manifolds

Let A be an open subset of $\mathbb{R}^n$, and define a scalar function that provides the mapping of A to the set of all real numbers $h : A \to \mathbb{R}$. The concept can be readily extended to being a scalar function of the state $x = [x_1, x_2, ..., x_n]^T$, where the superscript "T" denotes a transpose operator, $h(x) = h(x_1, x_2, ..., x_n)$. In the case that h has continuous partial derivatives up to and including an arbitrary positive integer k, then it is defined as C^k, k times continuously differentiable. Should the premise hold true for all k, h is referred to as smooth, C^∞. A separate consideration is the mapping H, defined as a set of functions $(H_1, H_2, ..., H_m)$ that maps $A \to \mathbb{R}^m$. It then follows

that mappings h and H are only considered C^k if each and every component of such are proven so. A given matrix mapping of functions $G : A \to \mathbb{R}^{m_1 \times m_2}$, which consists of entries that map A to a real number, also sees this property.

Let S denote sets that demonstrate topology, fittingly known as topological spaces. Further, an open set containing an arbitrary point p within a topological space identifies a neighborhood of point p. It then follows that a subset of space S, denoted as S_o, includes a unique open set referred to as the the interior of S_o, or $int(S_o)$, which by definition is contained in S_o and includes any other open set in S_o. An empty interior for S_o exists if and only if the empty set $\emptyset$ is contained in any arbitrary open set of S in S_o. Consider a mapping between topological spaces $F : S_1 \to S_2$. F may be described as continuous if the inverse image of every S_2 open set is an open set of S_1. Should the image of every S_2 open set be an open set of S_1, then the mapping is considered open. Therefore, an open, continuous, bijection mapping is by definition a homeomorphism.

A locally Euclidean space E composed of n dimensions is a topological space where an arbitrary $p \in E$ may be operated on by a homeomorphism ψ from an open neighborhood of p onto an open set in $\mathbb{R}^n$. It then follows that an n-dimensional manifold M can be defined as a locally Euclidean space observing a countable basis allowing any two unique points to have disjoint neighborhoods. Coordinate charts can exist on such manifolds in the form of the pair (U, ψ); U denotes an open set of M, while ψ represents a homeomorphism mapping U onto an open set of $\mathbb{R}^n$. A noteworthy case is when ψ may be divided into $(\psi_1, \psi_2, ..., \psi_n)$ coordinate functions. Should this be true, and if $p \in U$, then the operation of those coordinate functions on p can be defined as the set of local coordinates of p in the coordinate chart (U, ψ).

Consider a C^∞ atlas on a manifold M as a collection of coordinate charts $\{(U_i, \psi_i)\}_{i \in I}$ with I being an index set, that are pairwise C^∞-compatible given the property that

$\cup_{i\in I} U_i = M$. The C^∞ atlas is considered complete if and only if it is not contained by any other atlas. It then follows that a manifold with a complete atlas is defined as smooth.

Also important to discuss is the matter of embedding. Consider two unique, smooth manifolds M_1 and M_2 of respective dimensions m_1 and m_2. An embedding can therefore be defined as a smooth injective map $F : M_1 \to M_2$ if F is found to be homeomorphism onto its image and $rank\frac{\partial F(p)}{\partial x} = dim(M_1)$. For clarity, $\frac{\partial F(p)}{\partial x}$ denotes the Jacobian matrix operator:

$$\frac{\partial F}{\partial x} = \begin{bmatrix} \frac{\partial F_1}{\partial x_1} & \cdots & \frac{\partial F_1}{\partial x_{m_1}} \\ \cdots & \cdots & \cdots \\ \frac{\partial F_{m_2}}{\partial x_1} & \cdots & \frac{\partial F_{m_2}}{\partial x_{m_1}} \end{bmatrix}. \tag{2.1}$$

It can be surmised that the embedded submanifold of M_2 is the image of the embedding operation $F(M_1)$. If the manifolds in question have identical dimension, a bijection mapping between may be defined as diffeomorphic if and only if both itself and its inverse are smooth. In this case, the manifolds are referred to as diffeomorphic.

2.2 Generalized Coordinates and Lagrange's Equations of Motion

To describe a certain system's configuration, a set of generalized coordinates $q = [q_1, q_2, ..., q_n]^T \in \mathbb{R}^n$ can be used that are independent from each other, and thus can parametrize the configuration space for the system as n-dimensional. Furthermore, the configuration's time derivative $\dot{q} \in \mathrm{T}_q\mathbb{R}^n$ belongs to the tangent space diffeomorphic to $\mathbb{R}^n$, allowing their union $(q, \dot{q}) \in \mathrm{T}\mathbb{R}^n$ to exist in a tangent bundle that is

diffeomorphic to $\mathbb{R}^{2n}$. The set of coordinates can be given local or global considerations, to one's preference and foresight. It must be noted that the latter will provide a more complete understanding of the spaces described.

2.2.1 The Lagrangian Function

It can be seen that for a given classical system, a Lagrangian function $L : \mathrm{T}\mathbb{R}^n \to \mathbb{R}$ is defined as the total potential energy subtracted from the total kinetic energy:

$$L(q, \dot{q}) = T(q, \dot{q}) - U(q), \tag{2.2}$$

$T(q, \dot{q})$ being thus the kinetic energy, and $U(q)$ the potential. It then follows that the Lagrangian function is defined on the tangent bundle previously defined. Hamilton's Variation Principle can then be applied, through the use of a well-established action integral. Construction of the action requires variations from a curve $q : [t_0, t_f] \to \mathbb{R}^n$. Allow these variations to be parametrized by $\epsilon \in (-c, c), c \in \mathbb{R}^+$. The newly parametrized curve subsequently sees the following conditions:

$$q^0(t) = q(t), \tag{2.3}$$

$$q^\epsilon(t_0) = q(t_0), \tag{2.4}$$

$$q^\epsilon(t_f) = q(t_f), \tag{2.5}$$

identifying that the endpoints of the curve are fixed, and zero deviation is identically equal to the curve itself. Application of a Taylor Series expansion around ϵ, allows for the expression to be rewritten as

$$q^\epsilon(t) = q(t) + \epsilon\delta q(t) + \mathscr{O}(\epsilon^2). \tag{2.6}$$

The time derivative of the above expression observes mixed partials and term cancellation to produce

$$\dot{q}^\epsilon(t) = \dot{q}(t) + \epsilon\delta\dot{q}(t) + \mathscr{O}(\epsilon^2). \tag{2.7}$$

Each variation on the tangent bundle can then be expressed through the mapping $(q^\epsilon, \dot{q}^\epsilon) : [t_0, t_f] \to \mathbb{R}$. Infinitesimal variations shown above are also defined as

$$\frac{d}{d\epsilon} q^\epsilon \Big|_{\epsilon=0} = \delta q, \tag{2.8}$$

$$\frac{d}{d\epsilon} \dot{q}^\epsilon \Big|_{\epsilon=0} = \delta \dot{q}, \tag{2.9}$$

which by definition lie on the tangent bundle itself, and satisfy the endpoint conditions. Hamilton's Variation Principle can now be invoked.

2.2.2 Hamilton's Principle

With all prerequisites assembled, an action integral is then expressed that integrates the Lagrangian function over the fixed time period given

$$\mathscr{S} = \int_{t_0}^{t_f} L(q, \dot{q}) dt. \tag{2.10}$$

Shifting mathematical focus to motion variation, the integral becomes

$$\mathscr{S}^\epsilon = \int_{t_0}^{t_f} L(q^\epsilon, \dot{q}^\epsilon) dt. \tag{2.11}$$

The variation form of the action integral can then be given the same Taylor Series considerations used prior

$$\mathscr{S}^{\epsilon} = \mathscr{S} + \epsilon\delta\mathscr{S} + \mathscr{O}(\epsilon^2). \tag{2.12}$$

The second term represents infinitesimal variation for the action integral. Hamilton's Principle declares that

$$\frac{d}{d\epsilon}\mathscr{S}^{\epsilon}\Big|_{\epsilon=0} = 0, \tag{2.13}$$

in order to consider all possible variations that satisfy the previously stated conditions. This result is helpful for the explicit definition of the derivative

$$\frac{d}{d\epsilon}\mathscr{S}^{\epsilon}\Big|_{\epsilon=0} = 0 = \int_{t_0}^{t_f}\left(\frac{\partial L(q,\dot{q})}{\partial\dot{q}}\delta\dot{q} + \frac{\partial L(q,\dot{q})}{\partial q}\delta q\right)dt. \tag{2.14}$$

Through the use of integration-by-parts on the first term in the integrand, the following can be provided

$$\frac{\partial L(q,\dot{q})}{\partial\dot{q}}\delta q\Big|_{t_0}^{t_f} + \int_{t_0}^{t_f}\left\{-\frac{d}{dt}\left(\frac{\partial L(q,\dot{q})}{\partial\dot{q}}\right) + \frac{\partial L(q,\dot{q})}{\partial q}\right\}\delta q dt = 0. \tag{2.15}$$

For this expression to be zero for all variations with fixed endpoints, the integrand must be identically zero. Therefore, the familiar Lagrange's equations of motion emerge:

$$\frac{d}{dt}\left(\frac{\partial L(q,\dot{q})}{\partial\dot{q}}\right) - \frac{\partial L(q,\dot{q})}{\partial q} = 0. \tag{2.16}$$

However, (2.16) does not account for well-behaved dissipation functions, or generalized forces. The former is a straightforward matter, so long as a Rayleigh's function

$R(q, \dot{q})$ be provided with a continuous partial derivative with respect to $\dot{q}$, to provide the modified set of equations as

$$\frac{d}{dt}\left(\frac{\partial L(q,\dot{q})}{\partial \dot{q}}\right) - \frac{\partial L(q,\dot{q})}{\partial q} + \frac{\partial R(q,\dot{q})}{\partial \dot{q}} = 0. \tag{2.17}$$

The latter requires more insight and care. Depending on the source of the generalized force in question, the formulation may be resolved by methods ranging from the principle of virtual work to the use of constraint forces and Lagrange multipliers. Such considerations must exist on the tangent bundle for all given trajectories, necessitating care in the modeling and development.

Chapter 3

Manifold Constraint Formulation

Outlined in the previous chapter were the considerations necessary to define a manifold in mathematically general terms. In doing so, the grounds for validity of Lagrange's equations of motion were determined. However, further insight can be obtained from the structure of the manifolds themselves.

Observe first the configuration or initial manifold. By being a function of the state variables and being differentiable, such a space can be represented as an embedding onto $\mathbb{R}^n$, under the constraints the physical system requires:

$$M = \{x \in \mathbb{R}^n : f_i(x) = 0, i = 1, \ldots, m\}, \tag{3.1}$$

where $f_i : \mathbb{R}^n \to \mathbb{R}$ must be scalar differentiable functions with linearly independent gradient vectors $\frac{\partial f_i(x)}{\partial x}$ in $\mathbb{R}^n$ at each arbitrary x. An immediate advantage to the linearly independent gradients is to require $1 \leq m \leq n$, or otherwise individually identify each constraint in its own right.

Another benefit to the gradient condition follows when considering proper definition of the tangent space. At an arbitrary element x in the configuration, the set of all tangent vectors to the element can also be considered an embedding in $\mathbb{R}^n$, and

is most effectively defined by a shared orthogonality constraint. Making use of the inner product operator, the resulting tangent space at the element x can be written as

$$\mathrm{T}_x M = \left\{ \xi \in \mathbb{R}^n : \left(\frac{\partial f_i(x)}{\partial x} \cdot \xi \right) = 0, i = 1, \ldots, m \right\}, \tag{3.2}$$

where ξ is referred to as a tangent to M at the arbitrary element x. Naturally, this space houses the given system's velocities along with their physical restrictions. By applying a union between each element in the configuration with its corresponding tangent space, the resulting set $\mathrm{T}M$ is referred to as the tangent bundle. By incorporating the constraints from its constituent spaces, the tangent bundle allows for complete representation of the dynamics observed.

In light of these points, one can make use of the nature of manifold structure to rewrite a set of dynamical equations into a form usable for one's purposes. The scope of this document will be restricted to controls engineering applications, and thus will show interest in isolating acceleration terms for control inputs. To do so, orthogonality constraints will be applied along with a mathematical identity to avoid singular relationships. The following general formulation is outlined and expanded on both in the provided examples and in Hoffman and Reyhanoglu (2017a)

Considering the points made above, differential geometric techniques demand well-posed constraints for the given system. In particular, the corresponding configuration and tangent spaces apply orthogonality and other constraint requirements of the respective trajectories and velocities. In turn, the Lagrangian function created from the system lies in the appropriate tangent bundle, providing through the principle of least action global-coordinate equations of motion. To create the complete configuration

manifold, often a semiproduct of a number of n separate manifolds is required:

$$M = M_1 \times M_2 \times \cdots \times M_n. \tag{3.3}$$

With this expression, all necessary constraints present from the individual configurations are clearly shown. The most common of such constraints are those of orthogonality, as they are often well-defined for operations such as the tangent space and tangent bundle. As outlined in Lee et al. (2017), each configuration is paired to its orthogonal constraint projection through the expression

$$P_i(x_i)^T \left\{ \frac{d}{dt} \left(\frac{\partial L(x, \dot{x})}{\partial \dot{x}_i} \right) - \frac{\partial L(x, \dot{x})}{\partial x_i} \right\} = 0, i = 1, \ldots, n, \tag{3.4}$$

where each P_i is the required orthogonal projection, and x for solely this section denotes the collected global generalized coordinates. Once all P_i are defined, the system of equations is concatenated. It must be noted that the acceleration term cannot be defined in this manner alone due to the singular nature of the orthogonal projections. Thus, an additional identity is required that expands the first term of the equations of motion, providing

$$\begin{bmatrix} P(x)^T \frac{\partial^2 L(x,\dot{x})}{\partial \dot{x}^2} \\ I_{n \times n} - P(x) \end{bmatrix} \ddot{x} = \begin{bmatrix} -P(x)^T \left(\frac{\partial}{\partial x} \left(\frac{\partial L(x,\dot{x})}{\partial \dot{x}} \right) \dot{x} - \frac{\partial L(x,\dot{x})}{\partial x} \right) \\ \frac{\partial (P(x)\dot{x})}{\partial x} \dot{x} \end{bmatrix}. \tag{3.5}$$

Applying the transpose of the first bracketed term will yield a means of isolating the acceleration term, in essence allowing for control law design. In the examples that follow, foresight will be noted that allows for ease of control law design or equations of motion representation. Nevertheless, the above equations will provide these results or an equally-viable alternative.

Chapter 4

Constraint Embedding Formulation

The versatility of manifold notation cannot be understated. So long as mathematically valid constraints can be provided for a given set of trajectories, a singularity-free model can be created. For example, further constraints can be applied to a set of Lagrange's equations of motion after creating the original dynamics, often seen through the Lagrange's multiplier method. Moreover, the dynamics in question do not have to be generated from the action integral, allowing for kinematics and other dynamical methods to be equally valid for additional constraint modifications.

Once more requiring a restriction on scope, the following considerations will fixate on constraints sourced from a desire to avoid perturbation of unactuated degrees of freedom. The overview provided in this chapter will be elaborated on in the example chapters to follow, with additional coverage seen in Hoffman and Reyhanoglu (2018).

Presented below is a class of dynamical systems in terms of differential algebraic equations (DAEs):

$$J(q)\ddot{q} + F(q, \dot{q}) = Q, \tag{4.1}$$

$$A(q)\ddot{q} + S(q, \dot{q}) = 0, \tag{4.2}$$

where $q \in \mathbb{R}^n$, $J \in \mathbb{R}^{n-m \times n}$, $A \in \mathbb{R}^{m \times n}$, $F, Q \in \mathbb{R}^{n-m}$, $S \in \mathbb{R}^m$. Dynamically speaking, the general equation structure implies the result of Lagrangian formulations. However, this is not required for the following considerations. The latter expression identifies m constraints in the form of unactuated degrees of freedom. What naturally follows is the desire to maintain zero perturbation of such DOFs from rest. The objective can be incorporated to the original dynamics through the manifold

$$M = \{(q, \dot{q}) \in \mathbb{R}^{2n} : A(q)\ddot{q} + S(q, \dot{q}) = 0\}, \tag{4.3}$$

that defines a space within $\mathbb{R}^{2n}$ where all acceptable trajectories reside. In order to enforce this new subset, a Lagrange's constraint multiplier can be used to produce a projection of the original configuration onto the modified tangent space $\mathrm{T}_{(q,\dot{q})}M$:

$$\ddot{q} = G(q, \dot{q}) + B(q)u + A(q)^T\lambda, \tag{4.4}$$

where $G = -J^{-1}F(q, \dot{q})$, $Bu = J^{-1}Q$, and λ represents the constraint multiplier. To continue, it must be confirmed that the expression

$$C(q) = A(q)A(q)^T \tag{4.5}$$

be of full rank for all q. Then, multiplying (4.4) by $A(q)$ to replace the $\ddot{q}$ term results in an expression for λ:

$$\lambda = -C(q)^{-1}(S(q, \dot{q}) + A(q)(G(q, \dot{q}) + B(q)u)). \tag{4.6}$$

Replacing this term in (4.4) in turn provides the final constraint-embedded dynamics:

$$\ddot{q} = P(q)(G(q,\dot{q}) + B(q)u) - A(q)^T C(q)^{-1} S(q,\dot{q}), \tag{4.7}$$

where $P = I_{n\times n} - A(q)^T C(q)^{-1} A(q)$ indicates the projection operator. Through this derivation, the expression (4.7) sees M as an invariant manifold of its flow. It then follows that, provided an initial-value problem defined on M, the designed control effort $B(q)u$ and by extension the actuation term Q will be guaranteed to provide a unique solution in M. More often than not, the mappings provided yield nonholonomic considerations, and as a result will necessitate either a non-continuous or a time-varying control law for stability objectives.

Chapter 5

Examples: Local Coordinate Underactuated Systems

This chapter is based on papers by Hoffman, Reyhanoglu, and collaborators (Hoffman et al., 2017), (Reyhanoglu and Hoffman, 2016), (Reyhanoglu et al., 2016), (Reyhanoglu and Hoffman, 2017). Described are the identification and stabilization of a variety of underactuated systems, all of which in local-coordinate formulation. With the examples provided, this may be separated into 2 further categories: manipulator robotics and quadrotor attitude dynamics.

5.1 Robotic Manipulators

Flexible and hybrid structures are widely used throughout aerospace industries. Direct implementation can be seen in products such as spacecraft antennas and telescopes. Elastic considerations in mechatronics are quite common, requiring high-performance control laws to achieve strict control objectives. Published literature provides a number of mathematical formulation examples for these types of chal-

lenges. The most common approaches to modeling are finite element methods (see e.g., Aoustin et al. (1994), Tokhi et al. (2001)) and assumed mode methods (Azad (1994), Junkins and Kim (1993), Martins et al. (2003), Wie (1998)). The latter models the deflection of the elastic structure by a finite series of space-dependent shape functions that are multiplied by time-dependent amplitude functions. The book by Junkins and Kim (Junkins and Kim, 1993) outlines a thorough approach to developing mathematical models for infinite-dimensional flexible structures.

Flexible structure control has seen consistent interest throughout the years. Seen in Eckhart (2005) is the comparison of various conventional control laws for the single-link flexible manipulator. A popular solution towards the fast yet precise slewing maneuver is the use of finite-time control, an example of which is shown in Reyhanoglu (2008). On the other hand, a Lyapunov-based deflection feedback controller is outlined in Tso et al. (2003).

As can be expected, the presence of an additional link leads to increased complications. Finite element models for two-link flexible planar robot manipulators can be seen in Usoro et al. (1986) and Yang and Sadler (1990). Through the use of an assumed mode method, Ahmad et al. (2008) constructs a two-link flexible manipulator dynamical model, to include hub inertia and payload. The comparison of flexible robot model-based and model-free control schemes is shown in Rigatos (2009). Nonlinear energy-based approaches in the case of two-link flexible manipulators are outlined in Bo et al. (2005) and Rigatos (2009). Robust finite-time control is applied to a class of robotic manipulators in Zhao et al. (2010), making use of a finite-time Lyapunov stability analysis.

Hybrid two-link manipulators composed of flexible and rigid members have been tackled by researchers such as (Dogan and Iftar, 1998), (Goes et al., 2001), (Reyhanoglu and Hoffman, 2016), (Reyhanoglu et al., 2016), to name but a few. A com-

mon setup for such manipulators is the presence of a small rigid member with end effector attached to the end of a larger flexible arm. The latter is referred to as a macro manipulator, and the former a micro manipulator. It then follows that successful control of the system requires stability for both members and the suppression of macro manipulator structural oscillation, lest the residual vibrations harm overall performance. Some literature examples of authors who have addressed flexible-macro/rigid-micro manipulator systems include (Lew and Moon, 2001), (Sharf, 1995), (Torres and Dubowsky, 1993), (Yang et al., 2007), (Yoshikawa et al., 1996). A two-time scale model-based active damping control for micro/macro manipulators is presented in Lew and Moon (2001). Using a linear model, Sharf (1995) implements a damping controller that requires only the micro manipulator position. Outlined in reference (Torres and Dubowsky, 1993) is a technique called "the coupling map" to plan motions on an elastically constrained space manipulator system that results in relatively low residual vibrations to its supporting structure. Augmentation of inertial damping control is addressed in Yang et al. (2007) through the use of a neural network-based adaptive control implemented on a micro manipulator mounted at the tip of a cantilevered beam that resembles a macro manipulator with its joint locked. A tracking controller for micro/macro manipulators can be seen in Yoshikawa et al. (1996).

Hybrid manipulator control may be summarized as the motion control of a single manipulator attached to an oscillatory base, observing strong perturbations on the former's dynamics due to the latter's vibrations (Chong et al., 1997), (Lew and Moon, 1999), (Lin et al., 2007), (Lin and Huang, 2007), (Tilley and Cannon, 1986), (Yang et al., 2007). Active damping control objectives for robotic manipulators with oscillatory bases are solved in Lin et al. (2007). Specifically, a two-time scale fuzzy logic controller with a vibration stabilizer for such structures has been proposed. In

light of such complexity, Lin and Huang (2007) relegates the overall control task into two subtasks, to be distributed over two different levels. It is arranged such that, in the context of the hierarchical fuzzy control structure, the lower level controllers focus solely on the subtask requirements while the higher level controller handles subsystem coupling.

Compliant base systems in general can be seen in a variety of industrial and aerospace applications. In the case of mechatronics, ingenuity of control design is often required in order to obtain simultaneous control of base and manipulator. As a result, many publications demonstrate alternative solutions. For example, Nenchev et al. (1999) makes use of a reaction null space so as to input trajectories that do not induce base disturbances, in combination with the separate provision of base damping. A Cartesian compliance control is proposed in Ott et al. (2006) for a compliant base robotic manipulator, allowing for control of effective stiffness and damping for total system behavior. By regarding the flexible structure dynamics as uncertain, Wongratanaphisan and Cole (2009) creates a robust impedance control for the purpose of contact tasks. A space laboratory unit is interpreted as a large flexible structure in Casella et al. (2002), and its vibration suppression is achieved through various configurations of jet thrusters and piezoactuators. The above attempts to avoid the highly nonlinear system coupling through either the separation of the control objective into sub-objectives, or the simplification of the layout itself.

In the subsections that follow, various underactuated robotic manipulators will be considered that fall under the compliant base or hybrid robotic manipulator category. Following in-depth mathematical formulation is the establishment of a rigorous stability analysis for the proposed controller. This in turn is followed by simulation results highlighting controller effectiveness. Such controllers will address both base and manipulator stability simultaneously, and will make use of the nonlinear coupling

between members, an innovative approach not seen in the prior literature.

5.1.1 Hybrid Robotic Manipulator Cantilevered and Subjected to Single Torque

The problem in its entirety is outlined in Reyhanoglu and Hoffman (2016), for the reader's convenience. The objective of the following is to make use of the system's coupled behavior to produce a Lyapunov stability-based control law for a given slew maneuver. To do so, the partial feedback linearization approach will be used to implement the rigid body's angular acceleration as the control input, with the resulting torque requirement to be analyzed during implementation.

Model Formulation

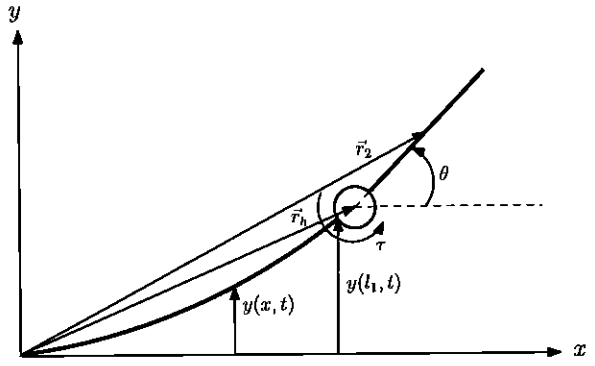

Figure 5.1: Schematic model of a one-torque hybrid robot manipulator.

Presented above is the schematic model of hybrid robotic manipulator composed of a flexible first link and rigid second link. The mass per unit length of link 1 will be referred to as ρ_1, while its length will be labeled as l_1. The hub, depicted as the circle, connects the two links and observes a radius l_o. The uniform flexural rigidity of the first link is denoted by EI_1. The sole control torque τ is applied at the joint via the motor hub. For the second link, let l_2 and m_2 denote the length and mass respectively,

while m_h represents the mass of the hub, to include the motor and mounting bracket. The combined structure of the rigid link, motor and mounting bracket produces a moment of inertia I_z.

Generalized coordinates will be assembled based on an inertial coordinate frame denoted as xyz. The angular position of the rigid link with respect to the x-axis will be defined as θ, while the actuation torque will be directed along the z-axis. The transverse deformation of the flexible link at a given point x and time t is defined as $y(x,t)$, to be parametrized appropriately in the following derivation.

The provided hybrid manipulator will in turn demand a hybrid modeling technique, making use of distributed and discrete parameter modeling (Junkins and Kim, 1993). To this end, the following assumptions are asserted:

1. The robot manipulator exists and acts solely on a horizontal plane;
2. Uniform beam theory is applied to both links;
3. Euler-Bernoulli assumptions appropriate for long and slender links are made, which can be summarized as negligible shear deformation and distributed rotary inertia;
4. Linear theory of elasticity for the first link is used based on small-deflection considerations;
5. Coulomb friction effects and backlash in the reduction gear are neglected;
6. The velocity component of the flexible link in the x-direction is neglected, asserting that all beam deflection is transverse to the x-axis.

These assumptions are mild, as they reflect common aerospace structural considerations for small-deflection scenarios. The first assumption allows for the only

potential term to be due to elastic energy in the first link:

$$U = \frac{1}{2}\int_0^{l_1} EI_1[y''(x,t)]^2 dx \tag{5.1}$$

To assemble the kinetic energy terms, let $\vec{r}_2$ denote the position vector of the center of mass of the rigid link, and $\vec{r}_h$ represent the position vector of the hub's center of mass. The system's total kinetic energy can then be defined as the summation of all translational and rotational energies from both links and the hub:

$$T = \frac{1}{2}\int_0^{l_1} \rho_1[\dot{y}(x,t)]^2 dx + \frac{1}{2}m_2\dot{r}_2^2 + \frac{1}{2}m_h\dot{r}_h^2 + \frac{1}{2}I_z\dot{\theta}^2, \tag{5.2}$$

where

$$\dot{r}_2^2 = [\gamma x_2\dot{\theta}\sin\theta]^2 + [\gamma\dot{y}(l,t) + x_2\dot{\theta}\cos\theta]^2, \tag{5.3}$$

$$\dot{r}_h^2 = [\gamma\dot{y}(l,t)]^2. \tag{5.4}$$

For convenience, the contracted terms are

$$\gamma = \frac{l_1 + l_0}{l_1},\ x_2 = l_0 + \frac{l_2}{2}.$$

The assumed mode method will be implemented on $y(x,t)$ to parametrize the deflection function into a shape and generalized coordinate:

$$y(x,t) = \sum_{j=1}^{N} \phi_j(x)q_j(t), \tag{5.5}$$

where $q_j(t)$ is the generalized coordinate corresponding to the jth vibrational mode,

and $\phi_j(x)$ is the jth mode shape function, which is given as (Junkins and Kim, 1993):

$$\phi_j(x) = 1 - \cos\left(\frac{j\pi x}{l_1}\right) + \frac{1}{2}(-1)^{(j+1)}\left(\frac{j\pi x}{l_1}\right)^2. \tag{5.6}$$

To obtain the simplest model, only the first mode will be considered, i.e., $j = 1$ so that

$$y(x,t) = \phi_1(x)q_1(t) \triangleq \phi(x)q(t). \tag{5.7}$$

The Lagrangian function $L = T - U$ can therefore be obtained as

$$L = \frac{1}{2}m_q\dot{q}^2 + \frac{1}{2}I_t\dot{\theta}^2 + m_{q\theta}\dot{q}\dot{\theta}\cos\theta - \frac{1}{2}kq^2, \tag{5.8}$$

where

$$\begin{aligned}
m_q &= \rho_1\int_0^{l_1}\phi^2 dx + (m_h + m_2)\phi^2(l_1)\gamma^2,\\
I_t &= I_z + m_2x_2^2,\\
m_{q\theta} &= m_2x_2\phi(l_1)\gamma,\\
k &= EI_1\int_0^{l_1}\phi''^2(x)dx.
\end{aligned}$$

Structural damping for the first link will be introduced via the Rayleigh dissipation function given by

$$R = \frac{1}{2}c\dot{q}^2, \tag{5.9}$$

where c is the damping constant for the first link, determined through conventional damped mass-spring oscillator theory. To assemble the applied non-conservative forces, the theory of virtual work will be implemented:

$$\delta W = \tau\delta\theta - \phi'(l_1)\tau\delta q. \tag{5.10}$$

Lagrange's equations of motion for the hybrid two-link robot manipulator can then be written as

$$I_t\ddot{\theta} + m_{q\theta}\ddot{q}\cos\theta = \tau, \tag{5.11}$$

$$m_{q\theta}\ddot{\theta}\cos\theta + m_q\ddot{q} + c\dot{q} + kq - m_{q\theta}\dot{\theta}^2\sin\theta = -\phi'(l_1)\tau. \tag{5.12}$$

For the purpose of practical implementation, a partial feedback linearization will be used to identify the angular acceleration as the virtual input

$$\ddot{\theta} = u, \tag{5.13}$$

$$(\alpha_1 + \alpha_2\cos\theta)\ddot{q} + c\dot{q} + kq = -(\beta_1 + \beta_2\cos\theta)u + \beta_2\dot{\theta}^2\sin\theta, \tag{5.14}$$

where

$$\alpha_1 = m_q,\ \alpha_2 = \phi'(l_1)m_{q\theta};\ \beta_1 = \phi'(l_1)I_t,\ \beta_2 = m_{q\theta}.$$

This setup is accomplished for the purpose of designing a feedback control law for u, to be in turn used to determine the required control torque via

$$\tau = I_t u + m_{q\theta}\ddot{q}\cos\theta. \tag{5.15}$$

The system (5.13), (5.14) has two degrees of freedom and one control input, identifying it as underactuated. Moreover, the strong coupling between links causes the control objective of precise slewing maneuvers to be challenging to achieve.

Stability Analysis

In this section, the system outlined in the previous section is considered for the purpose of devising a Lyapunov-based nonlinear controller.

Consider the following candidate Lyapunov function for the system:

$$V = \frac{1}{2}(\alpha_1 + \alpha_2 \cos\theta)\dot{q}^2 + \frac{1}{2}kq^2 + \frac{p_1}{2}\theta^2 + \frac{p_2}{2}\dot{\theta}^2 + (\beta_1 + \beta_2 \cos\theta)\dot{q}\dot{\theta},$$

where $p_1, p_2 \in \mathbb{R}^+$. Assume that

$$\mu = p_2 - \frac{(\beta_1 + \beta_2 \cos\theta)^2}{\alpha_1 + \alpha_2 \cos\theta} > 0$$

so that the function V is positive definite. Motivation for this assumption is given by the following use of Sylvester's Criterion:

Remark 1: *Let $z = [\dot{\theta},\ \dot{q}]^T$ and let $Q \in \mathbb{R}^{2\times 2}$ denote the symmetric matrix corresponding to the quadratic form*

$$z^T Q z = p_2\dot{\theta}^2 + 2(\beta_1 + \beta_2 \cos\theta)\dot{\theta}\dot{q} + (\alpha_1 + \alpha_2 \cos\theta)\dot{q}^2,$$

where

$$Q = \begin{bmatrix} p_2 & \beta_1 + \beta_2 \cos\theta \\ \beta_1 + \beta_2 \cos\theta & \alpha_1 + \alpha_2 \cos\theta \end{bmatrix}.$$

It then follows that the quadratic function is positive definite if and only if the leading principal minors of Q are all positive. It is therefore required that $p_2 > 0$ and $\mu > 0$.

The time derivative of V is taken along the trajectories of the given dynamics, and can be compressed into

$$\dot{V} = -c\dot{q}^2 + \left[\mu u + p_1\theta - 0.5\alpha_2\dot{q}^2 \sin\theta\right]\dot{\theta} - \left[\frac{\beta_1 + \beta_2 \cos\theta}{\alpha_1 + \alpha_2 \cos\theta}(\beta_2\dot{\theta}^2 \sin\theta - kq - c\dot{q})\right]\dot{\theta}.$$

By observation, the control law

$$u = \frac{1}{\mu}\left[-p_1\theta - d\dot{\theta} + 0.5\alpha_2\dot{q}^2\sin\theta\right] + \frac{1}{\mu}\left[\frac{\beta_1 + \beta_2\cos\theta}{\alpha_1 + \alpha_2\cos\theta}(\beta_2\dot{\theta}^2\sin\theta - kq - c\dot{q})\right], \quad (5.16)$$

where $d \in \mathbb{R}^+$, results in

$$\dot{V} = -c\dot{q}^2 - d\dot{\theta}^2,$$

which satisfies $\dot{V} \leq 0$, and can be described as negative semi-definite. Applying LaSalle's invariance principle (Khalil, 1996), we conclude that the closed-loop system is globally asymptotically stable to the origin.

Simulations

We now illustrate the ideas developed in the previous sections through a numerical simulation. The physical parameters used in the simulation are provided in the following table.

Table 5.1: Physical parameters of the one-torque hybrid robot manipulator.

Parameter	Value
ρ_1	0.7597 kg/m
l_0	0.06465 m
$l_1 = l_2$	0.22 m
m_h	0.9966 kg
m_2	0.0586 kg
EI_1	2.69 N·m^2
I_z	6.8195×10^{-4} kg·m^2

We implement the control algorithm described in the stability analysis with

$$(p_1, p_2) = (1.0, 1.0),$$

$$(\alpha_1, \alpha_2) = (86.34, 4.118),$$

$$(\beta_1, \beta_2) = (0.1108, 0.0918).$$

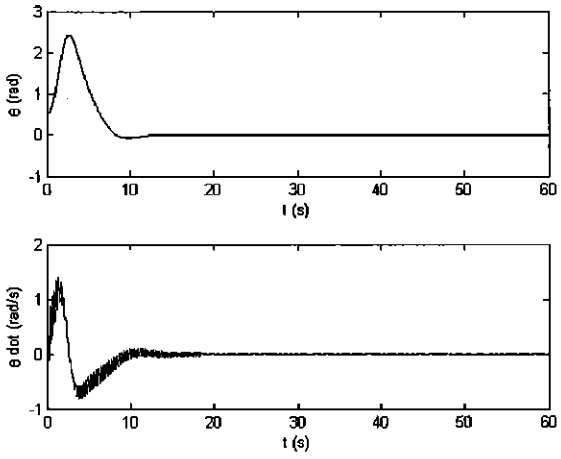

Figure 5.2: Time behavior of rigid member angle and angular velocity.

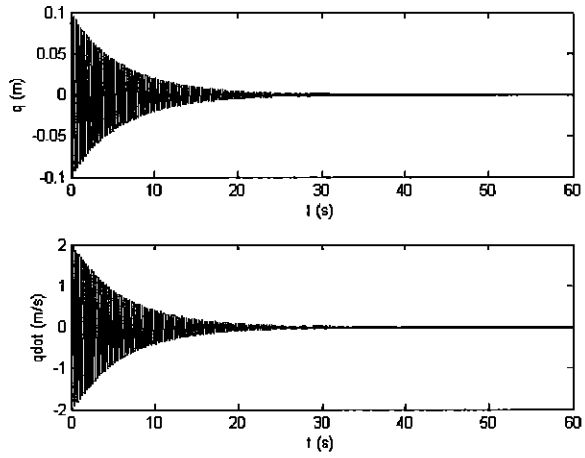

Figure 5.3: Time behavior of vibrational deflection and velocity.

The provided figures show the results of the simulation that correspond to initial

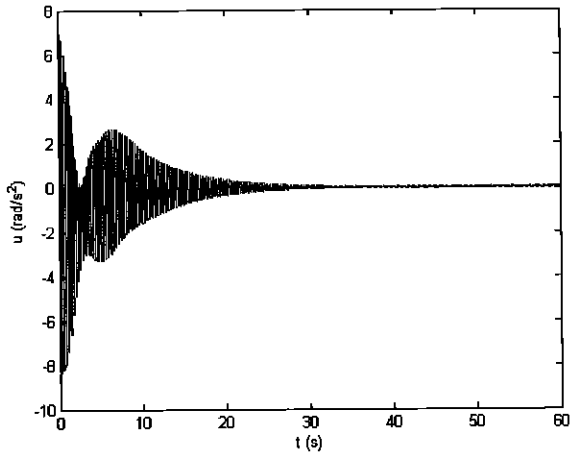

Figure 5.4: Time behavior of angular acceleration (u).

conditions given by

$$(\theta_0, q_0) = (0.5, 0.1),$$

$$\dot{\theta}_0 = \ddot{\theta}_0 = \dot{q}_0 = \ddot{q}_0 = 0.$$

As can be seen in the figures, the hybrid manipulator converges to equilibrium at zero in $30s$ and remains there. The time component of the deflection function q and its derivative also converge to zero and maintain equilibrium. Due to the partial feedback linearization, the angular acceleration is bounded and converging. The observed chatter will be motivation for the subsequent control designs.

5.1.2 Modeling and Control of a Two-Torque Hybrid Robotic Manipulator

The following is also seen in Reyhanoglu et al. (2016), but is described here in full. The system itself is rather similar to the previous section, with the addition of a second torque hub where the previously cantilevered point once existed. The objective of the presented work is to provide slewing maneuvers using a nonlinear finite-time controller

for the two-torque system, making use of a notch filter to avoid system disturbances.

Model Formulation

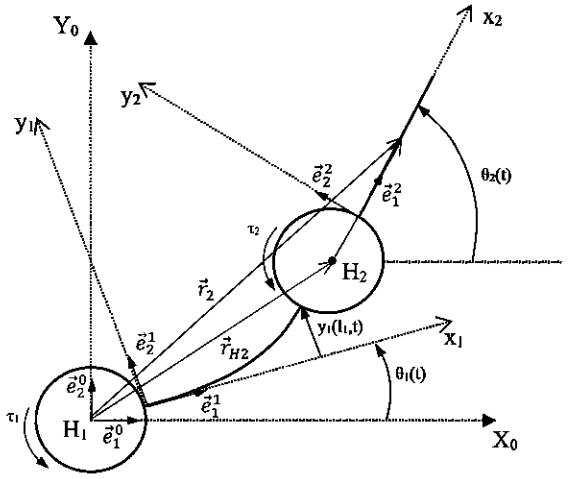

Figure 5.5: Schematic model of a two-torque hybrid robot manipulator.

The above denotes a schematic model of a two-torque hybrid robot manipulator composed of a flexible first and rigid second link. The mass per unit length, flexural rigidity, and length of the first link will be respectively labeled as ρ_1, EI_1, and l_1. The moment of inertia for the first motor and mounting bracket will be represented as I_{z_1}. The second link's length and mass will be denoted as l_2 and m_{l_2}. The mass of the second hub, m_{H_2}, and that of the corresponding mounting bracket, m_{b_2}, contribute to their collective moment of inertia, I_{z_2}.

The system's two points of actuation are through the individual motors integrated into the hubs represented by circles. Once more, an inertial coordinate frame is defined, this time as $X_0Y_0Z_0$. Each link observes a body-fixed frame of $x_iy_iz_i, i = 1, 2$.

With the applied body frames, the respective angular position of each link with respect to the inertial are labeled as θ_i. Both control torques are applied about the z-axis, to be defined as τ_1 and τ_2. The transverse deflection of the first link at an arbitrary point x_1 and time t is denoted as $y_1(x_1, t)$.

Due to the strikingly similar system as the previous section, the same hybrid modeling technique outlined in Junkins and Kim (1993) will be implemented. It then follows that a very similar set of mild assumptions must be made:

1. The robot manipulator is restricted to purely planar motion, and hence is not affected by gravity;
2. Both links observe uniform beam behavior;
3. Euler-Bernoulli assumptions for the long and slender links are made, i.e., negligible shear deformation and distributed rotary inertia are assumed;
4. Linear theory of elasticity is used on the first link, and hence small deflections are surmised;
5. Coulomb friction effects and backlash in the reduction gear are neglected;

Assuming that the manipulator is restricted to move in the horizontal plane, the elastic energy of the first link expressed as:

$$U = \frac{1}{2}\int_0^{l_1} EI_1(y_1''(x_1,t))^2 dx_1. \tag{5.17}$$

As shown in Figure 5.5, $\vec{r}_1$ and $\vec{r}_2$ represent the position vector of the first link at point x_1 and the position vector of the center of mass of the second link, respectively. As such, the total kinetic energy of the system can be assembled as

$$T = \frac{1}{2}\int_0^{l_1} \rho_1 \dot{r}_1^2 dx_1 + \frac{1}{2}m_2\dot{r}_2^2 + \frac{1}{2}m_{H_2}\dot{r}_{H_2}^2 + \frac{1}{2}I_{z_1}\dot{\theta}_1^2 + \frac{1}{2}I_{z_2}\dot{\theta}_2^2. \tag{5.18}$$

where $m_2 = m_{l_2} + m_{b_2}$ and

$$\dot{r}_1^2 = (y_1\dot{\theta}_1)^2 + [\dot{y}_1 + (x_1 + l_0)\dot{\theta}_1]^2, \tag{5.19}$$

$$\dot{r}_2^2 = \left[\gamma y_1(l_1,t)\dot{\theta}_1 + x_{C_2}\dot{\theta}_2 s(\theta_2 - \theta_1)\right]^2 + \left[\gamma\dot{y}_1(l_1,t) + (2l_0 + l_1)\dot{\theta}_1 + x_{C_2}\dot{\theta}_2 c(\theta_2 - \theta_1)\right]^2, \tag{5.20}$$

$$\dot{r}_{H_2}^2 = \left[\gamma y_1(l_1,t)\dot{\theta}_1\right]^2 + \left[\gamma\dot{y}_1(l_1,t) + (2l_0 + l_1)\dot{\theta}_1\right]^2. \tag{5.21}$$

Here

$$\gamma = \frac{l_1 + l_0}{l_1}, \quad x_{C_2} = \frac{(2l_0 + l_2)m_{l_2}}{2m_2}.$$

Note that the abbreviations $s(\cdot) = \sin(\cdot)$ and $c(\cdot) = \cos(\cdot)$ have been used.

The bending deflection $y_1(x_1, t)$ can be parameterized using the assumed mode method as:

$$y_1(x_1,t) = \sum_{j=1}^{N} \phi_j(x_1)q_j(t), \tag{5.22}$$

where $q_j(t)$ is the generalized coordinate corresponding to the jth vibrational mode, and $\phi_j(x_1)$ is the jth mode shape function of, which is given as (Junkins and Kim, 1993):

$$\phi_j(x_1) = 1 - \cos\left(\frac{j\pi x_1}{l_1}\right) + \frac{1}{2}(-1)^{(j+1)}\left(\frac{j\pi x_1}{l_1}\right)^2. \tag{5.23}$$

To obtain the simplest model, only the first mode will be considered, i.e., $j = 1$ so that

$$y_1(x_1,t) = \phi_1(x_1)q_1(t) \triangleq \phi_1(x_1)q(t). \tag{5.24}$$

The Lagrangian function $L = T - U$ can then be expressed as

$$\begin{aligned} L =& \frac{1}{2} m_q q^2 \dot{\theta}_1^2 + \frac{1}{2} m_q \dot{q}^2 + \frac{1}{2} I_{t_1} \dot{\theta}_1^2 + \frac{1}{2} I_{t_2} \dot{\theta}_2^2 + m_{1q} \dot{q} \dot{\theta}_1 + m_{2q}(\theta_1, \theta_2) \dot{q} \dot{\theta}_2 \\ & + m_{12}(\theta_1, \theta_2, q) \dot{\theta}_1 \dot{\theta}_2 - \frac{1}{2} k q^2, \end{aligned} \tag{5.25}$$

where

$$\begin{aligned} m_q &= \rho_1 \int_0^{l_1} \phi_1^2 dx_1 + (m_{H_2} + m_2) \phi_1^2(l_1) \gamma^2, \\ I_{t_1} &= \rho_1 \int_0^{l_1} (x_1 + l_0)^2 dx_1 + I_{z_1} + (m_{H_2} + m_2)(2l_0 + l_1)^2, \\ I_{t_2} &= I_{z_2} + m_2 x_{C_2}^2, \\ m_{1q} &= \rho_1 \int_0^{l_1} \phi_1 (x_1 + l_0) dx_1 + (m_{H_2} + m_2) \phi_1(l_1) \gamma (2l_0 + l_1), \\ m_{2q} &= m_2 x_{C_2} \phi_1(l_1) \gamma c(\theta_2 - \theta_1), \\ m_{12} &= m_2 x_{C_2} \left[\phi_1(l_1) \gamma q s(\theta_2 - \theta_1) + (2l_0 + l_1) c(\theta_2 - \theta_1) \right], \\ k &= E I_1 \int_0^{l_1} \phi_1''^2(x_1) dx_1. \end{aligned}$$

Structural damping seen in the first link is included through Rayleigh dissipation function:

$$R = \frac{1}{2} c \dot{q}^2, \tag{5.26}$$

where c is the damping constant for the first link.

The virtual work of non-conservative forces can be evaluated as

$$\delta W = (\tau_1 - \tau_2) \delta\theta_1 + \tau_2 \delta\theta_2 - \phi_1'(l_1) \tau_2 \delta q. \tag{5.27}$$

Therefore, the Lagrangian equations of motion for the two-torque hybrid robot

manipulator may be written as

$$(I_{t_1} + m_q q^2)\ddot{\theta}_1 + m_{12}\ddot{\theta}_2 + m_{1q}\ddot{q} + 2m_q q\dot{q}\dot{\theta}_1 + \partial m_{12}\theta_2\dot{\theta}_2^2 = \tau_1 - \tau_2, \tag{5.28}$$

$$m_{12}\ddot{\theta}_1 + I_{t_2}\ddot{\theta}_2 + m_{2q}\ddot{q} + 2\partial m_{2q}\theta_1\dot{q}\dot{\theta}_1 + \partial m_{12}\theta_1\dot{\theta}_1^2 = \tau_2, \tag{5.29}$$

$$m_{1q}\ddot{\theta}_1 + m_{2q}\ddot{\theta}_2 + m_q\ddot{q} - m_q q\dot{\theta}_1^2 + \partial m_{2q}\theta_2\dot{\theta}_2^2 + c\dot{q} + kq = -\phi_1'(l_1)\tau_2. \tag{5.30}$$

Once more applying partial feedback linearization yields

$$\ddot{\theta}_1 = u_1, \tag{5.31}$$

$$\ddot{\theta}_2 = u_2, \tag{5.32}$$

$$\ddot{q} + 2\zeta\omega_n\dot{q} + \omega_n^2 q = \sum_{i=1}^{2}(\alpha_i u_i + \beta_i\dot{\theta}_i^2) + \beta_3\dot{q}\dot{\theta}_1, \tag{5.33}$$

where

$$\omega_n = \sqrt{\frac{k}{\bar{m}_q}},\ \zeta = \frac{c}{2\sqrt{k\bar{m}_q}},\ \alpha_1 = -\frac{m_{1q} + \phi_1'(l_1)m_{12}}{\bar{m}_q},$$
$$\alpha_2 = -\frac{m_{2q} + \phi_1'(l_1)I_{t_2}}{\bar{m}_q},\ \beta_1 = \frac{m_q q - \phi_1'(l_1)\partial m_{12}\theta_1}{\bar{m}_q},$$
$$\beta_2 = -\frac{\partial m_{2q}\theta_2}{\bar{m}_q},\ \beta_3 = -2\frac{\phi_1'(l_1)\partial m_{2q}\theta_1}{\bar{m}_q}.$$

Here $\bar{m}_q = m_q + \phi_1'(l_1)m_{2q}$. Note that the control torques can be determined from the virtual control inputs through the expressions

$$\tau_1 = (I_{t_1} + m_q q^2 + m_{12})u_1 + (m_{12} + I_{t_2})u_2 + (m_{1q} + m_{2q})\ddot{q}$$
$$+ 2m_q q\dot{q}\dot{\theta}_1 + \frac{\partial m_{12}}{\partial\theta_2}\dot{\theta}_2^2 + \frac{\partial m_{12}}{\partial\theta_1}\dot{\theta}_1^2 + 2\frac{\partial m_{2q}}{\partial\theta_1}\dot{q}\dot{\theta}_1, \tag{5.34}$$

$$\tau_2 = m_{12}u_1 + I_{t_2}u_2 + m_{2q}\ddot{q} + 2\frac{\partial m_{2q}}{\partial\theta_1}\dot{q}\dot{\theta}_1 + \frac{\partial m_{12}}{\partial\theta_1}\dot{\theta}_1^2. \tag{5.35}$$

Once more this system is underactuated, and requires similar considerations to the previous section (see e.g., Reyhanoglu (2003), Reyhanoglu et al. (1999a), Reyhanoglu et al. (1998), Reyhanoglu and Hervas (2012) and references therein).

Filter and Controller Design

A notch filter, also known as a band-reject filter, is a specialized form of a second-order filter (Wie, 1998). The general form of such filters can be expressed as

$$\frac{u}{v} = \frac{s^2/\omega_z^2 + 2\zeta_z s/\omega_z + 1}{s^2/\omega_p^2 + 2\zeta_p s/\omega_p + 1}, \tag{5.36}$$

where u is the filter output, v is the filter input; and ω_z, ω_p, ζ_z, and ζ_p are filter parameters. Variations such as lead/lag and all-pass filters can be created through different parameter combinations.

For the proposed notch filter, the parameters are chosen as $\omega_z = \omega_p = \omega_n$, $\zeta_z = \zeta$, and $\zeta_p = 1$. Making these substitutions into the original generalized format yields the notch filter

$$\frac{u}{v} = \frac{s^2 + 2\zeta\omega_n s + \omega_n^2}{s^2 + 2\omega_n s + \omega_n^2}. \tag{5.37}$$

Consider the block diagram shown below, which corresponds to the controlled linearized system

$$\ddot{\theta}_1 = u_1, \tag{5.38}$$

$$\ddot{\theta}_2 = u_2, \tag{5.39}$$

$$\ddot{q} + 2\zeta\omega_n\dot{q} + \omega_n^2 q = \sum_{i=1}^{2} \alpha_i u_i. \tag{5.40}$$

The finite-time control signals are given by (without loss of generality, assuming

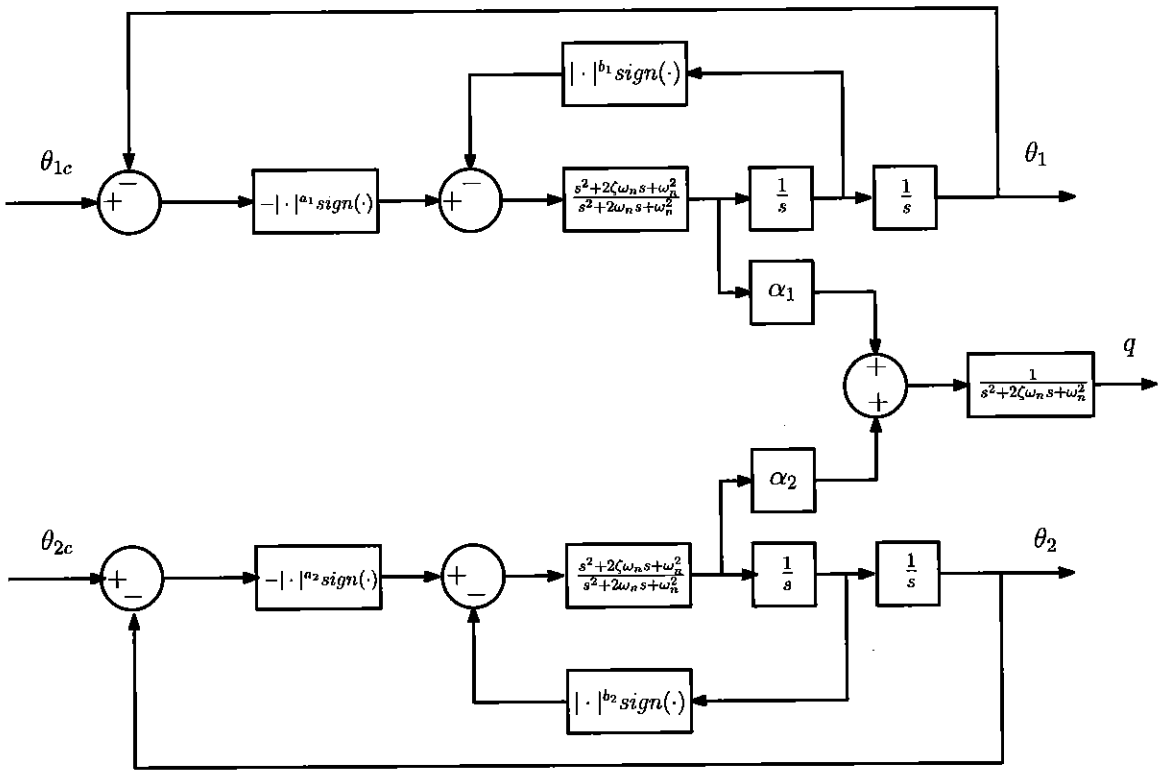

Figure 5.6: Finite-time system block diagram.

$\theta_{1c} = \theta_{2c} = 0$)

$$v_1 = -|\theta_1|^{a_1}\text{sign}(\theta_1) - |\dot{\theta}_1|^{b_1}\text{sign}(\dot{\theta}_1), \tag{5.41}$$

$$v_2 = -|\theta_2|^{a_2}\text{sign}(\theta_2) - |\dot{\theta}_2|^{b_2}\text{sign}(\dot{\theta}_2), \tag{5.42}$$

where $a_i,\ b_i \in (0,\ 1),\ a_i > b_i/(2 - b_i),\ i = 1, 2$, are controller parameters. These feedback laws control the rigid body motion to $(\theta_1, \dot{\theta}_1, \theta_2, \dot{\theta}_2) = (0, 0, 0, 0)$ in finite time (Haimo, 1986). The finite-time control signals (5.41), (5.42) provide input to their respective notch filter.

Identifying state-space representations of the notch filters requires the definition

of auxiliary variables z_i such that

$$\ddot{z}_i + 2\omega_n \dot{z}_i + \omega_n^2 z_i = v_i,\ i = 1, 2,$$

so that the transfer functions from v_i to z_i is given by

$$\frac{z_i}{v_i} = \frac{1}{s^2 + 2\omega_n s + \omega_n^2},\ i = 1, 2.$$

Clearly, the controls u_i for the system are the filters' outputs given by

$$u_i = \ddot{z}_i + 2\zeta\omega_n \dot{z}_i + \omega_n^2 z_i = v_i - 2\omega_n (1 - \zeta)\, \dot{z}_i,\ i = 1, 2.$$

The closed-loop system (nonlinearities included) can be written as:

$$\ddot{\theta}_1 = v_1 - 2\omega_n (1 - \zeta)\, \dot{z}_1, \tag{5.43}$$

$$\ddot{\theta}_2 = v_2 - 2\omega_n (1 - \zeta)\, \dot{z}_2, \tag{5.44}$$

$$\ddot{q} = -2\zeta\omega_n \dot{q} - \omega_n^2 q + \beta_1 \dot{\theta}_1^2 + \beta_2 \dot{\theta}_2^2 + \beta_3 \dot{q}\dot{\theta}_1 + \sum_{i=1}^{2} \alpha_i \left[v_i - 2\omega_n (1 - \zeta)\, \dot{z}_i \right], \tag{5.45}$$

$$\ddot{z}_1 = v_1 - 2\omega_n \dot{z}_1 - \omega_n^2 z_1, \tag{5.46}$$

$$\ddot{z}_2 = v_2 - 2\omega_n \dot{z}_2 - \omega_n^2 z_2, \tag{5.47}$$

where v_i are given by (5.41) and (5.42).

Simulations

The effectiveness of the proposed control algorithm is demonstrated in this section via a simulation. Specifically, the physical parameters used in the simulation are given in the following table (Quanser.com).

Table 5.2: Physical parameters of the two-torque hybrid robot manipulator.

Parameter	Value
ρ_1	0.7597 kg/m
l_0	0.06465 m
$l_1 = l_2$	0.22 m
m_{H_2}	0.593 kg
m_{b_2}	0.4036 kg
m_{l_2}	0.0586 kg
EI_1	2.69 Nm^2
I_{z_1}	7.424×10^{-4} kg m^2
I_{z_2}	4.456×10^{-4} kg m^2

The selected control gains for the nonlinear PD controller are selected to be

$$a_i = b_i = 1/3,\ i = 1, 2.$$

The following plots represent the closed-loop system behavior corresponding to initial conditions given by

$$(\theta_{10}, \theta_{20}) = (\pi/4, \pi/4) \text{ rad},\ \dot{\theta}_1 = \dot{\theta}_2 = q_0 = \dot{q}_0 = 0.$$

The states of the filters are initialized at zero, i.e., $z_{i0} = \dot{z}_{i0} = 0,\ i = 1, 2.$

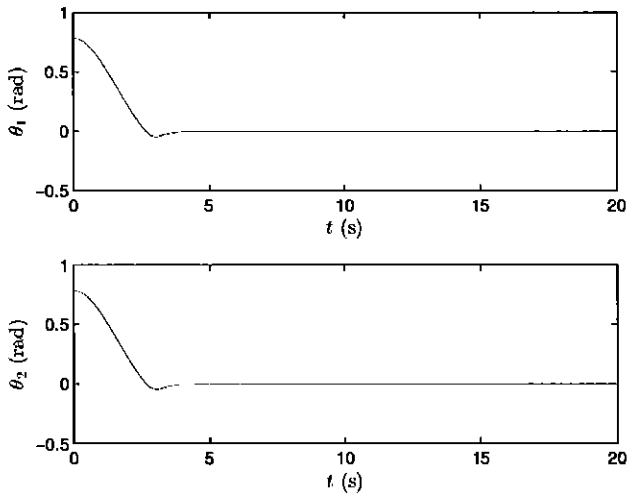

Figure 5.7: Angular position time behavior

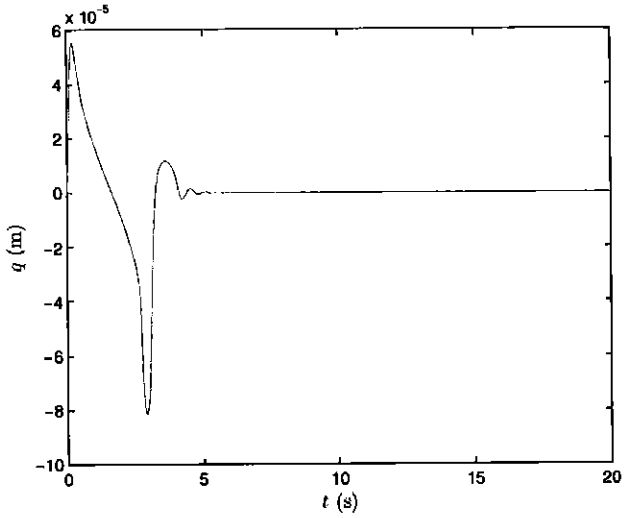

Figure 5.8: Vibration deflection time behavior.

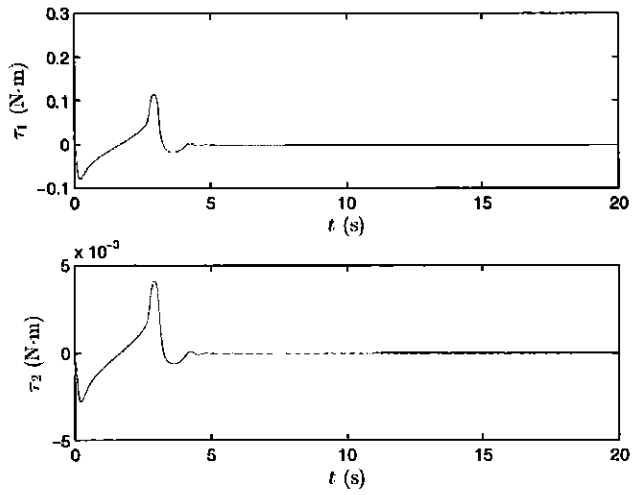

Figure 5.9: Torques for each hub.

The proposed finite-time control algorithm composed of nonlinear PD controller and notch filter successfully accomplishes the slew maneuver, reaching the origin within $5s$. The maximum torque required is less than $0.15Nm$, and thus can be easily accomplished by the simulated manipulator.

5.1.3 Finite-Time Control of a Compliant Base Robot Manipulator

The following has been published in Reyhanoglu and Hoffman (2017). A two-torque, two rigid member robotic manipulator is mounted to a translationally compliant

base, with the control objective of slew maneuvering. Similar to the previous section, a notch filter/nonlinear proportional-derivative (PD) controller combination is implemented to achieve finite-time convergence to the control objective.

Model Formulation

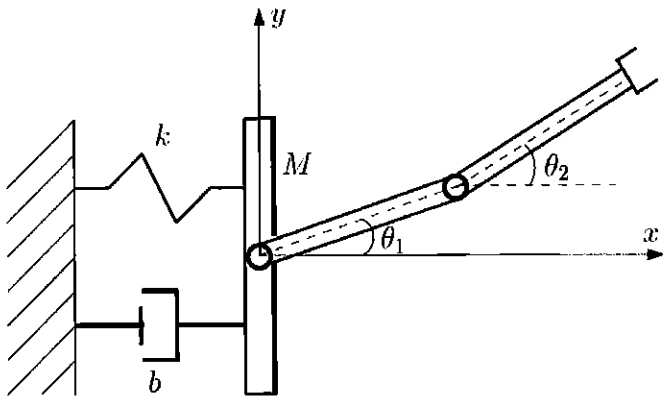

Figure 5.10: Schematic of the compliant base robotic manipulator.

The above figure provides a schematic model for a compliant base robot manipulator. The two rigid links that the manipulator is composed of observe lengths and masses $l_i, m_i, i = 1, 2$, which are joined together and to the base by the joint torque motors. The moment of inertia with respect to its center of mass is denoted as I_{z_i}. The compliant base will be given spring-mass-damper considerations, represented by mass M, spring constant k, and damping constant b. In the same spirit as the previous sections, an inertial frame xyz is established, with its origin located at the equilibrium

position such that deformation of the spring may be labeled as x. The control torques provided are applied from the attached links and are defined as τ_1 and τ_2. Angular positions of the links with respect to the x axis are given by θ_1 and θ_2.

To progress in the derivation, the following assumptions are made:

1. Motion is purely on horizontal plane,
2. Uniform beam behavior is expected of the links,
3. Coulomb friction and backlash are insignificant.

For the total potential energy, only the spring provides a term:

$$U = \frac{1}{2}kx^2. \tag{5.48}$$

Let $\vec{r}_1$ and and $\vec{r}_2$ represent the respective inertial position vectors of the links' center of masses, which can be written as:

$$\vec{r}_1 = (x + 0.5l_1c(\theta_1))\hat{i} + 0.5l_1s(\theta_1)\hat{j},$$
$$\vec{r}_2 = (x + l_1c(\theta_1) + 0.5l_2c(\theta_2))\hat{i} + (l_1s(\theta_1) + 0.5l_2s(\theta_2))\hat{j},$$

where the abbreviations $c(\cdot) = \cos(\cdot)$ and $s(\cdot) = \sin(\cdot)$ have been used. The total kinetic energy of the system can be expressed as:

$$T = \frac{1}{2}\left(M\dot{x}^2 + m_1\left\|\dot{\vec{r}}_1\right\|^2 + m_2\left\|\dot{\vec{r}}_2\right\|^2 + I_{z_1}\dot{\theta}_1^2 + I_{z_2}\dot{\theta}_2^2\right),$$

where

$$\left\|\dot{\vec{r}}_1\right\|^2 = \dot{x}^2 + \frac{1}{4}l_1^2\dot{\theta}_1^2 - l_1\dot{x}\dot{\theta}_1s(\theta_1),$$
$$\left\|\dot{\vec{r}}_2\right\|^2 = \dot{x}^2 + l_1^2\dot{\theta}_1^2 + \frac{1}{4}l_2^2\dot{\theta}_2^2 + l_1l_2\dot{\theta}_1\dot{\theta}_2c(\theta_2 - \theta_1) - \dot{x}\left(2l_1\dot{\theta}_1s(\theta_1) + l_2\dot{\theta}_2s(\theta_2)\right).$$

The non-conservative forces must be applied through the principle of virtual work:

$$\delta W = (\tau_1 - \tau_2)\delta\theta_1 + \tau_2\delta\theta_2 - b\dot{x}\delta x. \tag{5.49}$$

With all aspects assembled, Lagrange's equations of motion may be directly determined:

$$I_1\ddot{\theta}_1 + a_2 l_1 c(\theta_2 - \theta_1)\ddot{\theta}_2 - a_1 s(\theta_1)\ddot{x} - a_2 l_1 s(\theta_2 - \theta_1)\dot{\theta}_2^2 = \tau_1 - \tau_2, \tag{5.50}$$

$$a_2 l_1 c(\theta_2 - \theta_1)\ddot{\theta}_1 + I_2\ddot{\theta}_2 - a_2 s(\theta_2)\ddot{x} + a_2 l_1 s(\theta_2 - \theta_1)\dot{\theta}_1^2 = \tau_2, \tag{5.51}$$

$$m_t\ddot{x} + b\dot{x} + kx = \sum_{i=1}^{2} a_i \left(u_i s(\theta_i) + \dot{\theta}_i^2 c(\theta_i)\right), \tag{5.52}$$

where

$$I_1 = I_{z_1} + m_1\frac{l_1^2}{4} + m_2 l_1^2,$$

$$I_2 = I_{z_2} + m_2\frac{l_2^2}{4},$$

$$m_t = M + m_1 + m_2,$$

$$a_1 = (0.5m_1 + m_2)l_1,$$

$$a_2 = 0.5m_2 l_2.$$

Partial feedback linearization may be used once again to identify the angular accelerations as the control inputs:

$$\ddot{\theta}_1 = u_1, \tag{5.53}$$

$$\ddot{\theta}_2 = u_2, \tag{5.54}$$

$$\ddot{x} + 2\zeta\omega_n\dot{x} + \omega_n^2 x = \frac{1}{m_t}\sum_{i=1}^{2} a_i(u_i s(\theta_i) + \dot{\theta}_i^2 c(\theta_i)), \tag{5.55}$$

where

$$\omega_n = \sqrt{\frac{k}{m_t}}, \tag{5.56}$$

$$\zeta = \frac{b}{2\sqrt{km_t}}. \tag{5.57}$$

This transformation is in anticipation of the control design, and the actual torque actuation can be recovered through

$$\tau_1 = \bar{I}_1 u_1 + \bar{I}_2 u_2 - \bar{a}\ddot{x} + a_2 l_1 (\dot{\theta}_1^2 - \dot{\theta}_2^2) s(\theta_2 - \theta_1), \tag{5.58}$$

$$\tau_2 = (\bar{I}_1 - I_1) u_1 + I_2 u_2 - a_2 s(\theta_2)\ddot{x} + a_2 l_1 \dot{\theta}_1^2 s(\theta_2 - \theta_1), \tag{5.59}$$

where

$$\bar{I}_1 = I_1 + a_2 l_1 c(\theta_2 - \theta_1),$$

$$\bar{I}_2 = I_2 + a_2 l_1 c(\theta_2 - \theta_1),$$

$$\bar{a} = a_1 s(\theta_1) + a_2 s(\theta_2).$$

Filter and Controller Design

To avoid perturbation of the compliant base, the notch filter proposed will be identical in structure to the one shown in the previous section. In a similar fashion, $\omega_z = \omega_p = \omega_n$, $\zeta_z = \zeta$, and $\zeta_p = 1$. The general expression then becomes

$$\frac{u}{v} = \frac{s^2 + 2\zeta\omega_n s + \omega_n^2}{s^2 + 2\omega_n s + \omega_n^2}. \tag{5.60}$$

The simplified system can be represented by a block diagram, seen below. It

corresponds to the partially linearized equations

$$\ddot{\theta}_1 = u_1, \tag{5.61}$$

$$\ddot{\theta}_2 = u_2, \tag{5.62}$$

$$\ddot{x} + 2\zeta\omega_n\dot{x} + \omega_n^2 x = \sum_{i=1}^{2} a_i^s u_i, \tag{5.63}$$

where $a_i^s = \frac{a_i}{m_t}\theta_i,\ i = 1, 2.$

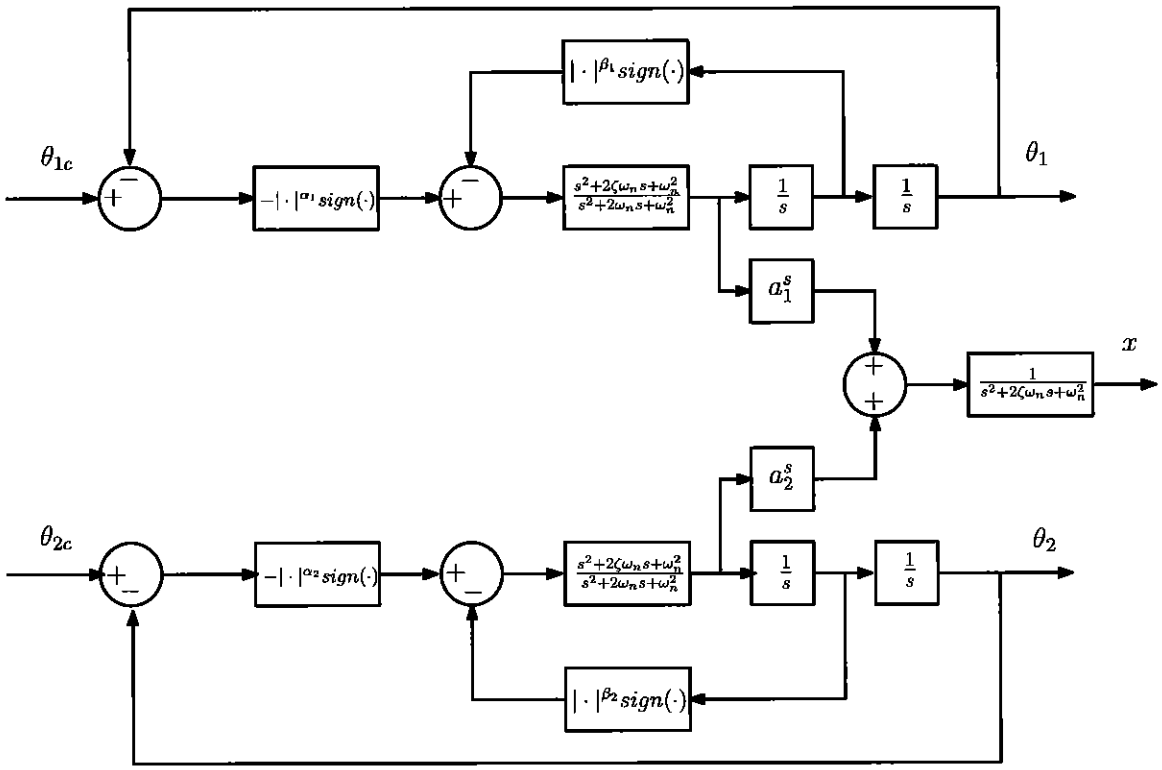

Figure 5.11: Block diagram representation of the simplified system.

Finite-time control inputs (prior to the filter) may be implemented in a similar

manner with the objective $\theta_{ic} = 0$ as follows.

$$v_i = -|\theta_i|^{\alpha_i}\text{sign}(\theta_i) - |\dot{\theta}_i|^{\beta_i}\text{sign}(\dot{\theta}_i), \tag{5.64}$$

with α_i, $\beta_i \in (0,\ 1)$, $\alpha_i > \beta_i/(2-\beta_i)$, $i = 1, 2$, are controller parameters. Note that generality is not lost here, as θ_i arguments may be replaced by $\theta_i - \theta_{ic}$ for any arbitrary command θ_{ic}. The feedback law seen thus brings the rigid links to $(\theta_1, \dot{\theta}_1, \theta_2, \dot{\theta}_2) = (0, 0, 0, 0)$ with finite-time control performance.

State-space representation of the notch filter dynamics is required. Here, auxiliary signals z_i will be defined as

$$\ddot{z}_i + 2\omega_n \dot{z}_i + \omega_n^2 z_i = v_i, \tag{5.65}$$

providing the transfer function between v_i and z_i as

$$\frac{z_i}{v_i} = \frac{1}{s^2 + 2\omega_n s + \omega_n^2}. \tag{5.66}$$

It then follows that the filter outputs u_i are represented as

$$u_i = \ddot{z}_i + 2\zeta\omega_n \dot{z}_i + \omega_n^2 z_i = v_i - 2\omega_n (1-\zeta)\, \dot{z}_i. \tag{5.67}$$

With the filter dynamics augmented, the full closed-loop system of equations (non-

linearities included), are shown below:

$$\ddot{\theta}_1 = v_1 - 2\omega_n(1-\zeta)\dot{z}_1, \tag{5.68}$$

$$\ddot{\theta}_2 = v_2 - 2\omega_n(1-\zeta)\dot{z}_2, \tag{5.69}$$

$$\ddot{x} = -2\zeta\omega_n\dot{x} - \omega_n^2 x + \sum_{i=1}^{2}\left(\frac{a_i s(\theta_i)}{m_t}u_i + \frac{a_i}{m_t}\dot{\theta}_i^2 c(\theta_i)\right), \tag{5.70}$$

$$\ddot{z}_1 = v_1 - 2\omega_n\dot{z}_1 - \omega_n^2 z_1, \tag{5.71}$$

$$\ddot{z}_2 = v_2 - 2\omega_n\dot{z}_2 - \omega_n^2 z_2, \tag{5.72}$$

with v_i previously defined by (5.64).

Simulations

Controller performance will be displayed in a similar manner, through a simulation-based compliant base robot manipulator with physical quantities shown in the table below.

Table 5.3: Physical parameters of the compliant base robot manipulator.

Parameter	Value
M	3.0 kg
m_1	0.4 kg
m_2	0.2 kg
$l_1 = l_2$	0.15 m
b	30 Ns/m
k	800 N/m
I_{z_1}	7.5×10^{-4} kg m^2
I_{z_2}	3.75×10^{-4} kg m^2

We implement the control algorithm with control parameters

$$\alpha_i = \beta_i = \frac{1}{3},\ i = 1, 2.$$

The following figures show the results of a simulation corresponding to the initial conditions

$$(\theta_{10}, \theta_{20}) = (\pi/3, \pi/3) \text{ rad}, \ \dot{\theta}_{10} = \dot{\theta}_{20} = x_0 = \dot{x}_0 = 0.$$

The states of the filters are initialized at zero, i.e.,

$$z_{i0} = \dot{z}_{i0} = 0, \ i = 1, 2.$$

It can be seen that the $\pi/3$ rad slewing of the links is achieved in around $5s$, avoiding residual vibrations in the process. An important note is the required control effort, u_1 and u_2, do not exceed 0.9 rad/s^2.

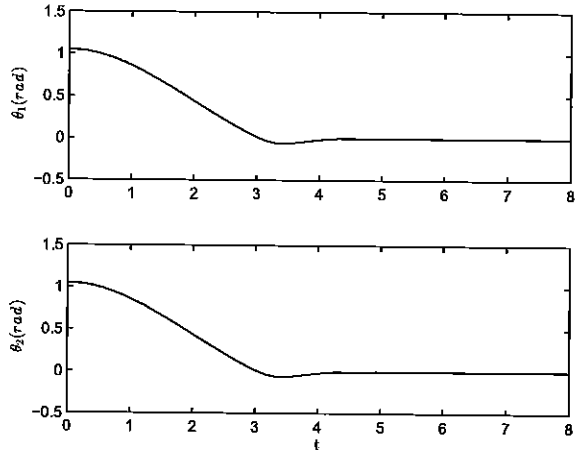

Figure 5.12: Time behavior of θ_i.

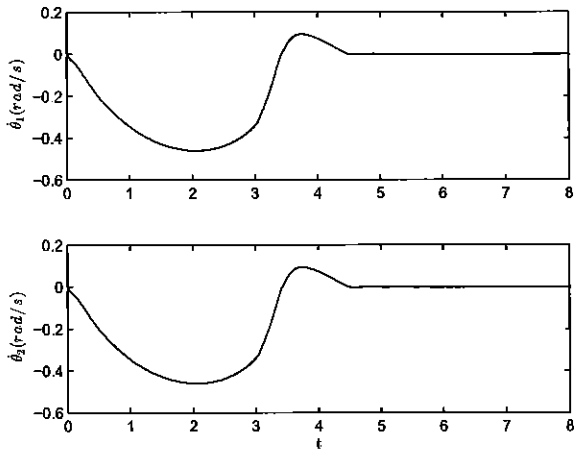

Figure 5.13: Time behavior of $\dot{\theta}_i$.

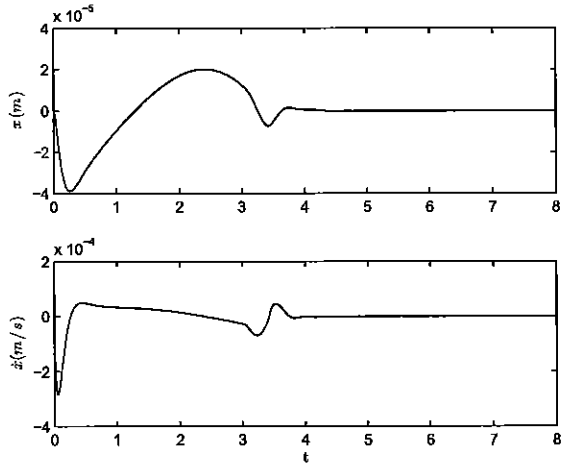

Figure 5.14: Time behavior of $x, \dot{x}$.

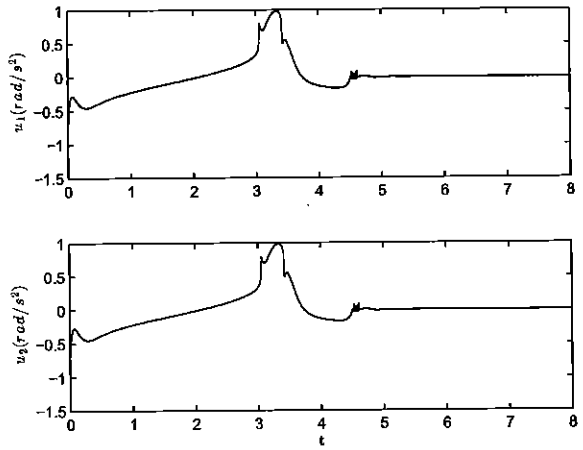

Figure 5.15: Time behavior of u_i.

5.2 Robust Quaternion-based Nonlinear Tracking Control of a Quadrotor Attitude Test Bed

Implementation of quadrotor unmanned aerial vehicles (UAVs) has seen growing intrigue in current research ventures. This is largely due to their increase in versatility along with a significant decrease in cost and implementation difficulty. Quadrotors may be used for various reconaissance missions, or for search and rescue operations where human life may be endangered. Equally of interest is their dynamical coupling, resulting in strong nonlinearity that exemplifies a noteworthy control challenge. It is therefore not surprising that many publications exist to address quadrotor control. Due to the numerous control objectives and model uncertainties however, a constant demand for mathematically rigorous control designs still exist. A need for controllers able to address system-inherent practical limitations is especially desired.

Many of the applications of quadrotor control inherently involve autonomous trajectory tracking. Some examples of published literature that address quadrotor track-

ing include (Choi and Ahn, 2015), (Faessler et al., 2017), (Fanni and Khalifa, 2017), (Ghomman and Saad, 2017), (Kayacan and Maslim, 2017), (Reinoso et al., 2016), (Yu and Ding, 2016), (Zhao et al, 2015), (Zuo, 2017), (Zuo, 2010). Aerial robotics in a complete experimental environment is seen in Fanni and Khalifa (2017), specifically highlighting new methods of identifying inverse kinematics. Fuzzy logic techniques are explored in Kayacan and Maslim (2017), through comparing the performances of type-1 and type-2 neural networks on a disturbance-plagued experimental quadrotor. The harrowing task of autonomous quadrotor landing upon a moving platform is outlined in Ghomman and Saad (2017), with solely relative position measurement feedback. This is achieved by dividing the task into phases, and done so with respect to a virtual target point and a safety radius sphere. The demands of practical implementation very frequently give rise to inventive approaches to quadrotor control design.

The presence of uncertainties in real-world applications demands control law designs to account for and suppress them. Such designs are referred to as robust. Robust control laws are elaborated on in (Chen et al., 2016), (Islam et al., 2015), (Lee, 2013), (Liu et al., 2017a), (Liu et al., 2017b), (Ma et al., 2016), (Mebarki et al., 2015), (Ortiz et al., 2016), (Ryan and Kim, 2013), (Satici et al., 2013), although more literature exists. Making use of the sliding mode control (SMC) property of disturbance rejection, Chen et al. (2016) applies a combination of such and a backstepping-based algorithm to produce quadrotor position tracking. By regarding system dynamics in the special orthogonal group in three dimensions (i.e., $SO(3)$), Lee (2013) uses global coordinates to attain robust attitude tracking for a quadrotor. Both actuation time delay and model uncertainty are addressed in Liu et al. (2017a), Liu et al. (2017b), in light of the behavior of digital components. To avoid GPS measurements, Mebarki et al. (2015) applies visual targeting for a UAV to estimate translational velocity mea-

surements. In spite of the multitude of previous publications, the varied nature of system disturbances and uncertainty provides still-open avenues of research potential.

The goal of the following section is the development and implementation of a robust nonlinear attitude tracking controller designed for the suppression of uncertainties affecting a 3-DOF experimental quadrotor hover system test bed. The analysis includes both rigorous dynamic and stability formulation and a formal consideration of the test bed actuators' input voltage constraints. It will be shown that the proposed control algorithm compensates for input-multiplicative parametric uncertainty intrinsic to the dynamic model, the result of unknown drag and friction multipliers in the propeller dynamics. Feed-forward constant estimates of the aforementioned uncertainty will be used to circumvent computational burden inherent with adaptive control laws. In the same spirit, the traditional sliding mode observer will be replaced with a bank of dynamic filters for the purpose of velocity estimate provisions for the control law. Thus, only position measurements will be required. Asymptotic trajectory tracking will be proved through a rigorous Lyapunov stability analysis. Particularly, the sufficient conditions on control gain selection will be identified to obtain uncertainty compensation. Simulation results are provided to demonstrate the performance of the proposed control system, and experimental results are also provided to demonstrate the performance of the attitude control law on the Quanser 3-DOF hover system test bed.

5.2.1 Dynamic Model Formulation

For a standard quadrotor, the Euler's equations for rigid-body rotation noted in Hughes (1994) may be used:

$$J\dot{\omega} = -\omega^{\times} J\omega + \tau. \tag{5.73}$$

In (5.73), $J \in \mathbb{R}^{3\times3}$ represents the positive-definite, symmetric inertia matrix, and $\omega(t) \triangleq \left[\begin{array}{ccc} \omega_x(t) & \omega_y(t) & \omega_z(t) \end{array}\right]^T \in \mathbb{R}^3$ is the angular velocity of the quadrotor body-fixed frame with respect to an inertial frame. Also in (5.73), $\zeta^\times$, $\forall\, \zeta \in \mathbb{R}^3$, expresses the standard skew-symmetric matrix equivalent to the vector cross-product operation, and $\tau(t) \triangleq \left[\begin{array}{ccc} \tau_x(t) & \tau_y(t) & \tau_z(t) \end{array}\right]^T \in \mathbb{R}^3$ is the generalized torque.

Uncertain Electromechanical Actuator Model

The generalized torque $\tau(t)$ is the result of combined propeller forces F_i, for $i = 1, ..., 4$. These forces are, in turn, generated by the input voltages V_i, for $i = 1, ..., 4$, applied to the propellers. It can therefore be said that the generalized torque can be expressed in terms of the input voltages as

$$\tau \triangleq \left[\begin{array}{c} \tau_x(t) \\ \tau_y(t) \\ \tau_z(t) \end{array}\right] = \left[\begin{array}{c} blK_v^2\left(V_4^2 - V_2^2\right) + J_r\omega_y\Omega_r \\ blK_v^2\left(V_3^2 - V_1^2\right) - J_r\omega_x\Omega_r \\ dK_v^2\left(V_1^2 - V_2^2 + V_3^2 - V_4^2\right) \end{array}\right] \tag{5.74}$$

where $\Omega_r = K_v\left(V_1 - V_2 + V_3 - V_4\right)$ denotes the overall residual angular speed of the propellers. The gyroscopic terms containing Ω_r in (5.74) are treated as disturbances in the dynamic model, and are to be compensated for in the subsequent analysis. In (5.74), $b, d \in \mathbb{R}^+$ denote uncertain thrust and drag coefficients; $l \in \mathbb{R}^+$ is the uncertain distance from the pivot to the motor, $K_v \in \mathbb{R}^+$ denotes an uncertain voltage transformation constant; and $J_r \in \mathbb{R}^+$ is the uncertain rotor inertia ((Damen et al., 2016)).

In light of the parametric uncertainty in the torque model in (5.74), an auxiliary

(virtual) voltage control signal $u(t) \in \mathbb{R}^3$ is defined via the parameterization

$$Bu = \begin{bmatrix} blK_v^2 (V_4^2 - V_2^2) \\ blK_v^2 (V_3^2 - V_1^2) \\ dK_v^2 (V_1^2 - V_2^2 + V_3^2 - V_4^2) \end{bmatrix}. \tag{5.75}$$

In (5.75), the uncertain matrix $B \in \mathbb{R}^{3\times3}$ and the virtual control input $u(t) \triangleq [u_1(t), u_2(t), u_3(t)]^T$ are explicitly defined as

$$B \triangleq \begin{bmatrix} blK_v^2 & 0 & 0 \\ 0 & blK_v^2 & 0 \\ 0 & 0 & dK_v^2 \end{bmatrix} \tag{5.76}$$

and

$$u = \begin{bmatrix} u_1 \\ u_2 \\ u_3 \end{bmatrix} = \begin{bmatrix} V_4^2 - V_2^2 \\ V_3^2 - V_1^2 \\ V_1^2 - V_2^2 + V_3^2 - V_4^2 \end{bmatrix}. \tag{5.77}$$

Remark 1. ***(Consideration of Voltage Constraints)*** *The establishment of the virtual control input $u(t)$ in (5.75) and (5.77) is done in foresight of the subsequent control design. In the steps to follow, the control law will be designed in terms of the virtual inputs $u_i(t)$, for $i = 1, 2, 3$; and in simulation and experimental implementation, the virtual inputs are transformed to non-negative input voltages by solving (5.77) for $V_i^2(t)$, for $i = 1, ..., 4$. It can be shown that the solution guarantees that the voltage inputs adhere to the constraints $V_i(t) \geq V_b$, for $i = 1, ..., 4$, where $V_b \in \mathbb{R}^+$ represents a bias voltage. Details on this proof are provided in Damen et al. (2016) and are omitted here for brevity.*

5.2.2 Kinematic Model Formulation

The hover system's rotational kinematics can be expressed in terms of standard quaternion notation seen in Hughes (1994):

$$\dot{q}_v = \frac{1}{2}(q_v^{\times}\omega + q_s\omega), \tag{5.78}$$

$$\dot{q}_s = -\frac{1}{2}q_v^T\omega, \tag{5.79}$$

where $q_v(t) \in \mathbb{R}^3$ and $q_s(t) \in \mathbb{R}$ represent the respective vector and scalar components. The quaternion vector observes the compact form $q(t) \triangleq \{q_v(t), q_s(t)\} \in \mathbb{R}^3 \times \mathbb{R}$, along with the constraint

$$q_v^T q_v + q_s^2 = 1.$$

The desired unit quaternion $q_d(t) \triangleq \{q_{vd}(t), q_{sd}(t)\} \in \mathbb{R}^3 \times \mathbb{R}$ represents the orientation of the desired body-fixed frame with respect to the fixed inertial frame. Standard quaternion kinematics can be used to show that rotation matrices $R(q_v, q_s) \in SO(3)$ and $R_d(q_{vd}, q_{sd}) \in SO(3)$ can be established to bring the inertial frame to the actual and desired frames, respectively.

5.2.3 Control Objective

The control objective can be defined as having the test bed's actual body-fixed frame track the desired frame. This objective can be mathematically defined through a rotational error matrix $\tilde{R}(e_v, e_s) \in \mathbb{R}^{3\times3}$, defined as

$$\tilde{R} \triangleq RR_d^T = (e_s^2 - e_v^T e_v)I_3 + 2e_v e_v^T - 2e_s e_v^{\times}, \tag{5.80}$$

where $e(t) \triangleq \{e_v(t), e_s(t)\} \in \mathbb{R}^3 \times \mathbb{R}$ is the quaternion error, and I_3 denotes the 3×3 identity matrix. Physically, the rotation matrix $\tilde{R}(e_v, e_s)$ represents the rotation that brings the desired body-fixed frame to the actual frame. In turn an angular velocity error between the actual and desired frames viewed in the actual body-fixed frame can be obtained as

$$\tilde{\omega} = \omega - \tilde{R}\omega_d. \tag{5.81}$$

In foresight of the stability analysis, the auxiliary error signal $r(t) \in \mathbb{R}^3$ is defined as

$$r \triangleq \tilde{\omega} + 2\alpha e_v + e_f, \tag{5.82}$$

where $\alpha \in \mathbb{R}^+$ is a constant control gain, and $e_f(t) \in \mathbb{R}^3$ is an auxiliary error signal to be defined during the bank of dynamic filters. Note that (5.82) can be used to express the angular velocity error as

$$\tilde{\omega} = r - 2\alpha e_v - e_f. \tag{5.83}$$

By using (5.81), the quaternion error kinematics can be expressed as

$$\dot{e}_v = \frac{1}{2} W(e)\, \tilde{\omega}, \tag{5.84}$$

$$\dot{e}_s = -\frac{1}{2} e_v^T \tilde{\omega}, \tag{5.85}$$

where the auxiliary matrix $W(e) \in \mathbb{R}^{3\times 3}$ is defined as

$$W(e) = e_v^{\times} + e_s I_3. \tag{5.86}$$

With the assembled error definitions, it can be seen that the quaternion error satisfies

$$e_v^T e_v + e_s^2 = 1. \tag{5.87}$$

Based on (5.80) and (5.87), the control objective can be stated mathematically as $\|e_v(t)\| \to 0$, which in turn implies that $\tilde{R}(e_v, e_s) \to I_3$.

Assumption 1: Throughout the following error dynamics derivations and stability analysis, it is assumed that the desired trajectory is bounded in the sense that $\omega_d(t)$, $\dot{\omega}_d(t) \in \mathcal{L}_\infty$ and $q_d(t)$, $\dot{q}_d(t)$, $\ddot{q}_d(t) \in \mathcal{L}_\infty$ throughout closed-loop controller operation.

5.2.4 Control Development

The development of the error dynamics and premises leading to the robust control design are discussed in detail here. The goal is to obtain a robust control law that is proven to achieve attitude tracking for the given physical system in spite of input-multiplicative parametric uncertainty, unmodeled dynamics, and control voltage input constraints. Under the practical assumption that only angular position measurements are reliable for output feedback, an innovative error and stability analysis is used with the implementation of a bank of dynamic filters.

Open-Loop Error Dynamics

The previously-seen auxiliary error signal $e_f(t)$ introduced in (5.82) is an output of a bank of dynamic filters defined as (Xian et al., 2004)

$$\dot{p} = -(k+2\alpha)p - \eta + 2(k+\alpha)^2 e_v + e_v, \tag{5.88}$$

$$\dot{\eta} = p - \alpha\eta - 2(k+\alpha)e_v, \tag{5.89}$$

$$e_f = p - 2(k+\alpha)e_v. \tag{5.90}$$

In (5.88) - (5.90), k, $\alpha \in \mathbb{R}^{3\times3}$ denote constant, diagonal, positive definite control gain matrices; $\eta(t) \in \mathbb{R}^3$ denotes another output of the filter; and $p(t) \in \mathbb{R}^3$ is an internal filter variable.

After taking the time derivative of (5.90) and using (5.83), (5.84), and (5.88), $\dot{e}_f(t)$ can be expressed as

$$\dot{e}_f = -\alpha e_f - \eta + e_v - (k+\alpha)r - (k+\alpha)\Delta(e)\tilde{\omega}, \tag{5.91}$$

where $\Delta(e) \in \mathbb{R}^{3\times3}$ is defined as

$$\Delta(e) = W(e) - I_3. \tag{5.92}$$

The expression in (5.91) will be used in the stability analysis to follow.

Assumption 2: It is assumed that the matrix mismatch term $\Delta(e)$ is bounded by

$$\|\Delta(e)\|_{i\infty} \leq \varepsilon < 1, \tag{5.93}$$

where $\varepsilon \in \mathbb{R}^+$ is a known bounding constant, and $\|\cdot\|_{i\infty}$ represents the induced infinity norm of a matrix. The bounding condition in (5.93) can be interpreted as a limit

on the region of convergence of the proposed control law. Essentially, this bounding presents itself as control design trade-off that is required to prove asymptotic attitude regulation in the presence of the input-multiplicative parametric uncertainty that plagues the hover system test bed. The provided results show that Assumption 2 is mild in the sense that the proposed control law achieves asymptotic attitude tracking over a wide operational range.

Taking the time derivative of $r(t)$ in (5.82) and premultiplying the result by J, provides the open-loop error dynamics as

$$J\dot{r} = J\dot{\omega} + J\tilde{\omega}^{\times}\tilde{R}\omega_d - J\tilde{R}\dot{\omega}_d + 2J\alpha\dot{e}_v + \dot{e}_f, \tag{5.94}$$

where the fact that $\dot{\tilde{R}} = -\tilde{\omega}^{\times}\tilde{R}$ was utilized. By substituting the original dynamics into (5.94), the open-loop system can be expressed as

$$\begin{aligned} J\dot{r} &= -\omega^{\times}J\omega + Bu + J\tilde{\omega}^{\times}\tilde{R}\omega_d - J\tilde{R}\dot{\omega}_d + J\alpha W(e)\tilde{\omega} - \alpha e_f \\ &\quad -\eta + e_v - (k+\alpha)r - (k+\alpha)\Delta(e)\tilde{\omega} + \chi(\omega), \end{aligned} \tag{5.95}$$

where (5.74), (5.75), (5.84), and (5.91) were utilized. In (5.95), the auxiliary term $\chi(\omega) \in \mathbb{R}^3$ represents the gyroscopic terms

$$\chi(\omega) \triangleq \begin{bmatrix} J_r\omega_y\Omega_r \\ -J_r\omega_x\Omega_r \\ 0 \end{bmatrix}. \tag{5.96}$$

For the purpose of more straightforward stability analysis, the open-loop error system

(5.95) is rewritten as

$$J\dot{r} = \tilde{N} + Bu + \Lambda\alpha e_f - \Lambda e_v - (k+\alpha) r, \tag{5.97}$$

where $\Lambda \in \mathbb{R}^{3\times3}$ is a subsequently defined uncertain auxiliary matrix, and the unmeasurable auxiliary term $\tilde{N}(t) \in \mathbb{R}^3$ is explicitly defined as

$$\begin{aligned} \tilde{N} \triangleq\ & -\omega^{\times} J\omega + J\tilde{\omega}^{\times}\tilde{R}\omega_d - J\tilde{R}\dot{\omega}_d + J\alpha W(e)\tilde{\omega} \\ & - (\Lambda+\alpha) e_f - \eta + e_v + \Lambda e_v - (k+\alpha)\Delta(e)\tilde{\omega} + \chi(\omega). \end{aligned} \tag{5.98}$$

The motivation for the grouping of terms in (5.98) is based on the subsequent stability analysis and in light of the upper bound

$$\left\|\tilde{N}\right\| \leq \rho(\|z\|)\|z\|, \tag{5.99}$$

where $\rho(\cdot) \in \mathbb{R}$ is a positive, globally invertible nondecreasing function; and $z(t) \in \mathbb{R}^{12}$ is defined as

$$z(t) \triangleq \left[\begin{array}{cccc} e_v^T(t) & e_f^T(t) & r^T(t) & \eta^T(t) \end{array}\right]^T. \tag{5.100}$$

Closed-Loop Error System

Following the derivation for the open-loop error system, and in foresight of the stability analysis to follow, the control input $u(t)$ is designed as

$$u(t) = \hat{B}^{-1}(ke_f(t)), \tag{5.101}$$

where k is a control gain introduced in (5.88) - (5.90). In (5.101), $\hat{B} \in \mathbb{R}^{3\times3}$ is a feedforward matrix containing constant, 'best guess' estimates $\hat{b}$, $\hat{d}$, $\hat{l}$, $\hat{K}_v \in \mathbb{R}^+$ of the

uncertain parameters b, d, l, K_v in (5.75). It is therefore prudent to define $\hat{B}$ as

$$\hat{B} \triangleq \begin{bmatrix} \hat{b}\hat{l}\hat{K}_v^2 & 0 & 0 \\ 0 & \hat{b}\hat{l}\hat{K}_v^2 & 0 \\ 0 & 0 & \hat{d}\hat{K}_v^2 \end{bmatrix}. \tag{5.102}$$

After substituting (5.101) into (5.97), the closed-loop error system is obtained:

$$J\dot{r} = \tilde{N} + \Lambda\left(ke_f\right) + \Lambda\alpha e_f - \Lambda e_v - \left(k+\alpha\right)r, \tag{5.103}$$

where the uncertain constant mismatch matrix $\Lambda \in \mathbb{R}^{3\times 3}$ is defined as

$$\Lambda \triangleq B\hat{B}^{-1}. \tag{5.104}$$

Property 1: The establishment of Λ as positive definite and symmetric allows for the consideration of the inverse Λ^{-1} being also positive definite and symmetric. This property will be critical in the subsequent stability analysis.

Remark 2. ***(Constant Estimates Application)*** *The use of constant parameter estimates in the control law (5.101) is done with the desire to reduce the computational burden in the closed-loop system. The simulation and experimental results demonstrate that the proposed control law achieves reliable attitude control under significant parametric uncertainty.*

By leveraging Property 1, the closed-loop error system in (5.103) can be rewritten as

$$\Lambda^{-1}J\dot{r} = \tilde{N}_1 + \left(k+\alpha\right)e_f - e_v - \Lambda^{-1}\left(k+\alpha\right)r, \tag{5.105}$$

where $\tilde{N}_1 \in \mathbb{R}^3$ is defined as

$$\tilde{N}_1 \triangleq \Lambda^{-1}\tilde{N}. \tag{5.106}$$

Based on Property 1 and Inequality (5.99), the auxiliary term $\tilde{N}_1(t)$ can be bounded as

$$\left\|\tilde{N}_1\right\| \leq \rho_1(\|z\|)\|z\|, \tag{5.107}$$

where $\rho_1(\cdot) \in \mathbb{R}$ is a positive, globally invertible nondecreasing function.

5.2.5 Stability Analysis

Consider the nonnegative Lyapunov candidate function $V(t)$ defined as

$$V = e_v^T e_v + (1-e_s)^2 + \frac{1}{2}e_f^T e_f + \frac{1}{2}r^T\Lambda^{-1}Jr + \frac{1}{2}\eta^T\eta. \tag{5.108}$$

After taking the time derivative of (5.108) and utilizing (5.84), (5.85), (5.89), (5.91), and (5.105) and canceling common terms, $\dot{V}(t)$ can be upper bounded as

$$\dot{V} \leq -\lambda_\alpha\|z\|^2 + \varepsilon(\lambda_k+\lambda_\alpha)\|z\|^2 - \lambda_{\Lambda k}\left(\|r\|^2 - \frac{\rho_1(\|z\|)}{\lambda_{\Lambda k}}\|z\|\|r\|\right),$$

where Inequality (5.93) of Assumption 2 was utilized. In (5.2.5), $\lambda_\alpha \triangleq \lambda_{\min}(\alpha)$, $\lambda_k \triangleq \lambda_{\min}(k)$, and $\lambda_{\Lambda k} \triangleq \lambda_{\min}(\Lambda^{-1}k)$, with $\lambda_{\min}(\cdot)$ denoting the minimum eigenvalue of the argument. After completing the squares in the parenthetic terms in (5.2.5), the upper bound in (5.2.5) can be expressed as

$$\dot{V} \leq -\left(\lambda_\alpha - \left(\frac{\rho_1^2(\|z\|)}{4\lambda_{\Lambda k}} + \varepsilon(\lambda_k+\lambda_\alpha)\right)\right)\|z\|^2. \tag{5.109}$$

Inequality (5.109) can be expressed as

$$\dot{V} \leq -c_0\|z\|^2, \tag{5.110}$$

where $c_0 \in \mathbb{R}^+$ denotes a bounding constant that is defined over the domain $\mathcal{D}$ given by

$$\mathcal{D} \triangleq \left\{ z \in \mathbb{R}^{12} : \|z\| < \rho_1^{-1} \left(\sqrt{4\lambda_{\Lambda k}\lambda_\alpha - \varepsilon\left(\lambda_k + \lambda_\alpha\right)} \right) \right\}. \tag{5.111}$$

The existence of the region of convergence can be ensured so long as the control gain matrices k and α are selected to satisfy the sufficient condition

$$\lambda_{\min}\left(\Lambda^{-1}k\right) \frac{\lambda_{\min}(\alpha)}{\lambda_{\max}(k) + \lambda_{\max}(\alpha)} > \frac{\varepsilon}{4}, \tag{5.112}$$

where Λ is introduced in (5.104), and ε is introduced in (5.93). The control gain matrices k and α can be selected to satisfy the sufficient condition in (5.112), provided Assumption 2 is satisfied.

Remark 4. ***(Sufficient Gain Conditions Under Uncertainty)*** *The expression in (5.112) can be viewed as the maximum discrepancy between actual and estimated input gain matrices B and $\hat{B}$ that can be allowed for the proposed closed-loop system to achieve asymptotic attitude tracking. It should be noted that Inequality (5.112) represents a* sufficient, not necessary, *condition. The subsequent simulation and experimental results demonstrate that the closed-loop system achieves asymptotic attitude tracking in the presence of significant input-multiplicative parametric uncertainty.*

Based on (5.108) and (5.110), it follows that $z(t) \in \mathcal{L}_\infty$ in $\mathcal{D}$, hence $e_v(t)$, $e_s(t)$, $e_f(t)$, $r(t)$, $\eta(t) \in \mathcal{L}_\infty$ in $\mathcal{D}$. Given that $r(t)$, $e_v(t)$, $e_f(t) \in \mathcal{L}_\infty$, (5.83) can be used to prove that $\tilde{\omega}(t) \in \mathcal{L}_\infty$ in $\mathcal{D}$; and Assumption 1 can be used along with (5.81) to conclude $\omega(t) \in \mathcal{L}_\infty$ in $\mathcal{D}$. Since $\tilde{\omega}(t)$, $e_v(t)$, $e_s(t) \in \mathcal{L}_\infty$, Equations (5.84) and (5.85) can be used to show that $\dot{e}_v(t)$, $\dot{e}_s(t) \in \mathcal{L}_\infty$ in $\mathcal{D}$. Given that $e_v(t)$, $e_f(t)$, $r(t)$, $\tilde{\omega}(t) \in \mathcal{L}_\infty$, (5.91) can be used to show that $\dot{e}_f(t) \in \mathcal{L}_\infty$ in $\mathcal{D}$. Since $\eta(t)$, $e_v(t) \in \mathcal{L}_\infty$, Theorem 1.1 of (Dawson et al., 1995) can be used with (5.88) to prove

that $p(t)$, $\dot{p}(t) \in \mathcal{L}_\infty$ in $\mathcal{D}$. Given that $p(t)$, $\eta(t)$, $e_v(t) \in \mathcal{L}_\infty$, it follows from (5.89) that $\dot{\eta}(t) \in \mathcal{L}_\infty$ in $\mathcal{D}$. Since $e_f(t) \in \mathcal{L}_\infty$, (5.101) can be used to show that the control input $u(t) \in \mathcal{L}_\infty$ in $\mathcal{D}$. Given that $e_v(t)$, $e_s(t)$, $e_f(t)$, $r(t)$, $\eta(t)$, $\omega(t)$, $\tilde{\omega}(t)$, $u(t) \in \mathcal{L}_\infty$, the expressions in (5.95) and (5.96) can be utilized along with Assumption 1 to show that $\dot{r}(t) \in \mathcal{L}_\infty$ in $\mathcal{D}$. Since $\dot{e}_v(t)$, $\dot{e}_f(t)$, $\dot{r}(t)$, $\dot{\eta}(t) \in \mathcal{L}_\infty$, the definition in (5.100) can be used to show that $\dot{z}(t) \in \mathcal{L}_\infty$ in $\mathcal{D}$; hence, $z(t)$ is uniformly continuous in $\mathcal{D}$. The expressions in (5.108) and (5.110) can then be used to prove that $z(t) \in \mathcal{L}_\infty \cap \mathcal{L}_2$ in $\mathcal{D}$. Barbalat's lemma (seen in Khalil (1996)) can now be invoked to prove that

$$\|z(t)\|^2 \to 0 \qquad \text{as} \qquad t \to \infty \qquad \forall\, z(0) \in \mathcal{D}. \tag{5.113}$$

Hence, (5.113) can be used along with (5.100) to prove that

$$\|e_v(t)\| \to 0 \qquad \text{as} \qquad t \to \infty \qquad \forall\, z(0) \in \mathcal{D}. \tag{5.114}$$

Due to the region of convergence's dependence on the initial conditions, it follows that the result is locally asymptotically stable (LAS), where the radius of convergence has been shown to depend on the degree of parametric uncertainty in the input gain matrix B (see (5.111)).

5.2.6 Numerical Simulation Results

The derived robust control law is demonstrated in the following simulation. The original dynamics are applied with the nominal values that construct B, but are in no way used by the control law. Both nominal and best guess estimate values are provided in the following table.

Table 5.4: Physical parameters of the quadrotor attitude test bed.

Parameter		Value
Thrust Coef. *Nominal*	b	$3.935 \times 10^{-6}\ \frac{N}{V}$
Estimate	$\hat{b}$	$4.317 \times 10^{-5}\ \frac{N}{V}$
Drag Coef. *Nominal*	d	$1.193 \times 10^{-7}\ \frac{Nm}{V}$
Estimate	$\hat{d}$	$3.054 \times 10^{-6}\ \frac{Nm}{V}$
Trans. Const. *Nominal*	K_v	$54.945\ \frac{rad}{sV}$
Estimate	$\hat{K}_v$	$34.341\ \frac{rad}{sV}$
Pivot to Motor *Nominal*	l	$0.197\ m$
Estimate	$\hat{l}$	$0.276\ m$

Dynamical insight was applied for judgment of the provided estimates. The simulation results presented here were obtained using control gains selected as

$$\alpha = diag\{2.7, 3, 3\},\ k = diag\{4.2, 0.7, 0.7\}.$$

In order to clearly show the wide range of allowable initial conditions provided by the feed-forward estimate paradigm, a Monte Carlo-esque simulation scheme is provided, that investigates a family of initial angle conditions spanning from 5 to 25 degrees for all three Euler angles. The remaining initial conditions of angular velocities and filter starting points were set to 0. Two separate goals of roll $\phi(t)$ and pitch $\theta(t)$ tracking of a desired sinusoidal trajectory (i.e., $\phi_d(t)$ and $\theta_d(t)$) were demonstrated, where the desired trajectory is defined as

$$\phi_d(t) = \theta_d(t) = 10\sin(0.5t). \tag{5.115}$$

The desired trajectory in (5.115) is expressed in degrees for convenience, and the desired yaw angle is set to 0, with the remaining Euler angle in both cases following a step command of 10 degrees, without loss of generality. In order to demonstrate

a realistic scenario, a 10 percent noise factor was added to the quaternion position measurement. The results of the control algorithm described can be seen in the following figures.

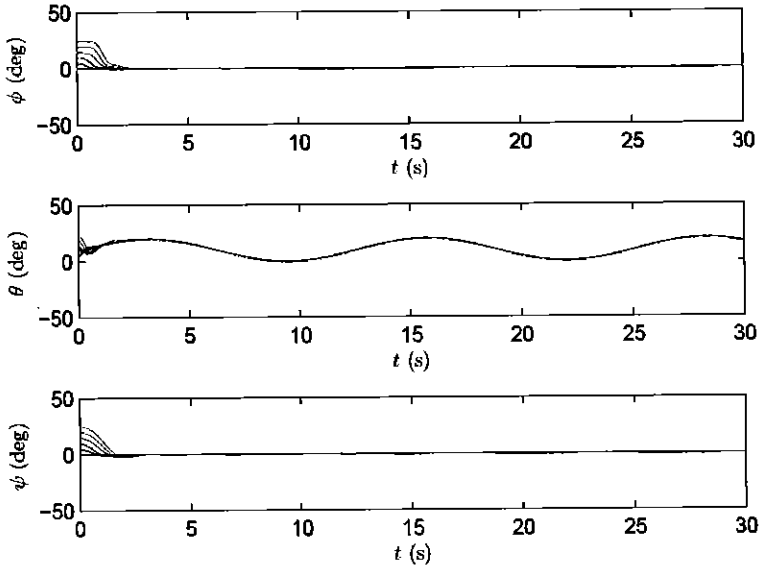

Figure 5.16: Angular position behavior of pitch tracking.

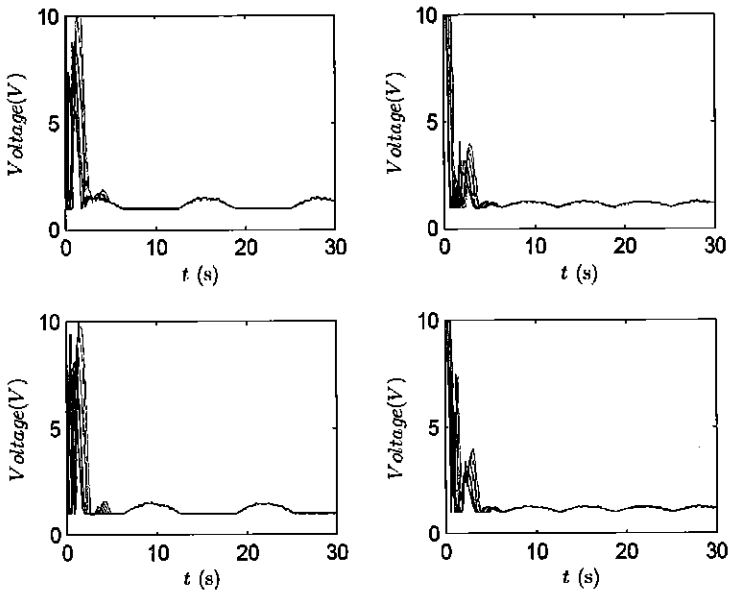

Figure 5.17: Voltage requirements of pitch tracking.

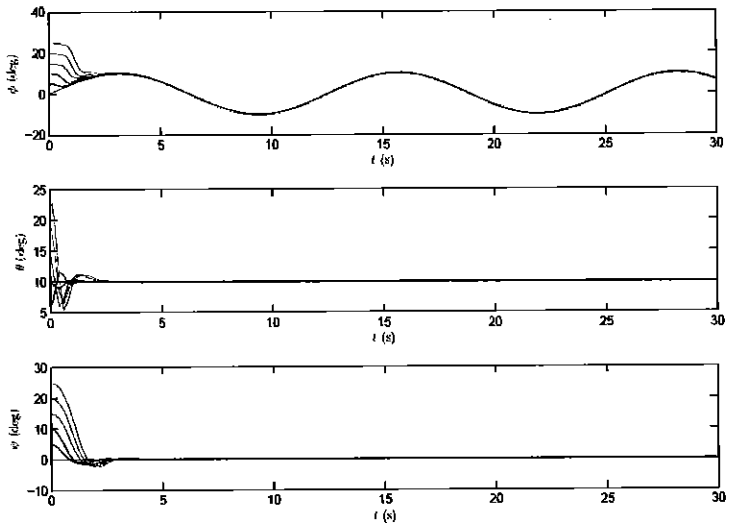

Figure 5.18: Angular position behavior of roll tracking.

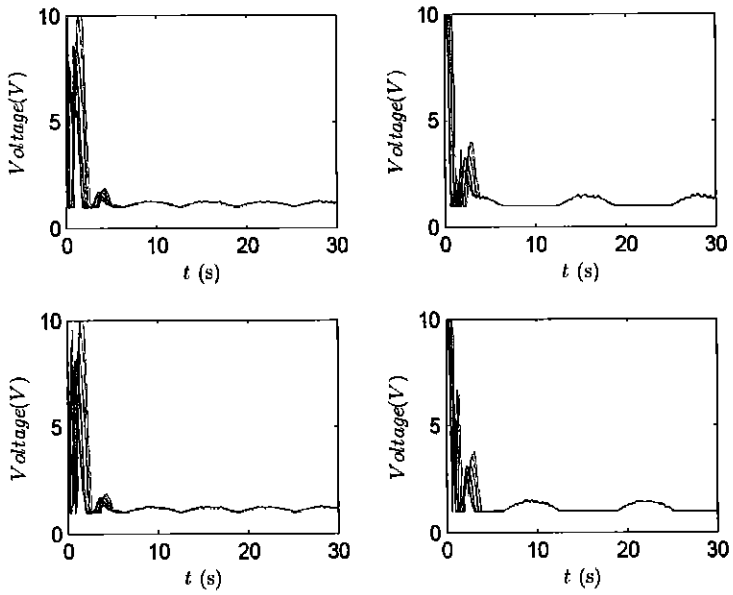

Figure 5.19: Voltage requirements of roll tracking.

Attitude tracking is clearly obtained within 4s for the provided range of initial angular positions, while the corresponding voltage plots prove that the saturation voltage constraint is respected, given the absence of control saturation.

5.2.7 Experimental Results

Further insight into the performance of the control law proposed is its application on the Quanser 3-DOF hover system test bed. Composed of a quadrotor helicopter system mounted at the center of gravity to an air bearing joint, the attitude behavior

of the quadrotor can be observed. The same setup as seen in the simulation is applied, to include the best guess estimates in the prior table, and the same control gains. The objective of the experiment is identical to the simulation, observing a tracking and step combination command to the respective roll and pitch angles, with regulation of yaw from zero initial displacement.

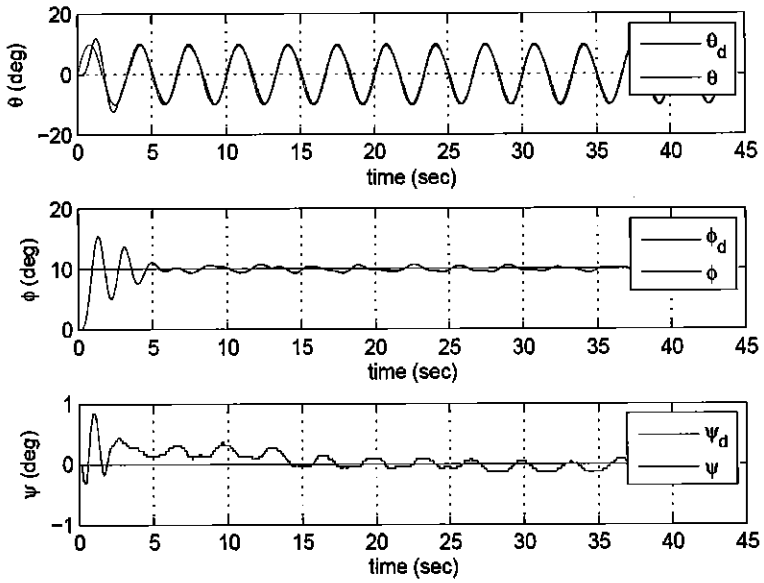

Figure 5.20: Pitch tracking behavior of Quanser test bed.

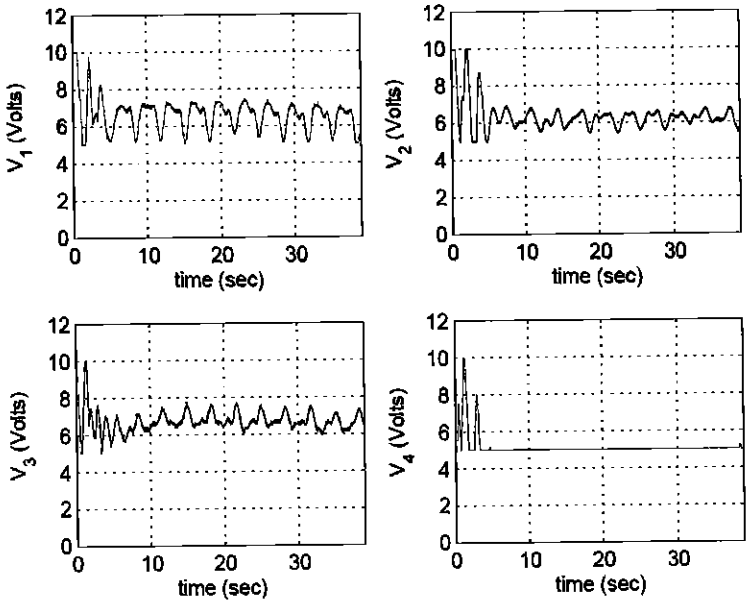

Figure 5.21: Voltage requirements of Quanser test bed pitch tracking.

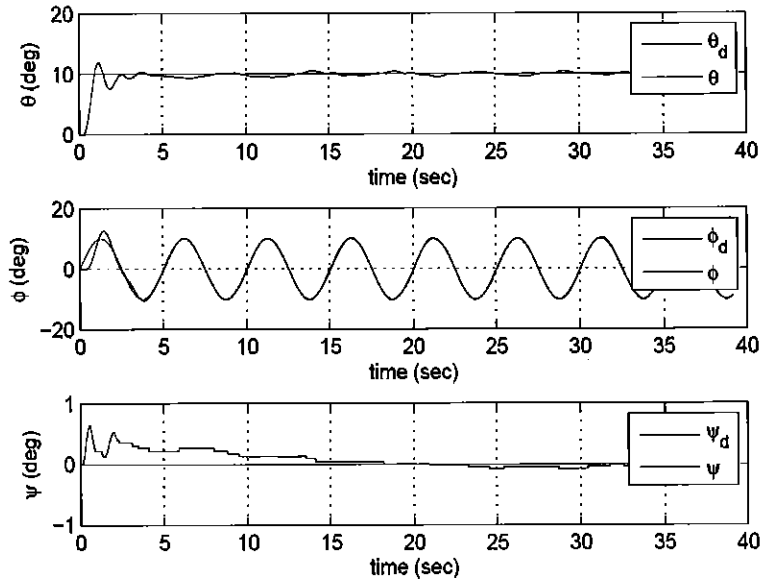

Figure 5.22: Roll tracking behavior of Quanser test bed.

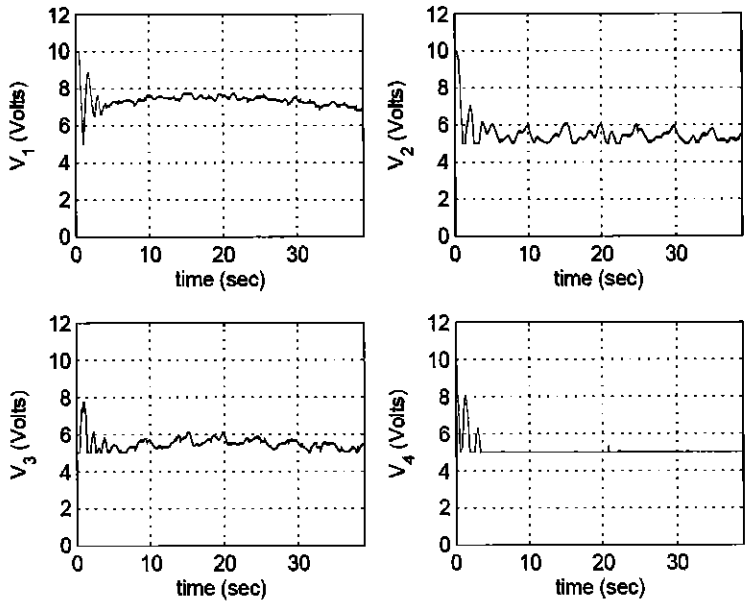

Figure 5.23: Voltage requirements of Quanser test bed roll tracking.

Convergence to the desired tracking is obtained in both cases within 5s, with no saturation observed from the motor voltage.

Chapter 6

Examples: Global Coordinate Underactuated Systems

The following chapter provides overview for challenges seen in (Hoffman et al., 2018), (Hoffman and Reyhanoglu, 2017a), (Hoffman and Reyhanoglu, 2017b). The elegance and mathematical rigor of global coordinates via manifolds will be demonstrated for dynamical formulation and controller design, to be compared to the prior chapter's local coordinate considerations. Because the previous chapter identified the unique considerations between quadrotors and robotics, only an overview on the topic of global coordinates and robust considerations in general will be provided prior to the given examples. Furthermore, a single-section format will be used in lieu of the separated sections seen previously.

The presence of uncertainties must be elaborated upon in their own right, for it is important to consider for robot performance. Robust surgical planning of a minimally-invasive cardiac surgery assisted by robotics but afflicted by naturally-present uncertainties are handled in Azimian et al. (2015). Tethered space robots facing dynamical uncertainty attain target capturing control objectives making use

of adaptive neural network control in Huang et al. (2016). Nonlinear parametrized uncertainties affecting robotic manipulators are handled through inventive adaptive control means in Hung et al. (2008). A non-holonomic wheeled robot addresses parametric and non-parametric uncertainties through the application of robust adaptive control with adaptive backstepping in Dong and Kuhnert (2005). Surgical robotic manipulators composed of parallel flexible structures are analyzed for performance regarding state estimation and shape sensing in the presence of uncertainties in Anderson et al. (2017). Robot localization error affecting motion planning is explored in Takeda et al. (1994), taking an anticipatory approach to minimize the expected errors.

Local coordinate focus is clearly seen in the majority of existing literature. While providing intuitive insight at first, the consequence of sacrificing mathematical rigor is the addition of singularities and ambiguities to the dynamical formulation. In turn, application of controllers derived in such a manner yields errors as benign as measurement error to disaster-inducing gimbal lock. A somewhat unexpected example is that of the quaternion, which avoids singularity outright but in exchange faces rotational uncertainty for any given command (Mayhew et al., 2011a). In practice this leads to discontinuous behavior and endangerment of the control objective, a clear example of which is seen in Mayhew et al. (2011b). Through applying manifolds described by thorough constraint definitions, differential geometric techniques circumvent this issue, providing controllers that operate on the entire tangent bundle subset within which the dynamics exist. Background literature demonstrating the use of differential geometry includes (Lee, 2017), (Lee, 2015a), (Lee, 2015b), (Lee, 2013), (Lee et al., 2017).

6.1 Hybrid Robotic Manipulator Cantilevered and Subjected to Single Torque Revisited

The problem in its entirety is outlined in Reyhanoglu and Hoffman (2016), for the reader's convenience. The objective of the following is to improve upon the local coordinate counterpart's results by providing a robust tracking controller free of dynamical singularities. The appropriate configuration and tangent spaces will be derived, culminating in the complete dynamical formulation and controller design. Simulation results will then be provided to demonstrate controller effectiveness.

6.1.1 Model Formulation

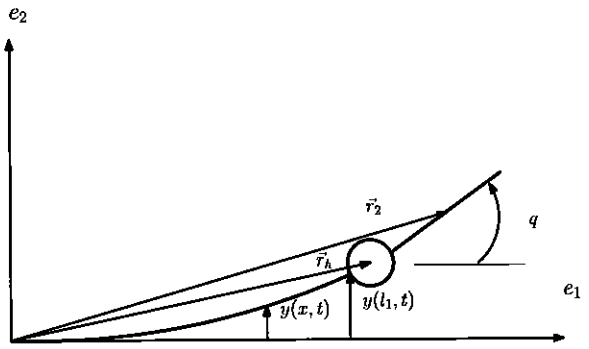

Figure 6.1: Schematic model of a one-torque hybrid robot manipulator, global configuration.

The above is a modified diagram of the same two-link hybrid robot manipulator seen in Figure 5.1. The inertial frame will now be defined by horizontal and vertical projections $\{\vec{e}_1, \vec{e}_2\}$, whose origin resides at the cantilevered point. Vectors $\vec{r}_h, \vec{r}_2$ once more represent the motion of the motor hub/mounting bracket assembly and center of mass of the rigid member, respectively. The lengths of links 1 and 2 are denoted as $l_i, i = 1, 2$. The flexible link has a moment of inertia I and a modulus of elasticity E,

with a mass per unit length ρ. The hub observes a mass m_h and radius l_o while the second link has a mass m_2, the combined moment of inertia with mounting bracket being I_z. The motor applies a torque τ to the system, producing an angular velocity ω. This system is considered in 5.1, but through local coordinate considerations, causing ambiguity in the angle representation with respect to the horizontal. Avoiding this requires re-definition of the rigid link in terms of a global unit vector, q. In doing so, the link exists in a plane but provides only one degree of freedom, as can be surmised by its fixed length. Specifically, the link resides in a one-sphere configuration manifold

$$S^1 = \{q \in \mathbb{R}^2 : ||q|| = 1\}, \tag{6.1}$$

The deflection of the flexible link is another challenge altogether. Lee et al. (2017) applies finite element considerations by dividing an elastic member into n minute rigid bodies, producing a configuration of $(S^2)^n$ for a three-dimensional version. While geometrically exact, this approach makes accurate and efficient mapping of the control torque difficult. To avoid this and facilitate modeling, the assumptions used in Section 5.1 will be applied again, as they are inherent qualities of the system.

Making use of the statement that all deflection is transverse to the orientation of the flexible member, and with the restrictions of a cantilevered beam, the deflection can be taken as a transverse, purely vertical behavior that is mapped as a function of time and the position along the length of the beam, shown as $y(x,t)$ in either figure. Thus, no further orthogonal projection is required, and the complete configuration is $M = (q, y) \in S^1 \times \mathbb{R}$.

For the purpose of error analysis, formulation of the equations of motion will be done with respect to the link's angular velocity. The time derivative of the configu-

ration can be reclaimed nonetheless through the conversion

$$\dot{q} = \omega S q,$$

where $\dot{q} \in T_q S^1$ is the configuration time derivative residing in the appropriate tangent space, $\omega \in \mathbb{R}$ is the scalar angular velocity, and S represents the skew symmetric 2×2 matrix

$$S = \begin{bmatrix} 0 & -1 \\ 1 & 0 \end{bmatrix}.$$

Potential energy is taken from the bending stress of the flexible member:

$$U = \frac{1}{2} \int_0^{l_1} EIy''^2(x,t)dx, \tag{6.2}$$

the $'$ denoting a derivative with respect to x. The kinetic energy terms are found to be

$$T = \frac{1}{2}\rho \int_0^{l_1} (\dot{y}(x,t))^2 dx + \frac{1}{2} I_z \omega^2 + \frac{1}{2} m_h \dot{r}_h^2 + \frac{1}{2} m_2 \dot{r}_2^2, \tag{6.3}$$

which are to be expanded in terms of generalized coordinates. First, the hub and

rigid link velocities are defined as

$$\dot{r}_h^2 = (l_s \dot{y}(l_1, t))^2, \tag{6.4}$$

$$\dot{r}_2^2 = (l_s x_2 \omega e_2^T q)^2 + (l_s \dot{y}(l_1, t) + l_s x_2 \omega e_1^T q)^2, \tag{6.5}$$

$$l_s = \frac{l_o + l_1}{l_1}, \tag{6.6}$$

$$x_2 = l_o + \frac{l_2}{2}, \tag{6.7}$$

taking into consideration the assumption of purely vertical deflection. Expanding and collecting terms provides

$$T = \frac{1}{2}\rho \int_0^{l_1} (\dot{y}(x,t))^2 dx + \frac{1}{2}\bar{I}\omega^2 + \frac{1}{2}(m_h + m_2) l_s^2 (\dot{y}(l_1,t))^2 + m_2 x_2 l_s^2 \omega \dot{y}(l_1,t) e_1^T q, \tag{6.8}$$

where

$$\bar{I} = I_z + \frac{1}{2} m_2 l_s^2 x_2^2.$$

From this point, the assumed mode method theory of deflection will be used. That is to say, the deflection function is considered to be a summation of parametrized functions of position and time:

$$y(x,t) = \sum_{i=1}^{N} \phi_i(x) f_i(t), \tag{6.9}$$

$$\phi_i(x) = 1 - \cos\left(\frac{i\pi x}{l_1}\right) + \frac{1}{2}(-1)^{i+1}\left(\frac{i\pi x}{l_1}\right)^2. \tag{6.10}$$

Once more it shall be taken that $N = 1$ and by extension that $f(t)$ will represent the generalized coordinate for flexible member deflection. The use of a cosine in the position function does not violate configuration mapping, as the function only exists

within the domain of $0 \leq x \leq l_1$. Therefore all possible arguments and operations are well-defined. Applying this substitution allows for the Lagrangian function to be represented in generalized coordinates:

$$L = \frac{1}{2}\begin{bmatrix}\omega \\ \dot{f}\end{bmatrix}^T \begin{bmatrix}\bar{I} & m_{fq}e_1^T q \\ m_{fq}e_1^T q & m_f\end{bmatrix}\begin{bmatrix}\omega \\ \dot{f}\end{bmatrix} - \frac{1}{2}Kf^2, \tag{6.11}$$

where

$$m_f = \rho\int_0^{l_1}\phi(x)^2dx + (m_h + m_2)l_s^2\phi(l_1)^2, \tag{6.12}$$

$$m_{fq} = m_2x_2l_s^2\phi(l_1), \tag{6.13}$$

$$K = \int_0^{l_1} EI(\phi''(x))^2dx. \tag{6.14}$$

Only the one-sphere portion of the semi-direct product requires an orthogonal projection for its equation of motion. D'Alembert's Principle is usable for non-conservative factors, providing the general form of

$$\frac{d}{dt}\left(\frac{\partial L(q,f,\omega,\dot{f})}{\partial\omega}\right) + q^TS\frac{\partial L(q,f,\omega,\dot{f})}{\partial q} = \tau, \tag{6.15}$$

$$\frac{d}{dt}\left(\frac{\partial L(q,f,\omega,\dot{f})}{\partial\dot{f}}\right) - \frac{\partial L(q,f,\omega,\dot{f})}{\partial f} = -c\dot{f} - \phi'(l_1)\tau, \tag{6.16}$$

where c is a positive damping coefficient that is a property of the flexible member. Lastly, a bounded disturbance will be introduced to both degrees of freedom, $[\Delta_q, \Delta_f]^T$, that are each bounded by a constant δ_q, δ_f. As such, the equations of

motion can be arranged as

$$\begin{bmatrix} \bar{I} & m_{fq}e_1^T q \\ m_{fq}e_1^T q & m_f \end{bmatrix} \begin{bmatrix} \dot{\omega} \\ \ddot{f} \end{bmatrix} + \begin{bmatrix} 0 \\ c\dot{f} + Kf - m_{fq}\omega^2 e_2^T q \end{bmatrix} = \begin{bmatrix} 1 \\ -\phi'(l_1) \end{bmatrix} \tau + \begin{bmatrix} \Delta_q \\ \Delta_f \end{bmatrix}. \quad (6.17)$$

This system is clearly underactuated, and can be compressed for future stability analysis as

$$M(q)\dot{v} + A(q, f, \omega, \dot{f}) = B\tau + \Delta, \quad (6.18)$$

where $||\Delta|| \leq \delta = \sqrt{\delta_q^2 + \delta_f^2}$.

Tracking Error

The following section will propose tracking errors for the rigid member for an arbitrary and smooth tracking command $q_d(t) \in S^1$ and likewise an angular velocity $\omega_d(t) \in \mathbb{R}$. Naturally, these considerations correspond to the following error functions

$$\Theta = \frac{1}{2}(1 - q_d^T q), \quad (6.19)$$

$$e_q = \frac{1}{2} q_d^T S^T q, \quad (6.20)$$

$$e_\omega = \omega - \omega_d, \quad (6.21)$$

Defining the errors as shown above allow for the following to be true:

1. Θ is positive definite about $q = q_d$;

   Proof: $q_d^T q$, being by definition the inner product of the two orientation vectors, identifies the cosine of the angle between them. This operator generates a maximum positive value of 1 if and only if the two "vectors" are identical. Thus, the statement holds for any arbitrary examples of q_d,q.

2. The combination of Darboux derivative, Lie group, and tangent space operators on Θ is given by

$$\mathrm{T}_I L_q(D_q\Theta(q, q_d)) = e_q. \tag{6.22}$$

Proof: Bullo and Lewis (2003) demonstrates more in-depth applications of this technique, however interpretation extends from the previous proof. Noting that Θ is a representation of the cosine of the angle between configurations, a trajectory-based derivative will provide an expression of their sine, noted by the configuration inner product operated on by S, a rotation of $\frac{\pi}{2}$. The order of operations can be seen as:

$$\begin{aligned} D_q(\Theta) &= -\frac{1}{2}q_d, \\ L_q(D_q\Theta) &= -\frac{1}{2}q_d^T q, \\ \mathrm{T}_I L_q(D_q\Theta) &= -\frac{1}{2}(Sq_d)^T q = \frac{1}{2}q_d^T S^T q = e_q. \end{aligned}$$

3. The critical points of Θ that are shown by $e_q = 0$ are defined by $\{q_d\} \cup \{q_d exp(\pi S)\}$.

   Proof: The only two configurations where a critical point is met occurs when $q = q_d$ and $q = -q_d$. The above union represents the set of both possibilities.

4. The lower bound of Θ is described as

$$||e_q||^2 \leq \Theta. \tag{6.23}$$

Proof: The sine/cosine correlation observed previously is needed. Let

$$\Theta = \frac{1-\cos\phi}{2},$$
$$e_q = \frac{\sin\phi}{2},$$

to clearly show the angle between configurations. Then,

$$\frac{||e_q||^2}{\Theta} = \frac{\sin^2\phi}{2(1-\cos\phi)} = \frac{1+\cos\phi}{2} \leq 1.$$

5. Consider a positive constant $\theta < 1$. Provided that $\Theta < \theta$, then an upper bound for Θ is represented as

$$\Theta \leq \frac{1}{1-\theta}||e_q||^2. \tag{6.24}$$

Proof: Similar considerations to that of 4) are necessary. A point of contention is the possibility of $q = -q_d$, which will yield a singularity with the current error expression. First,

$$\frac{\Theta}{||e_q||^2} = \frac{2}{1+\cos\phi}.$$

It then follows that

$$1-\theta < 1-\Theta \leq 1 - \frac{1-\cos\phi}{2} = \frac{1+\cos\phi}{2}$$

allows for replacement of the initial result with conclusion (6.24).

For the deflection f, only regulation will be considered to address more practical purposes. That is to say, $f_d = \dot{f}_d = 0$.

6.1.2 Stability Analysis

A nonlinear tracking and regulation controller for the one-torque hybrid robotic manipulator is considered through the coupled application of the input torque:

$$B\tau = -k_x e_x - k_v e_v - \beta \text{sgn}(e_x + e_v) + A + M\dot{v}_d, \tag{6.25}$$

$$e_x = [e_q, f]^T, \tag{6.26}$$

$$e_v = [e_\omega, \dot{f}]^T, \tag{6.27}$$

$$\dot{v}_d = [\dot{\omega}_d, 0]^T, \tag{6.28}$$

where $k_x, k_v \in \mathbb{R}^{2\times 2}$ are positive gain matrices, and $\beta \in \mathbb{R}^+$. Note that care must be taken when implementing this in an experiment environment, as the mapping is one sided: error inputs will produce a defined torque requirement, but the reverse cannot be uniquely determined. This controller design is motivated by the following error dynamics and stability analysis. Taking the time derivative of the provided error terms yields

$$\frac{d}{dt}\Theta = \frac{1}{2}(-\dot{q}_d^T q - q_d^T \dot{q}) = \frac{1}{2}(\omega - \omega_d)(q_d^T S^T q) = e_q e_\omega, \tag{6.29}$$

$$\frac{d}{dt}e_q = \frac{1}{2}(\dot{q}_d^T S^T q) + \frac{1}{2}(q_d^T S^T \dot{q}) = \frac{1}{2}E(q, q_d)e_\omega, \tag{6.30}$$

$$\frac{d}{dt}e_\omega = \dot{\omega} - \dot{\omega}_d, \tag{6.31}$$

$$E(q, q_d) = q_d^T q. \tag{6.32}$$

Noting that $||E|| \leq 1$, it can be said that

$$||\dot{e}_q|| \leq ||e_\omega||. \tag{6.33}$$

Replacing the original dynamics with the velocity error time derivative and control input will therefore produce the compressed result:

$$M\dot{e}_v = -k_x e_x - k_v e_v - \beta \text{sgn}(e_x + e_v) + \Delta. \tag{6.34}$$

Consider the Lyapunov candidate function

$$V = \frac{1}{2} e_v^T M e_v + \frac{1}{2} e_x^T (k_x + k_v) e_x + e_x^T M e_v, \tag{6.35}$$

which is positive definite so long as

$$\lambda_m(k_x + k_v) > \frac{\lambda_M(M)^2}{\lambda_m(M)} \tag{6.36}$$

through Sylvester's Criteria. The time derivative with respect to the trajectories produces

$$\begin{aligned}
\dot{V} &= e_v^T(-k_x e_x - k_v e_v - \beta \text{sgn}(e_x + e_v) + \Delta) + \frac{1}{2} e_v^T \dot{M} e_v + e_x^T (k_x + k_v) \dot{e}_x \\
&+ \dot{e}_x^T M e_v + e_x^T \dot{M} e_v + e_x^T (-k_x e_x - k_v e_v - \beta \text{sgn}(e_x + e_v) + \Delta) \\
&\leq -\left(\lambda_m(k_v) - \frac{1}{2} \lambda_M(\dot{M}) - \lambda_M(M) \right) ||e_v||^2 - \lambda_m(k_x) ||e_x||^2 + e_x^T \dot{M} e_v \\
&+ (e_x + e_v)^T (-\beta \text{sgn}(e_x + e_v) + \Delta).
\end{aligned}$$

It is therefore required that $\lambda_m(k_v) > \frac{1}{2}\lambda_M(\dot{M}) + \lambda_M(M)$. The signum function is able to overpower the constant-bounded uncertainty under the premise of

$$-\beta|z| + \delta z \leq (\delta - \beta)|z|, \tag{6.37}$$

thus only demanding that $\beta > \delta$. The cross term is then bounded through Young's Inequality

$$e_x^T \dot{M} e_v \leq \frac{\lambda_M(\dot{M})}{2}(||e_x||^2 + ||e_v||^2) = \frac{\lambda_M(\dot{M})}{2}||z||^2, \tag{6.38}$$

$$z = [e_x, e_v]^T. \tag{6.39}$$

Thus, the expression is further compressed as

$$\dot{V} \leq -\left(a - \frac{\lambda_M(\dot{M})}{2}\right)||z||^2, \tag{6.40}$$

$$a = \min\left\{\lambda_m(k_v) - \frac{1}{2}\lambda_M(\dot{M}) - \lambda_M(M), \lambda_m(k_x)\right\}. \tag{6.41}$$

So long as gains are chosen such that the argument in the parenthesis is positive, the system is identified to be globally asymptotically stable.

6.1.3 Simulations

Identification of control law success will be shown using parameters from a Quanser two-link robotic manipulator system (Quanser.com), shown in Table 5.1.

The implemented constant-bounded disturbance is

$$\Delta = \frac{1}{2}\begin{bmatrix}\cos(\pi t) \\ 0\end{bmatrix}$$

which is thus bounded by $\delta = \frac{1}{2}$. The control gains used are

$$k_x = \begin{bmatrix}3 & 0 \\ 0 & 10\end{bmatrix}, \; k_v = \begin{bmatrix}3 & 0 \\ 0 & 10\end{bmatrix}, \; \beta = 7.$$

The following figures depict system convergence to the desired command

$$q_d = [\cos(t), \sin(t)]^T, \ \omega_d = 1,$$

And the regulation of $f, \dot{f}$ to 0. The initial conditions were provided as

$$q(0) = \left[\frac{\sqrt{2}}{2}, \frac{\sqrt{2}}{2}\right]^T, \ \omega(0) = 0, \ f(0) = \dot{f}(0) = 0.$$

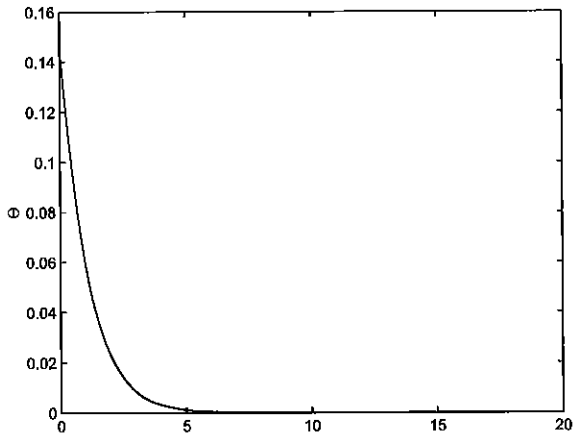

Figure 6.2: Time behavior of error function Θ.

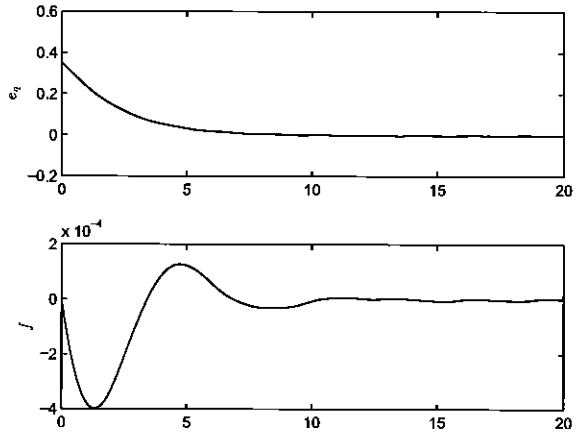

Figure 6.3: Time behavior of configuration error e_x.

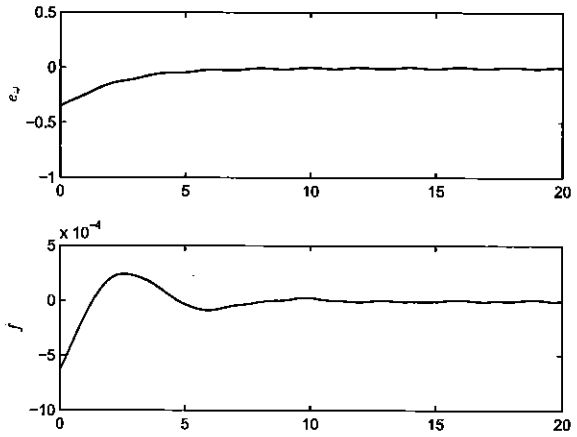

Figure 6.4: Time behavior of angular velocity error e_v.

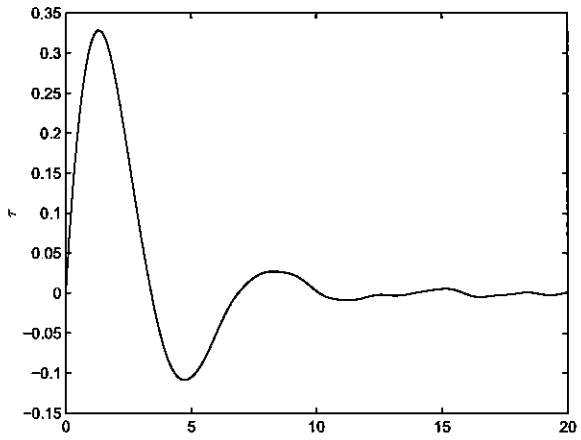

Figure 6.5: Time behavior of required torque.

The proposed robust tracking controller is shown to be successful. The control objective is achieved for all errors and regulation, completing the task within 11s.

6.2 Modeling and Control of a Two-Torque Hybrid Robotic Manipulator Revisited

The following is also seen in Reyhanoglu et al. (2016). The system itself, much like the previous section, was motivated by the desire to obtain a singularity-free robust tracking controller as an improvement on the locally-derived predecessor. A similar procedure as in the previous section will be presented, culminating in simulations proving controller capability.

6.2.1 Model Formulation

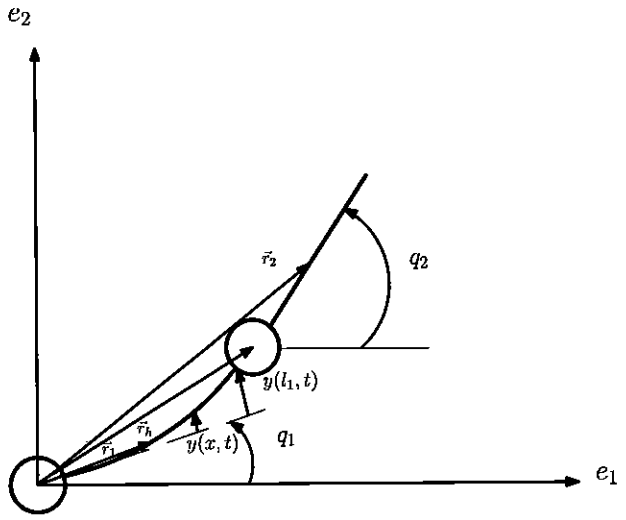

Figure 6.6: Hybrid robotic manipulator schematic, two torque configuration.

The above figure portrays a robotic manipulator nearly identical to that of Section 4.2, with the objective of obtaining a global formulation. Thus, two torques τ_1 and τ_2 act on the system, and the hubs' respective moments of inertia will be denoted as I_{z_i}, experiencing angular velocities ω_i. The same inertial frame, system quantities, and assumptions will be kept from the previous section, only redefining the vector to the combined center of mass of the mounting bracket and second link together as $\vec{r}_2$ and their combined mass as m_2, for the purpose of convenience during dynamical analysis.

As an extension of the previous section, the flexible member orientation alone can be described as an additional one-sphere degree of freedom, q_1, as member length is assumed to be unaffected by the transverse deflection mapping. It then follows that the orientation of the second link will now be denoted as q_2. As such, the complete manifold is $M = (q_1, q_2, y) \in (S^1)^2 \times \mathbb{R}$. The potential energy term is exactly that of

Equation 6.2, and the new kinetic energy expression is

$$T = \frac{1}{2}\rho \int_0^{l_1} \dot{r}_1^2 dx + \frac{1}{2} m_2 \dot{r}_2^2 + \frac{1}{2} m_h \dot{r}_h^2 + \frac{1}{2} I_{z_1} \omega_1^2 + \frac{1}{2} I_{z_2} \omega_2^2, \tag{6.42}$$

where the time derivatives of the vector magnitudes are defined as

$$\dot{r}_1^2 = (\dot{y}(x,t) + (l_o + x)\omega_1)^2 + (y(x,t)\omega_1)^2, \tag{6.43}$$

$$\dot{r}_h^2 = ((2l_o + l_1)\omega_1 + l_s \dot{y}(l_1,t))^2 + (l_s y(l_1,t)\omega_1)^2, \tag{6.44}$$

$$\begin{aligned}\dot{r}_2^2 =& ((2l_o + l_1)\omega_1 + l_s \dot{y}(l_1,t))^2 + (l_s y(l_1,t)\omega_1)^2 + (x_2\omega_2)^2 + l_s \dot{y}(l_1,t)) q_2^T q_1 \\ &+ 2x_2\omega_2((2l_o + l_1)\omega_1 + 2x_2\omega_2(l_s y(l_1,t)\omega_1) q_2^T S q_1.\end{aligned} \tag{6.45}$$

The assumed mode method of deflection may still be used, and $y(x,t)$ is parametrized once more into its shape function and generalized coordinate components. With significant effort, the Lagrangian function for this system can be arranged as

$$L = \frac{1}{2} \begin{bmatrix} \omega_1 \\ \omega_2 \\ \dot{f} \end{bmatrix}^T \begin{bmatrix} I_1 & m_{12} & m_{1f} \\ m_{12} & I_2 & m_{2f} \\ m_{1f} & m_{2f} & m_f \end{bmatrix} \begin{bmatrix} \omega_1 \\ \omega_2 \\ \dot{f} \end{bmatrix} - \frac{1}{2} K f^2, \tag{6.46}$$

where

$$I_1 = I_{z_1} + \rho \int_0^{l_1} (l_o + x)^2 dx + \rho \int_0^{l_1} \phi^2(x) dx f^2 + (m_2 + m_h)((2l_o + l_1)^2 + l_s^2 \phi^2(l_1) f^2),$$

$$I_2 = I_{z_2} + m_2 x_2^2,$$

$$m_f = \rho \int_0^{l_1} \phi^2(x) dx + (m_2 + m_h) l_s^2 \phi^2(l_1),$$

$$m_{1f} = \rho \int_0^{l_1} (l_o + x)\phi(x) dx + (m_2 + m_h) l_s (2l_o + l_1)\phi(l_1),$$

$$m_{2f} = m_2 x_2 l_s \phi(l_1) q_2^T q_1,$$

$$m_{12} = m_2 x_2 (2l_o + l_1) q_2^T q_1 + m_2 x_2 l_s \phi(l_1) f q_2^T S q_1,$$

and x_2 denotes the distance to the center of mass of the mounting bracket and second link. D'Alembert's Principle is applied once more to denote the general equations of motion:

$$\frac{d}{dt}\left(\frac{\partial L(q, f, \omega, \dot{f})}{\partial \omega_i}\right) + q_i^T S \frac{\partial L(q, f, \omega, \dot{f})}{\partial q_i} = Q_i, i = 1, 2 \tag{6.47}$$

$$\frac{d}{dt}\left(\frac{\partial L(q, f, \omega, \dot{f})}{\partial \dot{f}}\right) - \frac{\partial L(q, f, \omega, \dot{f})}{\partial f} = Q_f, \tag{6.48}$$

$$Q = \begin{bmatrix} \tau_1 - \tau_2 \\ \tau_2 \\ -c\dot{f} - \phi'(l_1)\tau_2 \end{bmatrix}, \tag{6.49}$$

adding a bounded disturbance on each degree of freedom $[\Delta_1, \Delta_2, \Delta_f]^T$, such that

$||\Delta_i|| \leq \delta_i, i = 1, 2, f$. The full equations of motion are then

$$\begin{bmatrix} I_1 & m_{12} & m_{1f} \\ m_{12} & I_2 & m_{2f} \\ m_{1f} & m_{2f} & m_f \end{bmatrix} \begin{bmatrix} \dot{\omega}_1 \\ \dot{\omega}_2 \\ \ddot{f} \end{bmatrix} + \begin{bmatrix} A_1 \\ A_2 \\ c\dot{f} + \bar{K}f - m_2 x_2 l_s \phi(l_1)\omega_2^2 q_2^T S q_1 \end{bmatrix} = \begin{bmatrix} 1 & -1 \\ 0 & 1 \\ 0 & -\phi'(l_1) \end{bmatrix} \begin{bmatrix} \tau_1 \\ \tau_2 \end{bmatrix} + \begin{bmatrix} \Delta_1 \\ \Delta_2 \\ \Delta_f \end{bmatrix}, \tag{6.50}$$

where

$$\bar{K} = K - \left(\rho \int_0^{l_1} \phi^2(x)dx + (m_2 + m_h) l_s^2 \phi^2(l_1) \right) \omega_1^2, \tag{6.51}$$

$$A_1 = \left(\rho \int_0^{l_1} \phi^2(x)dx + (m_2 + m_h)(l_s^2 \phi^2(l_1)) \right) f\dot{f}\omega_1 + m_2 x_2 l_s \phi(l_1) f \omega_2^2 q_2^T q_1, - m_2 x_2 (2l_o + l_1)\omega_2^2 q_2^T S q_1, \tag{6.52}$$

$$A_2 = m_2 x_2 (2l_o + l_1)\omega_1^2 q_2^T S q_1 - m_2 x_2 l_s \phi(l_1) f \omega_1^2 q_2^T q_1 + m_2 x_2 l_s \phi(l_1) \dot{f} \omega_1 q_2^T S q_1. \tag{6.53}$$

Once more the system is underactuated, and will be truncated into the expression

$$M(q_1, q_2, f)\dot{v} + A(q_1, q_2, f, \omega_1, \omega_2, \dot{f}) = C\tau + \Delta, \tag{6.54}$$

$$\tau = \begin{bmatrix} \tau_1 \\ \tau_2 \end{bmatrix}, \tag{6.55}$$

noting that $A \in \mathbb{R}^3, C \in \mathbb{R}^{3\times 2}$ and $||\Delta|| \leq \delta = \sqrt{\delta_1^2 + \delta_2^2 + \delta_f^2}$.

6.2.2 Tracking Error

The control objective can be expressed as smooth arbitrary tracking commands $q_{d_i}(t) \in S^1$ with corresponding angular velocities $\omega_{d_i}(t) \in \mathbb{R}$ for the two members. Error definitions seen in Equations 6.19 - 6.21 are called upon once more, with the propositions that follow, and the time derivatives defined. f and $\dot{f}$ will once more be subjected to regulation.

Assumption 1

A non-trivial observation is the matrix $M(q_1, q_2, f)$ being a function of the deflection explicitly. Although the magnitude of the links are constrained by definition, the deflection sees no such restraint. Instead, let the collection of errors as a vector be denoted as

$$z = [e_x, e_v]^T,\ e_x = [e_{q_1}, e_{q_2}, f]^T,\ e_v = [e_{\omega_1}, e_{\omega_2}, \dot{f}]^T. \tag{6.56}$$

In turn, the inertia matrix and its time derivative may each be bounded by positive, globally invertible non-decreasing functions of such error:

$$||M|| \leq \rho_1(||z||)||z||,\ ||\dot{M}|| \leq \rho_2(||z||)||z||. \tag{6.57}$$

Such an assumption is mild, as calculations for the magnitudes of each matrix demonstrate a straightforward function of $z(t)$.

6.2.3 Stability Analysis

Based on the previous considerations and the results of the previous section, a nonlinear tracking and regulation controller for the robotic manipulator is considered as

applied through the control input torque actuation:

$$C\tau = -k_x e_x - k_v e_v - \beta \text{sgn}(e_x + e_v) + A + M\dot{v}_d, \tag{6.58}$$

$$\dot{v}_d = [\dot{\omega}_{d_1}, \dot{\omega}_{d_2}, 0]^T, \tag{6.59}$$

where $k_x, k_v \in \mathbb{R}^{2\times 2}, \beta \in \mathbb{R}^+$ are tuning gains. Once more, the command-actuation mapping is one-sided. A similar process to the prior section yields very similar closed-loop error dynamics:

$$M\dot{e}_v = -k_x e_x - k_v e_v - \beta \text{sgn}(e_x + e_v) + \Delta, \tag{6.60}$$

warranting the use of an identical Lyapunov candidate function:

$$V = \frac{1}{2} e_v^T M e_v + \frac{1}{2} e_x^T (k_x + k_v) e_x + e_x^T M e_v, \tag{6.61}$$

with Sylvester's Criterion holding true. The initial time derivative with respect to the velocities is the same, but further bounding will now take into account the explicit assumption:

$$\begin{aligned}\dot{V} =& e_v^T(-k_x e_x - k_v e_v - \beta \text{sgn}(e_x + e_v) + \Delta) + \frac{1}{2} e_v^T \dot{M} e_v + e_x^T (k_x + k_v)\dot{e}_x \\ &+ \dot{e}_x^T M e_v + e_x^T \dot{M} e_v + e_x^T(-k_x e_x - k_v e_v - \beta \text{sgn}(e_x + e_v) + \Delta) \\ &\leq -\lambda ||z||^2 + e_v^T \left(\frac{1}{2}\dot{M} + M\right) e_v + e_x^T \dot{M} e_v,\end{aligned}$$

where $\lambda = \min\{k_v, k_x\}$. The last two terms can be represented as

$$e_v^T \left(\frac{1}{2}\dot{M} + M\right) e_v + e_x^T \dot{M} e_v = \bar{\rho}(\rho_1, \rho_2)||z||^2 = \bar{\rho}(||z||)||z||^2, \tag{6.62}$$

providing the result

$$\dot{V} \leq -(\lambda - \bar{\rho}(||z||))||z||^2. \tag{6.63}$$

The time derivative can be bounded as

$$\dot{V} \leq -p||z||^2, \tag{6.64}$$

p being a positive constant. Specifically, the expression $p||z||^2$ is a positive continuous semi-definite function residing within the set

$$F = \{z(t) \in \mathbb{R}^6 : ||z|| \leq \bar{\rho}^{-1}(\lambda)\}. \tag{6.65}$$

Signal chasing arguments then prove that $e_{q_i}, f, e_{\omega_i}, \dot{f} \in \mathcal{L}_\infty$ in F. It then follows that the time derivatives of the error functions and Θ_i exist in $\mathcal{L}_\infty$. Therefore, the remaining trajectories $q_i, \omega_i \in \mathcal{L}_\infty$. Therefore, $z(t)$ and the functions thereof are uniformly continuous in the domain F. Identifying viable initial conditions requires a subset $J \subset F$ to be defined as

$$J \triangleq \left\{z(t) \in \mathbb{R}^6 : z^T M z < \lambda_m(M)(\bar{\rho}^{-1}(\lambda))\right\}. \tag{6.66}$$

Using Theorem 8.4 of Khalil (1996), it can be determined that

$$||z||^2 \to 0, t \to \infty, \forall z(t_0) \in J. \tag{6.67}$$

Thus, all errors tend to 0, proving asymptotic tracking of the desired commands given the initial conditions exist within J. In turn, J can be made arbitrarily large through increasing the gain λ. Therefore, the result is semi-global in nature.

6.2.4 Simulations

The benchmark system used for control demonstration will be the same Quanser two-link manipulator as in Figure 5.5 (Quanser.com). Most physical parameters are largely the same, with a few additions or changes due to new notation, for example $m_2 = m_{l_2} + m_{b_2}$ as the summation of link and mounting bracket mass, used to find x_2.

The simulated system observes a constant bounded disturbance of

$$\Delta = \frac{1}{2\sqrt{2}} \begin{bmatrix} \cos(\pi t) \\ \sin(2\pi t) \\ 0 \end{bmatrix}$$

which is bounded by $\delta = \frac{1}{2}$. The control gains used are selected as

$$k_x = \begin{bmatrix} 1 & 0 & 0 \\ 0 & 2 & 0 \\ 0 & 0 & 15 \end{bmatrix}, \; k_v = \begin{bmatrix} 1 & 0 & 0 \\ 0 & 2 & 0 \\ 0 & 0 & 15 \end{bmatrix}, \; \beta = 10.$$

System convergence to desired trajectories of

$$q_{d_i} = [\cos(t), \sin(t)]^T, \; \omega_{d_i} = 1, i = 1, 2,$$

and the regulation of $f, \dot{f}$ are shown in the following figures. Initial conditions were given to be

$$q_1(0) = \left[\frac{\sqrt{2}}{2}, \frac{\sqrt{2}}{2}\right]^T, \; \omega_1(0) = 0, \; q_2(0) = \left[\frac{\sqrt{3}}{2}, \frac{1}{2}\right]^T, \; \omega_2(0) = 0, \; f(0) = \dot{f}(0) = 0.$$

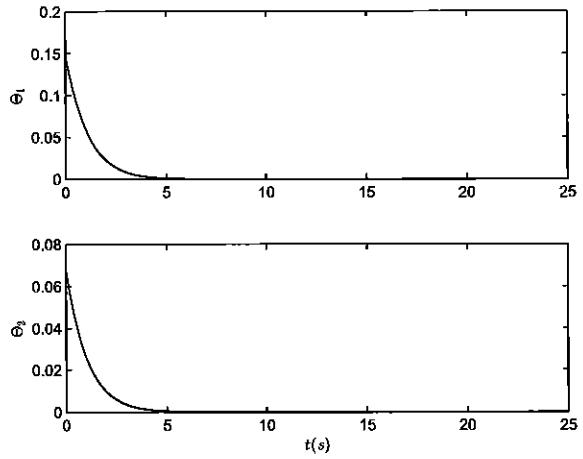

Figure 6.7: Time behavior of error functions Θ_i.

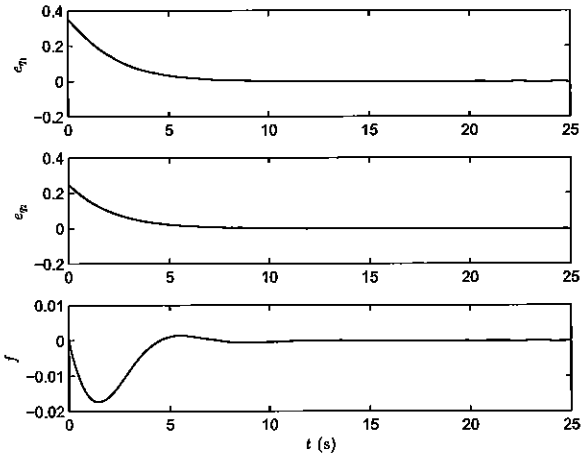

Figure 6.8: Time behavior of configuration errors e_{q_i}.

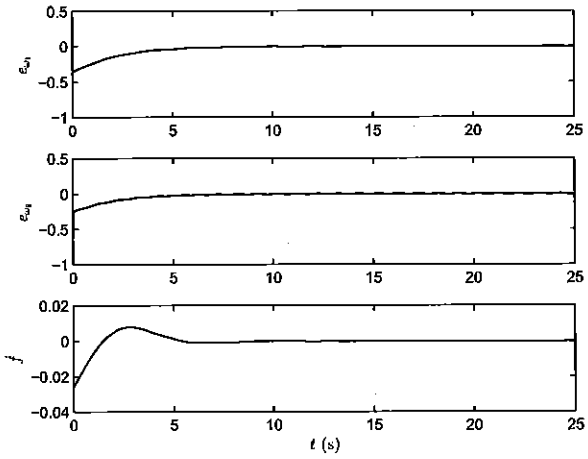

Figure 6.9: Time behavior of angular velocity errors e_{ω_i}.

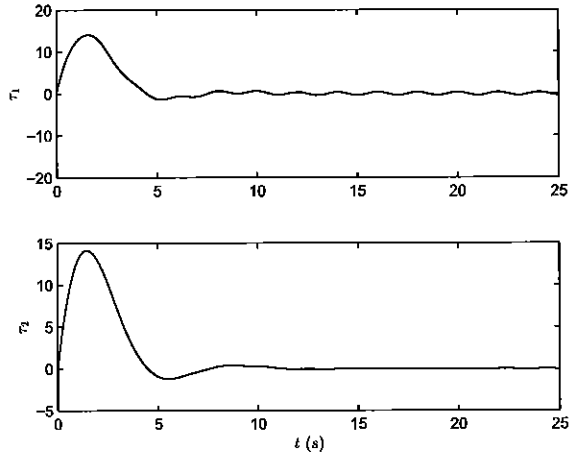

Figure 6.10: Time behavior of control torques.

Robust tracking and regulation is obtained within 7s despite the provided disturbances, thereby demonstrating controller effectiveness.

6.3 Geometric Tracking Control of a 3D Revolute Joint Robot

The following has been published in Hoffman and Reyhanoglu (2017b). A three-dimensional revolute robot composed of a rotating base and two rigid members linked together by motor hubs is subjected to a constant-bounded uncertainty. Global coordinate manifolds are used to design a tracking controller able to suppress the present uncertainties, with simulations on a benchmark system to determine effectiveness.

6.3.1 Model Formulation

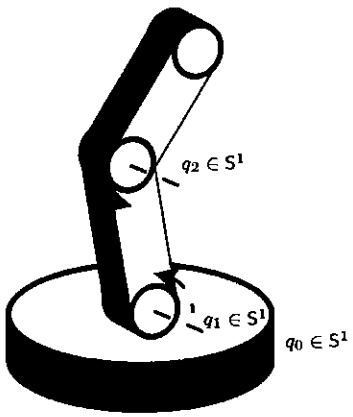

Figure 6.11: Schematic model of a three-dimensional revolute joint robot.

The physical representation of the three-dimensional revolute joint robot is given above, originally provided by Lee et al. (2017). An inertial frame composed of $\{\vec{e}_1, \vec{e}_2\}$ outlines horizontal and vertical projections with the origin fixed at the cylindrical base where the first link connects. This choice is made with insight towards the

horizontal rotation axes of the two links and vertical counterpart of the base. Due to the convenience of the fixed component dimensions, each component (link i and base) provides a degree of freedom that is concisely represented by a one-sphere configuration manifold:

$$S^1 = \{q_i \in \mathbb{R}^2 : ||q_i|| = 1\}, \tag{6.68}$$

where $i = 0, 1, 2$ to represent the base and links 1 and 2 respectively. The full configuration is thus $q = (q_0, q_1, q_2) \in (S^1)^3$.

The lengths of each rigid link are denoted as L_i, and their corresponding masses are represented by m_i. The base moment of inertia is labeled J, and the standard convention of g will be used for acceleration due to gravity. Integrated motors provide torques τ_i to each degree of freedom, and are such that the center of mass for each link resides in their respective centers.

As in the previous examples, a preference towards angular velocity will be observed, in order to provide more insightful error dynamics. Nomenclature will be kept the same in regards to the transformation between traditional velocity and angular:

$$\dot{q}_i = \omega_i S q_i,$$

where $\dot{q}_i \in \mathrm{T}_{q_i} S^1$ is the configuration time derivative residing in the appropriate tangent space, $\omega_i \in \mathbb{R}$ is the scalar angular velocity, and S represents the skew symmetric 2×2 matrix

$$S = \begin{bmatrix} 0 & -1 \\ 1 & 0 \end{bmatrix}.$$

Noting that the only potential energy is sourced from gravitational affects, the Lagrangian function can be expressed in terms of $(q, \omega) \in (S^1)^3 \times \mathbb{R}^3$ as

$$L = \frac{1}{2}\begin{bmatrix}\omega_0\\ \omega_1\\ \omega_2\end{bmatrix}^T \begin{bmatrix} M_{00} & 0 & 0\\ 0 & (m_1+4m_2)\frac{L_1^2}{4} & m_2\frac{L_1L_2}{2}q_1^Tq_2\\ 0 & m_2\frac{L_1L_2}{2}q_1^Tq_2 & m_2\frac{L_2^2}{4}\end{bmatrix}\begin{bmatrix}\omega_0\\ \omega_1\\ \omega_2\end{bmatrix} - m_1g\frac{L_1}{2}e_2^Tq_1 - m_2ge_2^T(L_1q_1 + \frac{L_2}{2}q_2) \tag{6.69}$$

where

$$M_{00} = J + m_1(e_1^T\frac{L_1}{2}q_1)^2 + m_2(e_1^T(L_1q_1 + \frac{L_2}{2}q_2))^2.$$

In turn, applying D'Alembert's Principle yields:

$$\frac{d}{dt}\left(\frac{\partial L(q,\omega)}{\partial \omega_i}\right) + q_i^TS\frac{\partial L(q,\omega)}{\partial q_i} = Q_i, \tag{6.70}$$

$$Q = \begin{bmatrix}\tau_0\\ \tau_1 - \tau_2\\ \tau_2\end{bmatrix}. \tag{6.71}$$

Bounded unstructured uncertainties will be affecting each degree of freedom, and later collected into a single column for stability analysis. Specifically, each uncertainty will be denoted as Δ_i and will be bounded as $||\Delta_i|| \leq \delta_i$, $\delta_i \in \mathbb{R}^+$. Collecting the terms

provides

$$\begin{bmatrix} M_{00}(q) & 0 & 0 \\ 0 & (m_1+4m_2)\frac{L_1^2}{4} & m_2\frac{L_1L_2}{2}q_1^Tq_2 \\ 0 & m_2\frac{L_1L_2}{2}q_1^Tq_2 & m_2\frac{L_2^2}{4} \end{bmatrix} \begin{bmatrix} \dot{\omega}_0 \\ \dot{\omega}_1 \\ \dot{\omega}_2 \end{bmatrix} + \begin{bmatrix} \omega_0(m_1\frac{L_1^2}{2}(e_1^Tq_1)(e_1^T\omega_1Sq_1)) \\ m_2\frac{L_1L_2}{2}\omega_2(\omega_1(Sq_1)^Tq_2+\omega_2q_1^T(Sq_2)) \\ m_2\frac{L_1L_2}{2}\omega_1(\omega_1(Sq_1)^Tq_2+\omega_2q_1^T(Sq_2)) \end{bmatrix}$$
$$+ \begin{bmatrix} 2\omega_0m_2e_1^T(L_1q_1+\frac{L_2}{2}q_2)e_1^T(L_1\omega_1Sq_1+\frac{L_2}{2}\omega_2Sq_2) \\ \frac{\omega_0^2}{2}[m_1\frac{L_1^2}{2}(e_1^Tq_1)+2m_2L_1e_1^T(L_1q_1+\frac{L_2}{2}q_2)](e_2^Tq_1)+P_1 \\ m_2[\frac{L_2\omega_0^2}{2}e_1^T(L_1q_1+\frac{L_2}{2}q_2)e_2^Tq_2+L_1L_2\frac{\omega_1\omega_2}{2}q_2^TSq_1]+P_2 \end{bmatrix} = \begin{bmatrix} \tau_0 \\ \tau_1-\tau_2 \\ \tau_2 \end{bmatrix} + \begin{bmatrix} \Delta_0 \\ \Delta_1 \\ \Delta_2 \end{bmatrix}, \tag{6.72}$$

where

$$P_1 = m_2L_1L_2\frac{\omega_1\omega_2}{2}q_1^TSq_2 + m_1g\frac{L_1}{2}e_1^Tq_1 + m_2gL_1(e_1^T(L_1q_1+\frac{L_2}{2}q_2))e_1^Tq_1,$$
$$P_2 = m_2g\frac{L_2}{2}(e_2^T(L_1q_1+\frac{L_2}{2}q_2))e_1^Tq_2.$$

For the purpose of simplicity in the subsequent development, this expression will be written as

$$M(q)\dot{\omega} + A(q,\omega) = \tau + \Delta, \tag{6.73}$$

where $A(q,\omega) \in \mathbb{R}^3$ and $||\Delta|| \leq \delta = \sqrt{\delta_0^2+\delta_1^2+\delta_2^2}$.

6.3.2 Tracking Error

Consider an arbitrary and smooth tracking command $q_{d_i}(t) \in S^1$ for each component, with in turn a desired angular velocity $\omega_{d_i}(t) \in \mathbb{R}$. Error functions are defined

similarly to previous sections, but must be properly indexed:

$$\Theta_i = \frac{1}{2}(1 - q_{d_i}^T q_i), \tag{6.74}$$

$$e_{q_i} = \frac{1}{2} q_{d_i}^T S^T q_i, \tag{6.75}$$

$$e_{\omega_i} = \omega_i - \omega_{d_i}. \tag{6.76}$$

The previously defined propositions are still valid, and the reader is referred to 6.1's Tracking Error subsection for brevity.

6.3.3 Stability Analysis

A nonlinear tracking controller for the system is proposed as follows:

$$\tau = -k_q e_q - k_\omega e_\omega + A(q, \omega) + M\dot{\omega}_d + \mu_q, \tag{6.77}$$

$$\mu_q = -\frac{\delta^2 e_\alpha}{\delta ||e_\alpha|| + \epsilon_q}, \tag{6.78}$$

$$e_\alpha = e_\omega + \beta M^{-1} e_q, \tag{6.79}$$

where $k_q, k_\omega, \beta, \epsilon_q \in \mathbb{R}^+$, and the errors without i indexing refer to the concatenation of the three errors. The μ_q term specifically addresses bounded uncertainty suppression, as can be seen with the use of the error norm in a sliding mode-esque fashion. This controller design is motivated by the following error dynamics and stability analysis.

Taking the time derivative of the provided error terms yields

$$\frac{d}{dt}\Theta_i = \frac{1}{2}(-\dot{q}_{d_i}^T q_i - q_{d_i}^T \dot{q}_i) = \frac{1}{2}(\omega_i - \omega_{d_i})(q_{d_i}^T S^T q_i) = e_{q_i} e_{\omega_i}, \tag{6.80}$$

$$\frac{d}{dt}e_{q_i} = \frac{1}{2}(\dot{q}_{d_i}^T S^T q_i) + \frac{1}{2}(q_{d_i}^T S^T \dot{q}_i) = \frac{1}{2}E(q_i, q_{d_i})e_{\omega_i}, \tag{6.81}$$

$$\frac{d}{dt}e_{\omega_i} = \dot{\omega}_i - \dot{\omega}_{d_i}, \tag{6.82}$$

$$E(q_i, q_{d_i}) = q_{d_i}^T q_i. \tag{6.83}$$

Noting that $||E|| \leq 1$, it can therefore be stated that

$$||\dot{e}_{q_i}|| \leq ||e_{\omega_i}||. \tag{6.84}$$

Replacing the error dynamics and designed controller into the original dynamics creates the closed loop error dynamics:

$$M\dot{e}_\omega = -k_q e_q - k_\omega e_\omega + \Delta + \mu_q. \tag{6.85}$$

To continue, consider the Lyapunov candidate function

$$V = \frac{1}{2}e_\omega^T M e_\omega + k_q \Theta(q, q_d) + \beta e_q^T e_\omega, \tag{6.86}$$

with respect to the appropriate system domain

$$D = \{q \in (S^1)^3 : \Theta(q, q_d) < \theta\}. \tag{6.87}$$

Being bounded within the domain D makes valid the bounding arguments provided by properties 4) and 5):

$$||e_q||^2 \leq \Theta(q, q_d) \leq \frac{1}{1-\theta}||e_q||^2, \tag{6.88}$$

with the conclusion that Θ is positive-definite and decrescent. Making use of this bounding with Sylvester's Criteria, the candidate function is therefore bounded by

$$z^T M_1 z \leq V \leq z^T M_2 z, \; z = [||e_q||, ||e_\omega||]^T \in \mathbb{R}^2, \tag{6.89}$$

$$M_1 = \frac{1}{2}\begin{bmatrix} 2k_q & -\beta \\ -\beta & \lambda_m(M) \end{bmatrix}, \; M_2 = \frac{1}{2}\begin{bmatrix} \frac{2k_q}{1-\theta} & \beta \\ \beta & \lambda_M(M) \end{bmatrix}, \tag{6.90}$$

where $\lambda_m()$ and $\lambda_M()$ denote the minimum and maximum eigenvalues, respectively, of the argument. Computing the time derivative along the trajectories yields

$$\begin{aligned} \dot{V} &= e_\omega^T M \dot{e}_\omega + k_q \dot{\Theta} + \beta \dot{e}_q^T e_\omega + \beta e_q^T \dot{e}_\omega + e_\omega^T \dot{M} e_\omega, \\ &\leq -(k_\omega - \beta E(q, q_d) - \lambda_M(\dot{M}))||e_\omega||^2 - \beta k_\omega e_q^T M^{-1} e_\omega - \beta k_q e_q^T M^{-1} e_q + e_\alpha^T(\Delta + \mu_q). \end{aligned}$$

Noting that $||E|| \leq 1$ allows for an upper bound of

$$\dot{V} \leq -z^T Q z + e_\alpha^T(\Delta + \mu_q),$$

where

$$Q = \begin{bmatrix} \frac{\beta k_q}{\lambda_M(M)} & -\frac{\beta k_\omega}{2\lambda_m(M)} \\ -\frac{\beta k_\omega}{2\lambda_m(M)} & k_\omega - \beta - \lambda_M(\dot{M}) \end{bmatrix}.$$

The second term is bounded by

$$e_\alpha^T(\Delta + \mu_q) \leq \delta||e_\alpha|| - \frac{\delta^2||e_\alpha||^2}{\delta||e_\alpha|| + \epsilon_q} = \epsilon_q \frac{\delta||e_\alpha||}{\delta||e_\alpha|| + \epsilon_q} \leq \epsilon_q,$$

ultimately giving

$$\dot{V} \leq -z^T Q z + \epsilon_q. \tag{6.91}$$

It is therefore implied that $\dot{V} < 0$ when $V > 1$. Furthermore, to ensure positive-definiteness of M_1, M_2, and Q, the condition

$$\beta < min\left\{k_\omega - \lambda_M(\dot{M}), \frac{4k_\omega k_q \lambda_m(M)^2}{k_\omega^2 \lambda_M(M) + 4k_q \lambda_m(M)^2}, \sqrt{2k_q \lambda_m(M)}\right\}$$

is required, along with $k_\omega > \lambda_M(\dot{M})$.

Define the constants d_1 and d_2 as

$$d_1 = \frac{\lambda_M(M_2)}{\lambda_m(Q)}\epsilon_q, \; d_2 = \lambda_m(M_1)\theta(1-\theta).$$

Let D_ψ denote a sub-level set of the candidate function given by

$$D_\psi = \{(q, \omega) \in (S^1)^3 \times \mathbb{R}^3 : V \leq \psi\}, \tag{6.92}$$

for some positive constant ψ. So long as the inequality $\psi < d_2$ is upheld, this subset resides in the original domain. If $d_1 < \psi < d_2$, D_ψ is a positively invariant set, with any solution beginning in D_ψ converging to D_{d_1}. Confirming this requires $d_1 < d_2$,

attained by the constraint

$$\epsilon_q < \frac{\lambda_m(M_1)\lambda_m(Q)}{\lambda_M(M_2)}\theta(1-\theta). \tag{6.93}$$

With the application of methods seen in Khalil (1996), it can be concluded that the tracking errors are uniformly ultimately bounded, estimated by the set

$$D_{d_1} \subset \left\{ \|z\|^2 \leq \frac{\lambda_M(M_2)}{\lambda_m(M_1)\lambda_m(Q)}\epsilon_q \right\}. \tag{6.94}$$

6.3.4 Simulations

A benchmark revolute robot system is provided to demonstrate controller effectiveness, with the following observed physical parameters:

Table 6.1: Physical parameters of the revolute robot.

Parameter	Value
$m_1 = m_2$	0.5 kg
J	1.0 kg·m^2
$L_1 = L_2$	1.0 m

The system is made subject to a disturbance of

$$\Delta = \frac{1}{\sqrt{3}} \begin{bmatrix} \sin(3\pi t) \\ \sin(\pi t) \\ \cos(2\pi t) \end{bmatrix},$$

which corresponds to a bounding of $\delta = 1$. The control parameters are chosen as

$$k_q = 1,\ k_\omega = 1,\ \beta = 5,\ \epsilon_q = 0.03.$$

The following figures show the results of a tracking command to the desired states of

$$q_{d_i} = [\cos t \;\; \sin t]^T, \; \omega_d = [1 \;\; 1 \;\; 1]^T,$$

from the initial conditions

$$q_0(0) = [0.5\sqrt{3} \;\; 0.5]^T, \; q_1(0) = [0.5\sqrt{2} \;\; 0.5\sqrt{2}]^T,$$
$$q_2(0) = [0.5 \;\; 0.5\sqrt{3}]^T, \; \omega(0) = [0 \;\; 0 \;\; 0]^T.$$

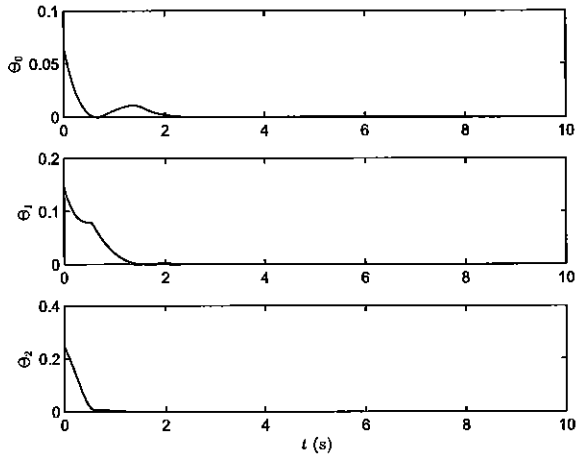

Figure 6.12: Time behavior of error function Θ.

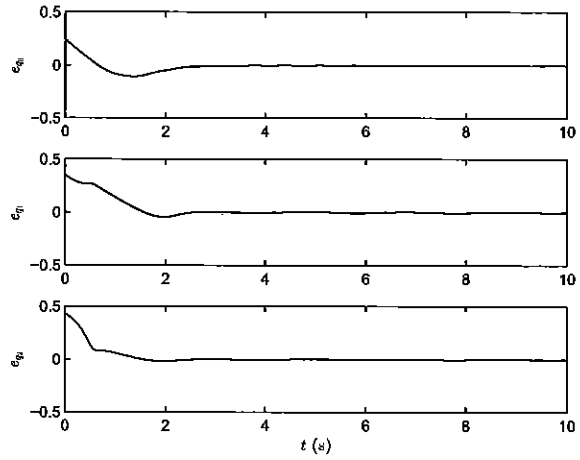

Figure 6.13: Time behavior of configuration error e_q.

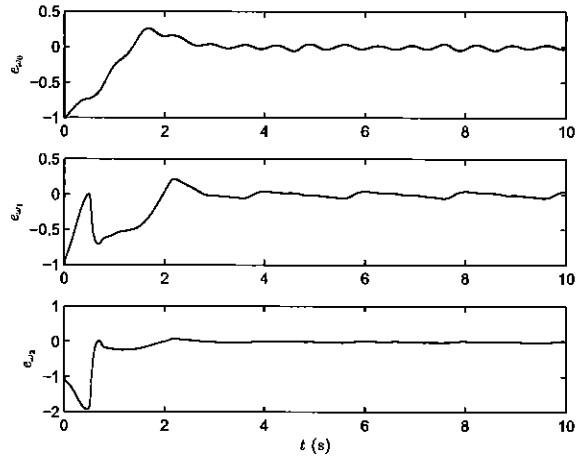

Figure 6.14: Time behavior of angular velocity error e_ω.

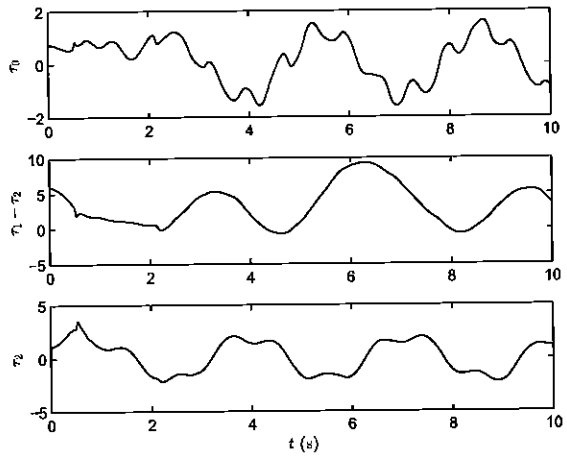

Figure 6.15: Time behavior of control torque τ.

Indicative of the ultimately uniformly bounded stability result, all errors converge within 3s, the largest of which is less than 0.05 in magnitude.

6.4 Robust Quaternion-based Nonlinear Tracking Control of a Quadrotor Attitude Test Bed Revisited

The following is to be published as a stand-alone journal paper, and attempts to create a direct global coordinate rendition of Hoffman et al. (2017). Robust tracking is once more desired of the quadrotor attitude test bed, but avoiding the ambiguities inherent in the quaternion-based derivation. Both the voltage input constraints and the measurements-only output feedback will be maintained. Experimental and simulation evidence of success will be provided.

6.4.1 Dynamic Model Formulation

Assuming a constant inertia matrix for the quadrotor hover system, the considered dynamics may be represented via Euler notation for rotating rigid bodies as (Hughes, 1994):

$$J\dot{\Omega} = -\Omega \times J\Omega + \tau, \tag{6.95}$$

where inertia matrix $J \in \mathbb{R}^{3\times 3}$ is positive definite and symmetric, $\Omega \in \mathbb{R}^3$ denotes the system angular velocity, and $\tau \in \mathbb{R}^3$ represents the generalized torque applied to the quadrotor. The operator $\times$ indicates a standard cross product between the column vectors on either side. The generalized torque term is a function of the same voltage inputs outlined in section 5.4, thus the reader is referred to the dynamic formulation remarks therein. Identifying the gyroscopic terms as bounded uncertainties to be separated from the control input, the control input and motor voltages can once more be defined as

$$Bu = \begin{bmatrix} blK_v^2\left(V_4^2 - V_2^2\right) \\ blK_v^2\left(V_3^2 - V_1^2\right) \\ dK_v^2\left(V_1^2 - V_2^2 + V_3^2 - V_4^2\right) \end{bmatrix}, \tag{6.96}$$

$$B \triangleq \begin{bmatrix} blK_v^2 & 0 & 0 \\ 0 & blK_v^2 & 0 \\ 0 & 0 & dK_v^2 \end{bmatrix}, \tag{6.97}$$

$$u = \begin{bmatrix} u_1 \\ u_2 \\ u_3 \end{bmatrix} = \begin{bmatrix} V_4^2 - V_2^2 \\ V_3^2 - V_1^2 \\ V_1^2 - V_2^2 + V_3^2 - V_4^2 \end{bmatrix}. \tag{6.98}$$

6.4.2 Kinematic Model Formulation

The following kinematic definitions demand exposition on the applied reference frames. An inertial frame and body-fixed frame share their origins at the center of mass of the hover system, to allow for the configuration of the quadrotor to be directly represented by the orientation of the body-fixed frame with respect to the inertial, specifically by a rotation matrix $R \in \mathsf{SO}(3)$. Special Orthogonal Group 3 is a well-defined manifold of 3×3 matrices subjected to the set of constraints

$$\mathsf{SO}(3) = \left\{ R \in \mathbb{R}^{3\times 3} : R^T R = I, \det R = 1 \right\}.$$

It then follows that the kinematics may be concisely defined by the expression

$$\dot{R} = R\hat{\Omega}, \tag{6.99}$$

where the $\hat{\cdot} : \mathbb{R}^3 \to so(3)$ operator denotes a conversion of the presented column vector into a skew-symmetric matrix that satisfies

$$\hat{a}b = a \times b, \ a, b \in \mathbb{R}^3.$$

It must be noted that at no point in the following derivation will a local consideration of $R(t)$ (quaternions, Euler angles, etc.) be used, ensuring that no singularities or ambiguities inherent in such representations will plague controller performance.

6.4.3 Control Objective

Consider the arbitrary and smooth attitude command $R_d(t) \in \mathsf{SO}(3)$, whose kinematics can be identified as

$$\dot{R}_d = R_d \hat{\Omega}_d, \tag{6.100}$$

where $\Omega_d(t) \in \mathbb{R}^3$ is the desired angular velocity. The objective of the proposed control law is to guide the quadrotor hover system to track the desired commands $R_d(t), \Omega_d(t)$. To accomplish this, error definitions for both system quantities are required, generated from a smooth, bounded, positive definite error measurement between actual and desired configuration. From this function, trajectory and time derivatives allow for expressions of the original two quantities that lie on the appropriate manifold and tangent space, respectively. (Lee, 2013) implements these error definitions to address a different source of system uncertainty, yet they are still relevant to the system presented:

$$\Psi(R, R_d) = \frac{1}{2} tr\left[G(I - R_d^T R)\right], \tag{6.101}$$

$$e_R(R, R_d) = \frac{1}{2} tr\left(G R_d^T R - R^T R_d G\right)^\vee, \tag{6.102}$$

$$e_\Omega = \Omega - R^T R_d \Omega_d, \tag{6.103}$$

where $\Psi(R, R_d) : \mathsf{SO}(3) \times \mathsf{SO}(3) \to \mathbb{R}$ denotes the attitude error function, $e_R(R, R_d) : \mathsf{SO}(3) \times \mathsf{SO}(3) \to \mathbb{R}^3$ represents the attitude error vector, $e_\Omega : \mathsf{SO}(3) \times \mathbb{R}^3 \times \mathsf{SO}(3) \times \mathbb{R}^3 \to \mathbb{R}^3$ is the angular velocity vector, and $G \in \mathbb{R}^{3\times3}$ is defined by $G = \mathsf{diag}\left[g_1, g_2, g_3\right], g_i \in \mathbb{R}^+$ and can be interpreted as a tuning gain for error conversion rate. This observation is made in light of the following statements, elaborated on in (Lee, 2013):

1. Ψ is positive definite about $R = R_d$.

Proof: $R_d^T R$ is the inner product between the actual and desired configurations, providing in simpler terms the cosine of the angle between them. This operator thus provides a maximum value of I if and only if the two configurations are identical. Thus, the statement holds for any arbitrary examples of R_d,R.

2. the combination of Darboux derivative, Lie group, and cotangent space operators on Ψ is given by

$$\mathrm{T}_I^* L_R(D_R\Psi(R, R_d)) = e_R. \tag{6.104}$$

Proof: More in-depth considerations of this technique are provided in Bullo and Lewis (2003), however the concept follows from above, and is referred to as a left-trivialized derivative. As Ψ is a function of the cosine of the angle between configurations, a trajectory-based derivative will provide a representation of their sine, noted by the skew nature of the expression within the parenthesis, an indication of a rotation by $\frac{\pi}{2}$. Each operator acts as follows:

$$\begin{aligned}
&D_R(\Psi) = -\frac{1}{2} G R_d, \\
&L_R(D_R\Psi) = -\frac{1}{2} G R_d^T R, \\
&\mathrm{T}_I^* L_R(D_R\Psi) = -\frac{1}{2}(R^T R_d G - G R_d^T R)^\vee \\
&= \frac{1}{2}(G R_d^T R - R^T R_d G)^\vee = e_R.
\end{aligned}$$

3. the critical points of Ψ that are shown by $e_R = 0$ are defined by $\{R_d\} \cup \{R_d exp(\pi \hat{s})\}, s \in \{e_1, e_2, e_3\}$.

Proof: The only scenarios where a critical point is seen occurs when $R = R_d$ and the rotation of such result of π about any of the three reference axes. The above union represents these scenarios.

4. the lower bound of Ψ is described as

$$b||e_{R,R_d}||^2 \leq \Psi(R, R_d), \tag{6.105}$$

such that b is defined as

$$\begin{aligned} b &= \frac{a_1}{a_2 + a_3}, \\ a_1 &= min\{g_1 + g_2, g_2 + g_3, g_3 + g_1\}, \\ a_2 &= max\{(g_1 - g_2)^2, (g_2 - g_3)^2, (g_3 - g_1)^2\}, \\ a_3 &= max\{(g_1 + g_2)^2, (g_2 + g_3)^2, (g_3 + g_1)^2\}. \end{aligned}$$

Proof: The above is elaborated in detail in Lee (2013).

5. consider a positive constant $\psi < a_1$. Provided that $\Psi < \psi$, an upper bound for Ψ is represented as

$$\Psi \leq \frac{a_1 a_4}{a_5(1 - \psi)}||e_R||^2, \tag{6.106}$$

$$a_4 = max\{g_1 + g_2, g_2 + g_3, g_3 + g_1\}, \tag{6.107}$$

$$a_5 = min\{(g_1 + g_2)^2, (g_2 + g_3)^2, (g_3 + g_1)^2\}. \tag{6.108}$$

Proof: Much like 4), the background to this conclusion is elaborated in Lee (2013).

The above five statements conclude that the original error function $\Psi(R, R_d)$ is not only positive definite but decrescent, indicating a convergence to the desired critical point (the control objective) with the application of an appropriate closed-loop system. Explicitly, $||\Psi|| \to 0$ as $||e_R||^2 \to 0$. Hence, it is only required that e_R be proven asymptotically converging to 0 in the subsequent stability analysis. On the

other hand, angular velocity error representation will require foresight. Consider the auxiliary error function

$$q(t) = e_\Omega + 2\alpha e_R - e_a, \tag{6.109}$$

where $e_a(t) \in \mathbb{R}^3$ is another auxiliary function to be defined in the following bank of filter statements, and $\alpha \in \mathbb{R}^{3\times3}$ is a positive diagonal tuning gain. While the control objective can be straightforwardly defined as

$$||e_R(t)|| \to 0, \ ||e_\Omega(t)|| \to 0,$$

It is best for the purpose of the following stability analysis that the complete error vector be defined as

$$z(t) = [e_R^T, q^T, e_a^T, \eta^T]^T, \tag{6.110}$$

where $\eta(t) \in \mathbb{R}^3$ is another filter output. Due to the definition of the auxiliary error signals, their convergence to 0 along with $e_R(t)$ ensures $e_\Omega(t)$'s convergence as well.

6.4.4 Control Development

It is the purpose of the designed control algorithm, and by extension the contribution of this section, to attain asymptotic tracking of the desired command through applying solely position measurements and outputs from the provided bank of dynamic filters, in spite of input-multiplicative uncertainty. The following subsections divide such considerations into open- and closed-loop aspects.

Open-Loop Error Dynamics

Auxiliary signals $\eta(t), e_a(t)$ are output variables from the following bank of dynamic filters (Xian et al., 2004):

$$\dot{p} = -(k+2\alpha)p - \eta + 2(k+\alpha)^2 e_R + e_R, \tag{6.111}$$

$$\dot{\eta} = p - \alpha\eta - 2(k+\alpha)e_R, \tag{6.112}$$

$$e_a = p - 2(k+\alpha)e_R, \tag{6.113}$$

where $k \in \mathbb{R}^{3\times3}$ is another positive diagonal tuning gain, and $p(t) \in \mathbb{R}^3$ denotes an internal filter variable. To progress, the remaining error dynamics are shown to be

$$\frac{d}{dt}(e_R) = E(R, R_d)e_\Omega, \tag{6.114}$$

$$\frac{d}{dt}(e_\Omega) = \dot{\Omega} + \hat{\Omega}R^T R_d \Omega_d - R^T R_d \dot{\Omega}_d, \tag{6.115}$$

$$E(R, R_d) = \frac{1}{2}(tr[R^T R_d G]I - R^T R_d G), \tag{6.116}$$

where it must be noted that the proof outlined in Lee (2013) concludes the bounding argument

$$||E(R, R_d)|| \leq \frac{1}{\sqrt{2}} tr[G].$$

Obtaining the time derivative of e_a, and applying the results of both the bank of filters and open loop error dynamics:

$$\dot{e}_a = -\alpha e_a - \eta + e_R - (k+\alpha)q - (k+\alpha)(2E - I)e_\Omega. \tag{6.117}$$

Also necessary is the time derivative of $q(t)$. Making use of both the above and the original dynamics, and multiplying through by the inertia matrix, the full open loop dynamics of such is

$$\begin{aligned} J\dot{q} = &-\Omega \times J\Omega + Bu + \chi(\Omega) + J\hat{\Omega}R^T R_d \Omega_d - JR^T R_d \dot{\Omega}_d \\ &- J\alpha e_a - J\eta + Je_R - J(k+\alpha)q - J(2kE - (k+\alpha))e_\Omega, \end{aligned} \tag{6.118}$$

where $\chi(\Omega)$ denotes the separated rotary inertia terms. To compress this expression in anticipation of the subsequent error analysis, the open loop error may be rewritten as

$$\begin{aligned} J\dot{q} &= \tilde{N} + Bu - J\alpha e_a - J(k+\alpha)q - J(2kE - (k+\alpha))e_\Omega, \\ \tilde{N} &= -\Omega \times J\Omega + \chi(\Omega) + J\hat{\Omega}R^T R_d \Omega_d - JR^T R_d \dot{\Omega}_d - J\eta + Je_R. \end{aligned} \tag{6.119}$$

By applying this substitution, the terms in $\tilde{N} \in \mathbb{R}^3$ can be bounded by a positive, globally invertible nondecreasing function of the total error vector defined in the control objective:

$$||\tilde{N}|| \leq \rho(||z||)||z||. \tag{6.120}$$

Closed-Loop Error System

Observing the final result for the open loop error dynamics and in foresight of the subsequent stability analysis yields the proposed control input term:

$$u(t) = (B^\sharp)^{-1}((k+\alpha)e_a(t) - (k+\alpha)e_R(t)), \tag{6.121}$$

where $B^\sharp \in \mathbb{R}^{3\times3}$ is composed of feedforward "best-guess" estimates $\hat{b}, \hat{d}, \hat{l}, \hat{K}_v \in \mathbb{R}^+$ of the uncertain physical parameters b, d, l, K_v. Moreover, $B^\sharp$ can be defined as

$$B^\sharp \triangleq \begin{bmatrix} \hat{b}\hat{l}\hat{K}_v^2 & 0 & 0 \\ 0 & \hat{b}\hat{l}\hat{K}_v^2 & 0 \\ 0 & 0 & \hat{d}\hat{K}_v^2 \end{bmatrix}. \tag{6.122}$$

Therefore, the closed-loop dynamics can be represented as

$$\begin{aligned} J\dot{q} =& \tilde{N} + \Gamma((k+\alpha)e_a - (k+\alpha)e_R) - J\alpha e_a \\ & - J(k+\alpha)q - J(2kE - (k+\alpha))e_\Omega, \end{aligned} \tag{6.123}$$

where $\Gamma = B(B^\sharp)^{-1}$ is the constant uncertain mismatch matrix, assumed to be positive definite and symmetric due to its components, as well as its inverse in turn.

The use of constant feed-forward estimates is justified in the local coordinate counterpart seen in section 5.4, and thus will be referred to for brevity.

It then follows that multiplying through by the inverse of the mismatch matrix provides

$$\begin{aligned} \Gamma^{-1}J\dot{q} =& \tilde{N}_1 + (k+\alpha)e_a - (k+\alpha)e_R - \Gamma^{-1}J\alpha e_a \\ & - \Gamma^{-1}J(k+\alpha)q - \Gamma^{-1}J(2kE - (k+\alpha))e_\Omega, \end{aligned} \tag{6.124}$$

where $\tilde{N}_1 = \Gamma^{-1}\tilde{N}$ is bounded by another positive globally invertible nondecreasing function

$$||\tilde{N}_1|| \leq \rho_1(||z||)||z||.$$

6.4.5 Stability Analysis

Consider the Lyapunov candidate function

$$V = \frac{1}{2}q^T\Gamma^{-1}Jq + \frac{1}{2}e_a^Te_a + \frac{1}{2}e_R^Te_R + \frac{1}{2}\eta^T\eta. \tag{6.125}$$

Taking its time derivative whilst applying filter definitions and closed-loop dynamics as appropriate yields

$$\begin{aligned}\dot{V} \leq & -\eta^T\alpha\eta - e_a^T\alpha(I+\Gamma^{-1}J)e_a - q^T\Gamma^{-1}J(k+\alpha)q \\ & - 2e_R^T\alpha(k+\alpha)e_R + \rho_2(||z||)||z||||q|| \\ & - e_\Omega^T\Gamma^{-1}J(2kE-(k+\alpha))e_\Omega \\ & - e_a^T[(k+\alpha)(2E-I)+k\Gamma^{-1}J(2E-I)]e_\Omega \\ & - e_a^T[2\alpha^2\Gamma^{-1}J+(k+\alpha)]e_R \\ & - e_\Omega^T[2\Gamma^{-1}J\alpha(2kE-(k+\alpha)+(k+\alpha)]e_R,\end{aligned} \tag{6.126}$$

where $\rho_2(||z||)||z||$, another positive globally invertible nondecreasing function, bounds the following expression $\tilde{N}_2$:

$$\tilde{N}_2 = \tilde{N}_1 + e_a^Te_R + e_R^TEe_\Omega.$$

Noting that all cross terms can be seen to be subtractions, they are thus allowable through the implementation of Sylvester's Criterion:

Sylvester's Criterion

Consider the cross terms and pertinent quadratics to represent a quadratic function

$$
\begin{aligned}
&r^T Q r = \\
&\begin{bmatrix} e_a \\ e_\Omega \\ e_R \end{bmatrix}^T \begin{bmatrix} \alpha(I+\Gamma^{-1}J) & A & B \\ A & \Gamma^{-1}J(2kE-(k+\alpha)) & C \\ B & C & 2\alpha(k+\alpha) \end{bmatrix} \begin{bmatrix} e_a \\ e_\Omega \\ e_R \end{bmatrix}, \\
&A = \frac{(k+\alpha)(2E-I)+k\Gamma^{-1}J(2E-I)}{2}, \\
&B = \frac{2\alpha^2\Gamma^{-1}J+(k+\alpha)}{2}, \\
&C = \frac{2\Gamma^{-1}J\alpha(2kE-(k+\alpha))+(k+\alpha)}{2}.
\end{aligned}
$$

So long as the leading principal minors are proven positive, the resulting quadratic function is positive definite.

Applying the above conditions requires the following to be true:

$$\lambda_m[\alpha] > 2\lambda_M[k]\frac{\lambda_M[(2E-I)(I+\Gamma^{-1}J)(2\Gamma^{-1}J-(2E-I))]}{\lambda_m[4(I+\Gamma^{-1}J)(\Gamma^{-1}J)+(2E-I)^2]},$$

provided that $2\lambda_m[\Gamma^{-1}J] > \lambda_M[2E-I]$ where λ_m, λ_M represent the minimum and maximum eigenvalues of their respective arguments, and

$$\Gamma^{-1}J : \mathsf{det}(Q) > 0.$$

The latter may be viewed as a limit on the allowable "best-guess" estimate mismatch with respect to the nominal system parameters, and equally so a limitation on the trace of the matrix G, the error convergence gain. Should all conditions be satisfied,

the time derivative can be further bounded as

$$\dot{V} \leq -a||z||^2 - \lambda_m[\Gamma^{-1}Jk]||q||^2 + \rho_2(||z||)||z||||q||,$$

where $a = \lambda_m[\alpha, \Gamma^{-1}J\alpha, Q]$. Completing the squares allows for further simplification:

$$\dot{V} \leq -\left(a - \frac{\rho_2^2(||z||)}{4\lambda_m[\Gamma^{-1}Jk]}\right)||z||^2. \tag{6.127}$$

The above inequality can therefore be expressed as

$$\dot{V} \leq -d||z||^2, \tag{6.128}$$

where $d \in \mathbb{R}^+$ represents a bounding constant defined over the domain D defined as

$$\mathsf{D} \triangleq \left\{z \in \mathbb{R}^{12} : ||z|| < \rho_2^{-1}\left(\sqrt{4\lambda_m[\Gamma^{-1}Jk]a}\right)\right\}.$$

The above domain, along with the completed time derivative of the candidate function, indicates that $z(t) \in \mathcal{L}_\infty$, along with all of its individual components within the given domain. By extension, $\Psi(t), e_\Omega(t) \in \mathcal{L}_\infty$. With bounded angular velocity tracking commands, $\Omega(t) \in \mathcal{L}_\infty$. With the original states confirmed bounded, $\dot{R}(t), \dot{e}_a(t) \in \mathcal{L}_\infty$. Given that both filter outputs are bounded, it can be said that $\dot{p}(t), p(t) \in \mathcal{L}_\infty$. Therefore, $\dot{\eta}(t) \in \mathcal{L}_\infty$. Both $e_R(t), e_a(t)$ being bounded confirm that $u(t) \in \mathcal{L}_\infty$. It then follows that the closed-loop error dynamics are bounded, represented as $\dot{q}(t) \in \mathcal{L}_\infty$. In doing so, all time derivatives of the components of $z(t)$ are bounded, thus $\dot{z}(t) \in \mathcal{L}_\infty$. Therefore, $z(t)$ is uniformly continuous in D. The candidate function and the final inequality (6.128) can then demonstrate that

$z(t) \in \mathcal{L}_\infty \cap \mathcal{L}_2$ in D. Barbalat's lemma may now be used to prove that (Khalil, 1996)

$$||z(t)||^2 \to 0 \text{ as } t \to \infty, \ \forall z(0) \in D.$$

Observing the original definition of $z(t)$ with the above conclusion determines that

$$||e_R(t)||, ||e_\Omega(t)|| \to 0 \text{ as } t \to \infty, \ \forall z(0) \in D.$$

The region of convergence is limited by given initial conditions, and therefore is considered locally asymptotically stable in the strictest sense. However, no restrictions exist on the governing control gain k, therefore it can be scaled arbitrarily large to incorporate larger sets of initial conditions. Hence, the complete result may be interpreted as semi-global asymptotic stability.

6.4.6 Numerical Simulation Results

To demonstrate the effectiveness of the derived attitude tracking controller, a simulation of the original dynamics were implemented with the proper virtual input - to - voltage conversion outlined in order to ensure voltage saturation considerations were in effect. The bank of dynamic filters shown in Equations (6.111) - (6.113) fulfill their purpose of providing velocity estimations for the control input seen in (6.121). It must be noted that while nominal values were applied for the inertia matrix, they are explicitly not used in the provided control law.

A direct comparison of the global-coordinate derived control law presented and a local-coordinate counterpart is also provided. Specifically, Hoffman et al. (2017) makes use of the same testbed and bank of filters system to address the same input-multiplicative uncertainty, but applies quaternion configuration and error. As a result,

a bound on the allowable initial conditions is established rather than one on the allowable mismatch. Therefore, by implementing identical system conditions and tracking commands, an exact comparison between local- and global-coordinate controllers can be firmly established. See (Hoffman et al., 2017) for the full derivation therein.

Both simulation results implement the following control gains:

$$\alpha = \mathsf{diag}\{2.7, 3, 3\},\ k = \mathsf{diag}\{4.2, 0.7, 0.7\},$$

with the feedforward "best-guess" estimate being determined from the estimated physical parameters seen in the following table and making use of Equation (6.122). In the case of the differential geometric controller, the matrix G is designed to be

$$G = \mathsf{diag}\{0.4, 0.4, 0.4\}.$$

In addition, a 10 percent noise factor was implemented to the position measurement to represent a more realistic scenario. Both control algorithms observed initial conditions corresponding to the following Euler angles:

$$\phi_o = 0\text{rad},\ \theta_o = 0.1\text{rad},\ \psi_o = \frac{\pi}{4}\text{rad}.$$

The desired tracking command was a regulation of yaw (ψ) to 0, a step command of $\frac{\pi}{18}$rad in pitch (θ), and a sinusoidal trajectory for roll described in radians as

$$\phi_d(t) = \frac{\pi}{9}\sin(0.1t).$$

The following first two figures demonstrate the convergence of the control laws' respective configuration error, while the latter two denote the required voltages to do

so, separated into each rotor.

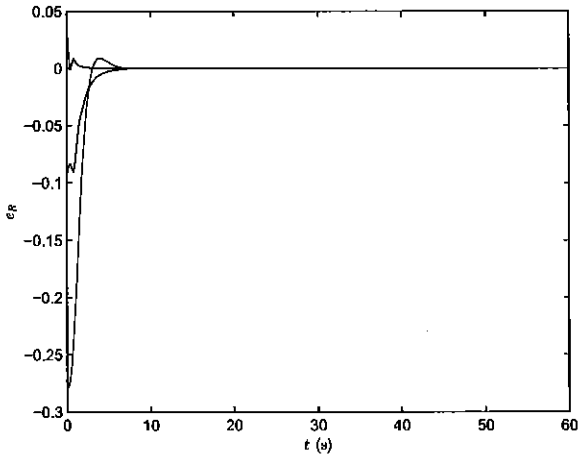

Figure 6.16: Configuration Error of Differential Geometric Controller.

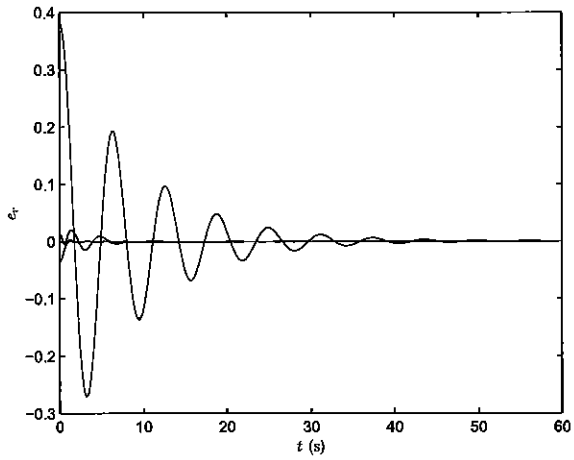

Figure 6.17: Configuration Error of Quaternion Controller.

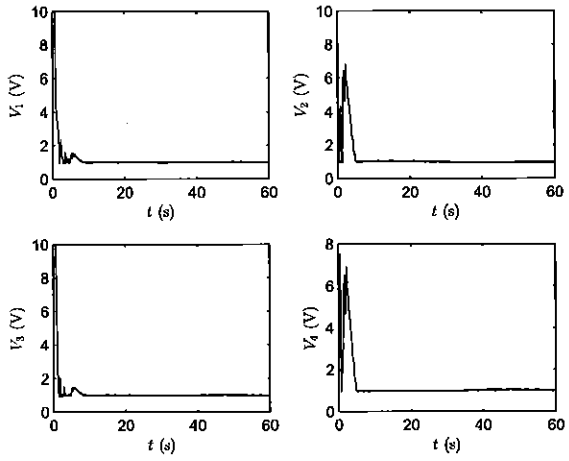

Figure 6.18: Applied Voltage Input of Differential Geometric Controller.

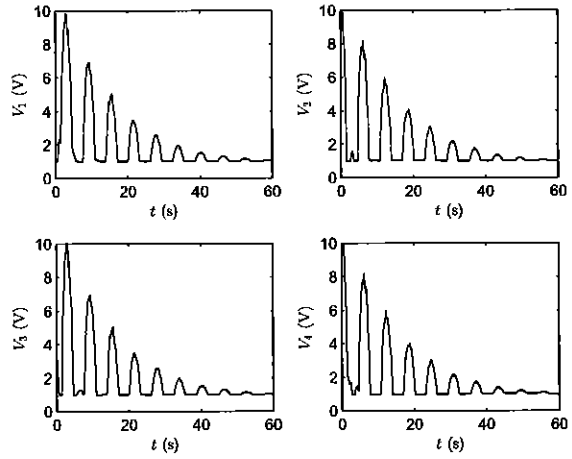

Figure 6.19: Applied Voltage Input of Quaternion Controller.

All provided figures clearly indicate the advantages of the proposed differential geometric controller. While the quaternion version requires a full minute to converge the error due to its limitation on initial conditions, the differential geometric controller efficiently arrives at the desired trajectory within 8s. This behavior is echoed in the voltage plots, where consecutive peaks from the former are required of the rotors

to obtain this pattern, whereas the latter rapidly arrives and maintains safe voltage levels.

6.4.7 Experimental Results

To confirm effectiveness of the derived controller in a real-life scenario, a experiment was conducted on standard Quanser quadrotor testbed, with the goal of tracking the combined step commands

$$\phi_d = \frac{\pi}{18} rad, \quad \theta_d = \frac{\pi}{18} rad, \quad \psi_d = \frac{\pi}{12} rad.$$

from the initial conditions of

$$\phi_o = 0 rad, \quad \theta_o = 0 rad, \quad \psi_o = 0 rad.$$

The estimated values from Table 5.4 and the simulation filter gains k and α are identical to the previous section, the only change being in matrix G to

$$G = \mathsf{diag}\{0.15, 0.15, 0.15\}.$$

The bank of dynamic filters still succeed in producing velocity estimates. The following figures demonstrate the error convergence and voltage use of the proposed control law.

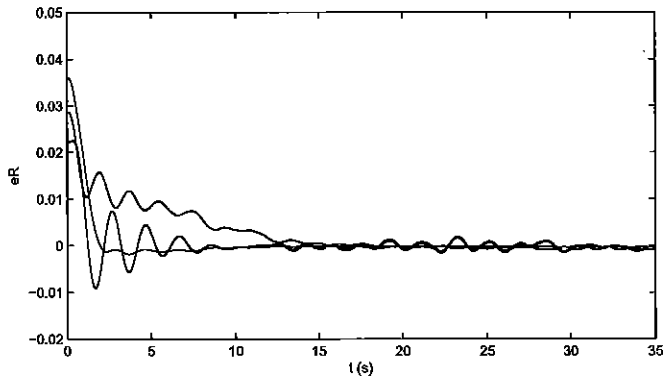

Figure 6.20: Experimental Configuration Error of Differential Geometric Controller.

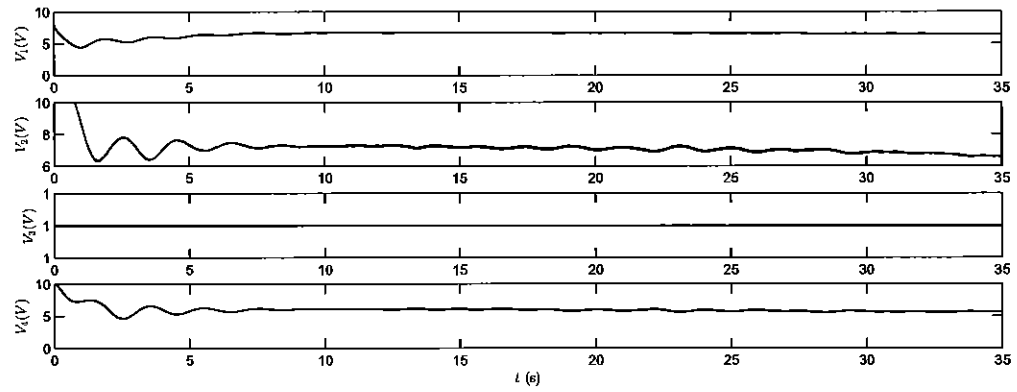

Figure 6.21: Experimental Applied Voltage Input of Differential Geometric Controller.

Despite the combined step commands, the control algorithm obtains effective convergence in 15s.

Chapter 7

Examples: Constraint Embedding of Unactuated Degrees of Freedom

The following chapter provides background literature on constraint embedding, as well as examples on the proposed manifold technique. Moreover, the examples shown are also seen in Hoffman and Reyhanoglu (2018). Overviews of unactuated constraints and robotic manipulators have been given in previous sections, and hence will be omitted to avoid redundancy.

7.1 Planar Rigid Body with Unactuated Sliding Mass

7.1.1 Model Formulation

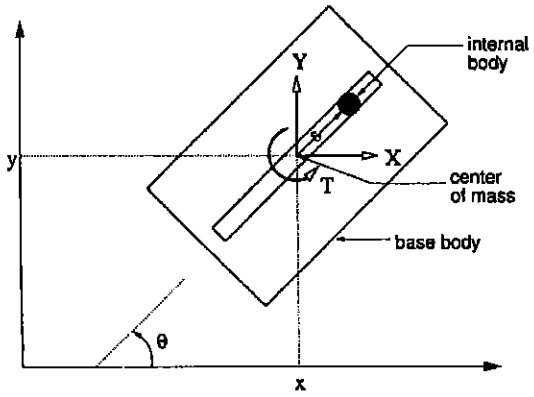

Figure 7.1: Planar Robot with Sliding Mass Schematic.

The system shown in the above figure, taken from Cho et al. (1998), depicts a robot composed of a base body and internal mass moving about a horizontal plane. Displacement of the main body's center of mass from the horizontal and vertical axes of an established inertial frame are denoted as x and y, respectively, while the rotational orientation of the body with respect to the horizontal is displayed as θ. The main body's mass is labeled as M while its moment of inertia is defined as I. The internal body is such that it slides along a track oriented along the longitudinal axis of the main body and is depicted as a point mass m. Thus, the distance from the mass to the main body center of mass is s. Three actuation efforts (X, Y, and T) act on the main body, while no direct actuation exists for the sliding mass.

In order to remain focused on the constraint operations, the Lagrangian dynamics

are directly presented:

$$(M+m)\ddot{x} + m\ddot{s}\cos\theta - ms\ddot{\theta}\sin\theta - 2m\dot{s}\dot{\theta}\sin\theta - ms\dot{\theta}^2\cos\theta = X, \tag{7.1}$$

$$(M+m)\ddot{y} + m\ddot{s}\sin\theta + ms\ddot{\theta}\cos\theta + 2m\dot{s}\dot{\theta}\cos\theta - ms\dot{\theta}^2\sin\theta = Y, \tag{7.2}$$

$$(I+ms^2)\ddot{\theta} + ms\ddot{y}\cos\theta - ms\ddot{x}\sin\theta = T, \tag{7.3}$$

$$\ddot{s} + \ddot{x}\cos\theta + \ddot{y}\sin\theta - s\dot{\theta}^2 = 0. \tag{7.4}$$

The control objective then becomes to avoid displacement of the sliding mass from the main body center of mass, or $s = 0$. The desired system dynamics are then expressed with the omission of the sliding mass's dynamics:

$$(M+m)\ddot{x} = X, \tag{7.5}$$

$$(M+m)\ddot{y} = Y, \tag{7.6}$$

$$I\ddot{\theta} = T, \tag{7.7}$$

$$\ddot{x}\cos\theta + \ddot{y}\sin\theta = 0. \tag{7.8}$$

Using the procedure outlined in Chapter 4, the components required for the general

formulation can be assembled as

$$q = [x, y, \theta]^T, \tag{7.9}$$

$$Q = [X, Y, T]^T, \tag{7.10}$$

$$A = [\cos\theta, \sin\theta, 0]^T, \tag{7.11}$$

$$M = \begin{bmatrix} M+m & 0 & 0 \\ 0 & M+m & 0 \\ 0 & 0 & I \end{bmatrix}, \tag{7.12}$$

$$F = S = 0, \tag{7.13}$$

$$C = 1. \tag{7.14}$$

By observation it can be seen that $G = 0$, and

$$Bu = \begin{bmatrix} \frac{1}{M+m} & 0 & 0 \\ 0 & \frac{1}{M+m} & 0 \\ 0 & 0 & \frac{1}{I} \end{bmatrix} \begin{bmatrix} X \\ Y \\ T \end{bmatrix} = \begin{bmatrix} \frac{X}{M+m} \\ \frac{Y}{M+m} \\ \frac{T}{I} \end{bmatrix}. \tag{7.15}$$

Following through, the projection operator is assembled as

$$P = \begin{bmatrix} 1 & 0 & 0 \\ 0 & 1 & 0 \\ 0 & 0 & 1 \end{bmatrix} - \begin{bmatrix} \cos^2\theta & \cos\theta\sin\theta & 0 \\ \cos\theta\sin\theta & \sin^2\theta & 0 \\ 0 & 0 & 0 \end{bmatrix} = \begin{bmatrix} \sin^2\theta & -\cos\theta\sin\theta & 0 \\ -\cos\theta\sin\theta & \cos^2\theta & 0 \\ 0 & 0 & 1 \end{bmatrix}. \tag{7.16}$$

These components culminate in the explicit mapping between control actuation and

embedded dynamics:

$$\begin{bmatrix} \ddot{x} \\ \ddot{y} \\ \ddot{\theta} \end{bmatrix} = \begin{bmatrix} \frac{\sin^2\theta}{M+m}X - \frac{\sin\theta\cos\theta}{M+m}Y \\ \frac{-\sin\theta\cos\theta}{M+m}X + \frac{\cos^2\theta}{M+m}Y \\ \frac{T}{I} \end{bmatrix}. \tag{7.17}$$

A singular relationship between $\ddot{x}$ and $\ddot{y}$ is readily seen and expected due to the second-order nonholonomic constraint. Through the criteria in Hervas and Reyhanoglu (2015), it is seen that the system is strongly reachable and controllable. As one example to achieve system stability (though far from being the only solution), a discontinuous feedback law will be created through the derivations shown in Reyhanoglu et al. (1999b) to obtain regulation to the origin.

7.1.2 Controller Design

The following control design is a variant of that seen in Reyhanoglu et al. (1999b), under the observation that the sliding mass case is a special case of the robotic system seen therein, where the sliding mass's constant displacement from the actuation focus point c is zero, and no spring parameters are observed. Thus, assume $\frac{-\pi}{2} < \theta < \frac{\pi}{2}$, and consider the control inputs as

$$\ddot{\theta} = u_1, \tag{7.18}$$

$$\ddot{y} = u_2, \tag{7.19}$$

$$\ddot{x} = u_3. \tag{7.20}$$

u_3 may then be written as a function of u_2:

$$u_3 = -u_2 \tan\theta. \tag{7.21}$$

Consider the reduced order system

$$\dot{\theta} = v_1, \tag{7.22}$$

$$\dot{y} = v_2, \tag{7.23}$$

$$\dot{x} = \omega - v_2 \tan\theta, \tag{7.24}$$

where

$$\omega = \dot{x} + \dot{y} \tan\theta, \tag{7.25}$$

$$\dot{\omega} = v_1 v_2 \sec^2\theta. \tag{7.26}$$

At this point, the assumption that the initial angle $\theta_o \neq 0$ is required. It then follows that a discontinuous coordinate transformation can be made such that

$$\eta_1 = y, \tag{7.27}$$

$$\eta_2 = \frac{x}{\theta}, \tag{7.28}$$

$$\eta_3 = \frac{\omega}{\theta}. \tag{7.29}$$

The transformed reduced system can now be arranged in the kinematic arrangement

$$\dot{\theta} = v_1, \tag{7.30}$$

$$\dot{\eta}_1 = v_2, \tag{7.31}$$

$$\dot{\eta}_2 = \eta_3 - \frac{v_1}{\theta}\eta_2 - \frac{\tan\theta}{\theta}v_2, \tag{7.32}$$

$$\dot{\eta}_3 = -\frac{v_1}{\theta}\eta_3 + \frac{v_1 v_2}{\theta}\sec^2\theta. \tag{7.33}$$

Let the feedback control law be defined as

$$(v_1, v_2) = (-k\theta, -l\eta), \tag{7.34}$$

$$l = [l_1, l_2, l_3], \tag{7.35}$$

$$\eta = [\eta_1, \eta_2, \eta_3]^T \tag{7.36}$$

where $k, l_i \in \mathbb{R}^+$ are tuning gains. Applying this controller produces the closed-loop dynamics

$$\dot{\theta} = -k\theta, \tag{7.37}$$

$$\dot{\eta}_1 = -l_1\eta_1 - l_2\eta_2 - l_3\eta_3, \tag{7.38}$$

$$\dot{\eta}_2 = k\eta_2 + \eta_3 + \frac{\tan\theta}{\theta}(l_1\eta_1 + l_2\eta_2 + l_3\eta_3), \tag{7.39}$$

$$\dot{\eta}_3 = k\eta_3 + k\sec^2\theta(l_1\eta_1 + l_2\eta_2 + l_3\eta_3), \tag{7.40}$$

Assembled into a matrix equation, the system then becomes

$$\dot{\eta} = (A_1 + A_2(\theta))\eta, \tag{7.41}$$

$$A_1 = \begin{bmatrix} -l_1 & -l_2 & -l_3 \\ l_1 & k + l_2 & 1 + l_3 \\ kl_1 & kl_2 & k + kl_3 \end{bmatrix}, \tag{7.42}$$

$$A_2 = \begin{bmatrix} 0 & 0 & 0 \\ l_1 r_1 & l_2 r_1 & l_3 r_1 \\ kl_1 r_2 & kl_2 r_2 & kl_3 r_2 \end{bmatrix}, \tag{7.43}$$

$$r_1(\theta) = \frac{\tan\theta}{\theta} - 1, \tag{7.44}$$

$$r_2(\theta) = \sec^2\theta - 1. \tag{7.45}$$

The above system of equations is exponentially convergent for $\theta, \eta \to 0$, so long as A_1 is a Hurwitz matrix. The original reduced order system must now be observed:

$$\dot{\theta} = -k\theta, \tag{7.46}$$

$$\dot{y} = -l_1 y - l_2 \frac{x}{\theta} - l_3 \frac{\omega}{\theta}, \tag{7.47}$$

$$\dot{x} = \omega + \tan\theta \left(l_1 y + l_2 \frac{x}{\theta} + l_3 \frac{\omega}{\theta} \right), \tag{7.48}$$

$$\dot{\omega} = k\theta \sec^2\theta \left(l_1 y + l_2 \frac{x}{\theta} + l_3 \frac{\omega}{\theta} \right), \tag{7.49}$$

In turn, the original control inputs are related through:

$$u_1 = \dot{v}_1, \tag{7.50}$$

$$u_2 = \dot{v}_2. \tag{7.51}$$

The complete control input may now be assembled as

$$u_1 = -K(\dot{\theta} + k\theta) - k\dot{\theta}, \tag{7.52}$$

$$u_2 = -L\left(\dot{y} + l_1 y + l_2\frac{x}{\theta} + l_3\frac{\omega}{\theta}\right) - l_1\dot{y} - l_2\left(\frac{\dot{x}\theta - x\dot{\theta}}{\theta^2}\right) - l_3\left(\frac{\dot{\omega}\theta - \omega\dot{\theta}}{\theta^2}\right), \tag{7.53}$$

$$u_3 = -u_2\tan\theta, \tag{7.54}$$

so long as $L \in \mathbb{R}^+$, $K > k$. With the application of a backstepping-esque procedure, a $\theta = 0$ scenario can be avoided. One final transformation is needed:

$$\zeta_1 = \dot{\theta} + k\theta, \tag{7.55}$$

$$\zeta_2 = \dot{y} + l_1 y + l_2\frac{x}{\theta} + l_3\frac{\omega}{\theta}. \tag{7.56}$$

The set of transformed coordinates (θ, η, ζ) can be arranged through their kinematics concisely:

$$\dot{\theta} = -k\theta + \zeta_1, \tag{7.57}$$

$$\dot{\zeta}_1 = -K\zeta_1, \tag{7.58}$$

$$\dot{\zeta}_2 = -L\zeta_2, \tag{7.59}$$

$$\dot{\eta} = (A_1 + \bar{A}_2)\eta + h, \tag{7.60}$$

$$\bar{A}_2 = \begin{bmatrix} 0 & 0 & 0 \\ l_1 r_1 & l_2 r_1 - \frac{\zeta_1}{\theta} & l_3 r_1 \\ -l_1 r_3 & -l_2 r_3 & -l_3 r_3 - \frac{\zeta_1}{\theta} \end{bmatrix}, \tag{7.61}$$

$$h = \begin{bmatrix} \zeta_2 \\ (r_1 - 1)\zeta_2 \\ (k + r_3)\zeta_2 \end{bmatrix}, \tag{7.62}$$

$$r_3(\zeta, \theta) = \frac{\zeta_1}{\theta} + \left(\frac{\zeta_1}{\theta} - k\right)(\sec^2\theta - 1). \tag{7.63}$$

where A_1, r_1 is identical to the factors seen in the first transformation. Once more, the presented system of equations is exponentially convergent under the criteria shown in Reyhanoglu et al. (1999b).

7.1.3 Simulations

To demonstrate controller effectiveness, the following benchmark system is established for simulation:

Table 7.1: Physical parameters of the planar robot with sliding mass.

Parameter	Value
M	1.0 kg
m	0.1 kg
I	1.5 kg m^2

The system is subjected to the initial conditions

$$x_o = y_o = 0.5m,$$
$$\theta_o = \frac{\pi}{4} rad,$$
$$\dot{x}_o = \dot{y}_o = 0m/s,$$
$$\dot{\theta}_o = 0rad/s,$$

The control gains selected to bring the system to the origin are

$$k = 1,$$
$$l = [3, -15, 11.5],$$
$$K = L = 5.$$

The following figures demonstrate controller efficiency.

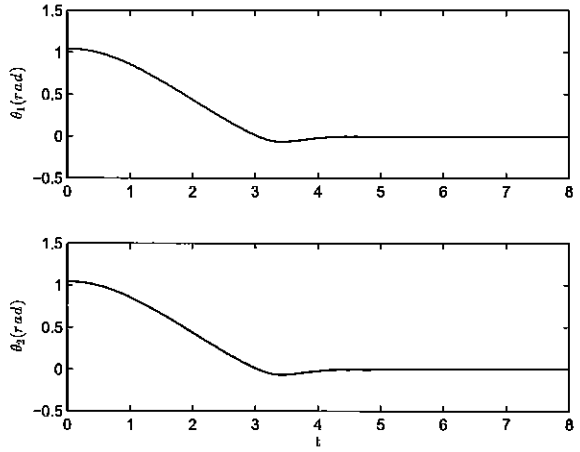

Figure 7.2: Planar robot angular behavior.

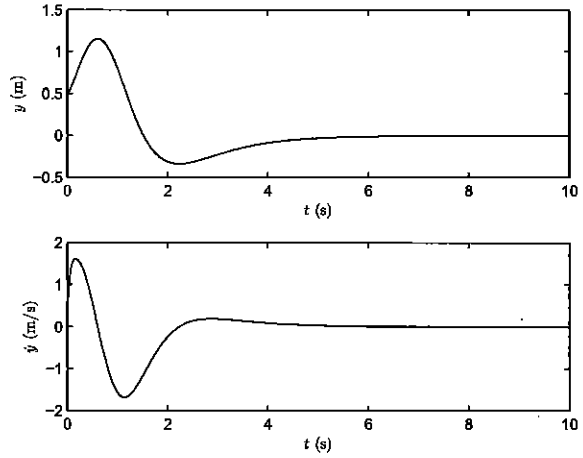

Figure 7.3: Planar robot vertical behavior.

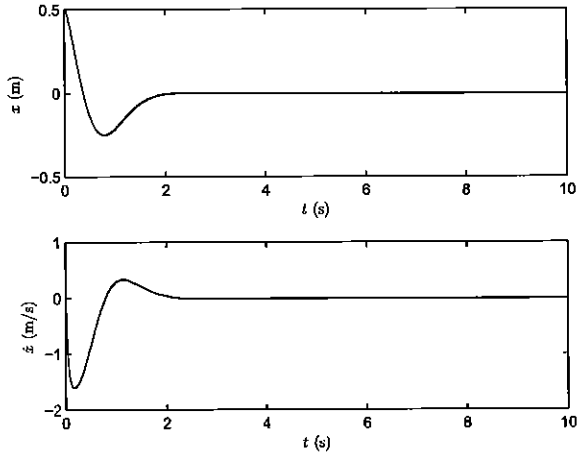

Figure 7.4: Planar robot horizontal behavior.

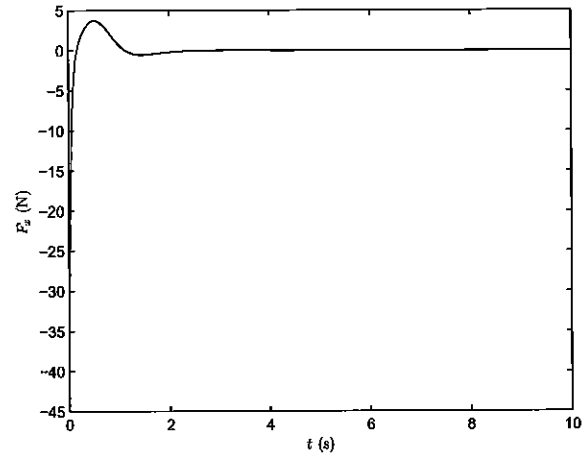

Figure 7.5: Planar robot horizontal actuation effort.

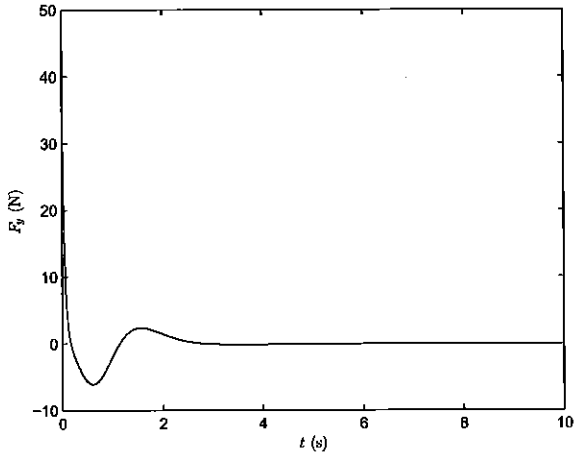

Figure 7.6: Planar robot vertical actuation effort.

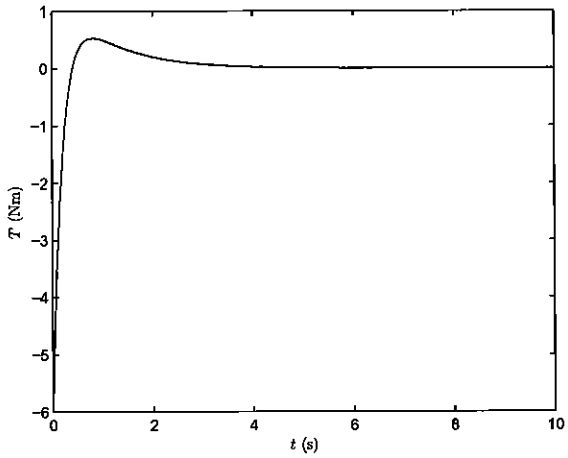

Figure 7.7: Planar robot torque actuation.

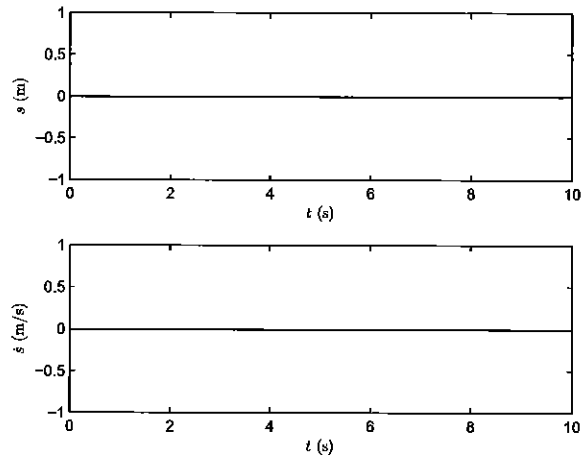

Figure 7.8: Planar robot sliding mass behavior.

It can be seen that the robot converges to the desired command within 6s. The last figure provides proof that the unactuated sliding mass is never provoked, proving modeling effectiveness.

7.2 PPR Robot with Unactuated Arm Oscillation

7.2.1 Model Formulation

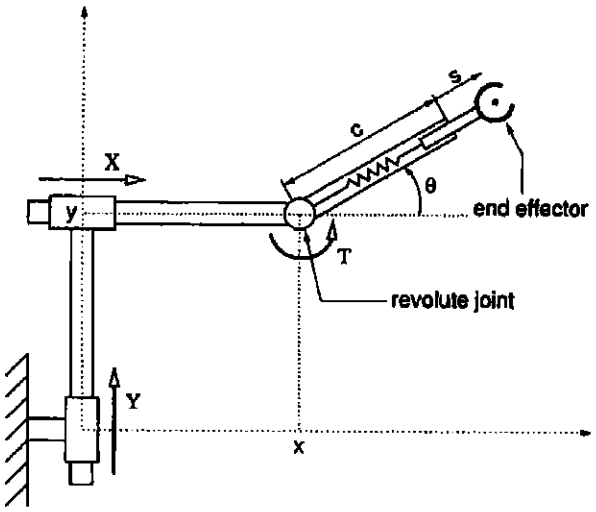

Figure 7.9: Prismatic-Prismatic-Revolute Robot Schematic.

The above diagram displays a prismatic-prismatic-revolute (PPR) robotic manipulator plagued by oscillations along the end effector arm, as explored in Reyhanoglu et al. (1999b). Referred to in the previous section, this system represents a more general case of the sliding mass scenario, where the sliding mass equilibrium is located a constant distance away from the actuated point while being subjected to spring considerations.

Let the mass of the oscillating end effector be m. The actuated hub moves on the

horizontal plane through the prismatic arms acting along the XY plane as shown, with the inertial frame for displacement reference. Thus, the displacement of the hub can be described as (x, y). A torque T acts directly on the hub, orienting the end effector arm an angle θ. The base length of the arm is c, but faces an unactuated deflection from equilibrium s. The spring that causes this is a restoring constant denoted k_s.

For convenience, Lagrange's equations of motion for the end effector are provided directly:

$$m(\ddot{x} + \ddot{s}\cos\theta - 2\dot{s}\dot{\theta}\sin\theta - (c+s)[\ddot{\theta}\sin\theta + \dot{\theta}^2\cos\theta]) = X, \tag{7.64}$$

$$m(\ddot{y} + \ddot{s}\sin\theta + 2\dot{s}\dot{\theta}\cos\theta + (c+s)[\ddot{\theta}\cos\theta - \dot{\theta}^2\sin\theta]) = Y, \tag{7.65}$$

$$(I_a + m(c+s)^2)\ddot{\theta} - m(c+s)\ddot{x}\sin\theta + m(c+s)\ddot{y}\cos\theta + 2m(c+s)\dot{s}\dot{\theta} = T, \tag{7.66}$$

$$\ddot{s} + \ddot{x}\cos\theta + \ddot{y}\sin\theta - (c+s)\dot{\theta}^2 + \frac{k_s}{m}s = 0, \tag{7.67}$$

where I_a is the moment of inertia for the revolute arm. It is desired that the unactuated degree of freedom never be perturbed, $s = 0$. Then, the original dynamics are simplified:

$$m(\ddot{x} - c[\ddot{\theta}\sin\theta + \dot{\theta}^2\cos\theta]) = X, \tag{7.68}$$

$$m(\ddot{y} + c[\ddot{\theta}\cos\theta - \dot{\theta}^2\sin\theta]) = Y, \tag{7.69}$$

$$(I_a + mc^2)\ddot{\theta} - mc\ddot{x}\sin\theta + mc\ddot{y}\cos\theta = T, \tag{7.70}$$

$$\ddot{x}\cos\theta + \ddot{y}\sin\theta - c\dot{\theta}^2 = 0. \tag{7.71}$$

In preparation for the constraint mapping, identification of the required terms is

determined:

$$q = [x, y, \theta]^T, \tag{7.72}$$

$$A = [\cos\theta, \sin\theta, 0], \tag{7.73}$$

$$C = 1, \tag{7.74}$$

$$S = -c\dot{\theta}^2, \tag{7.75}$$

$$Q = [X, Y, T]^T, \tag{7.76}$$

$$F = [-mc\dot{\theta}^2\cos\theta, -mc\dot{\theta}^2\sin\theta, 0]^T, \tag{7.77}$$

$$M = \begin{bmatrix} m & 0 & -mc\sin\theta \\ 0 & m & mc\cos\theta \\ -mc\sin\theta & mc\cos\theta & I_a' \end{bmatrix}, \tag{7.78}$$

where $I'_a = I_a + mc^2$. Identifying the final result terms produces

$$
\begin{aligned}
G &= -M^{-1}F \\
&= \frac{1}{I_a}\begin{bmatrix} c^2\cos^2\theta - \frac{I'_a}{m} & c^2\cos\theta\sin\theta & -c\sin\theta \\ c^2\cos\theta\sin\theta & c^2\sin^2\theta - \frac{I'_a}{m} & c\cos\theta \\ -c\sin\theta & c\cos\theta & -1 \end{bmatrix}\begin{bmatrix} -mc\dot{\theta}^2\cos\theta \\ -mc\dot{\theta}^2\sin\theta \\ 0 \end{bmatrix} \\
&= \begin{bmatrix} c\dot{\theta}^2\cos\theta \\ c\dot{\theta}^2\sin\theta \\ 0 \end{bmatrix}, \qquad (7.79)
\end{aligned}
$$

$$
\begin{aligned}
Bu &= M^{-1}Q \\
&= \frac{1}{I_a}\begin{bmatrix} c^2\cos^2\theta - \frac{I'_a}{m} & c^2\cos\theta\sin\theta & -c\sin\theta \\ c^2\cos\theta\sin\theta & c^2\sin^2\theta - \frac{I'_a}{m} & c\cos\theta \\ -c\sin\theta & c\cos\theta & -1 \end{bmatrix}\begin{bmatrix} X \\ Y \\ T \end{bmatrix} \\
&= \begin{bmatrix} \frac{1}{I_a}\left[X\left(\frac{I'_a}{m} - c^2\cos^2\theta\right) - Yc^2\cos\theta\sin\theta + Tc\sin\theta\right] \\ \frac{1}{I_a}\left[Y\left(\frac{I'_a}{m} - c^2\cos^2\theta\right) - Xc^2\cos\theta\sin\theta + Tc\sin\theta\right] \\ \frac{1}{I_a}(Xc\sin\theta - Yc\cos\theta + T) \end{bmatrix}, \qquad (7.80)
\end{aligned}
$$

$$
\begin{aligned}
P &= \begin{bmatrix} 1 & 0 & 0 \\ 0 & 1 & 0 \\ 0 & 0 & 1 \end{bmatrix} - \begin{bmatrix} \cos^2\theta & \cos\theta\sin\theta & 0 \\ \cos\theta\sin\theta & \sin^2\theta & 0 \\ 0 & 0 & 0 \end{bmatrix} \\
&= \begin{bmatrix} \sin^2\theta & -\cos\theta\sin\theta & 0 \\ -\cos\theta\sin\theta & \cos^2\theta & 0 \\ 0 & 0 & 1 \end{bmatrix}. \qquad (7.81)
\end{aligned}
$$

Dynamic-actuation mapping is then explicitly shown by

$$\begin{bmatrix} \ddot{x} \\ \ddot{y} \\ \ddot{\theta} \end{bmatrix} = \begin{bmatrix} \sin^2\theta & -\cos\theta\sin\theta & 0 \\ -cos\theta\sin\theta & \cos^2\theta & 0 \\ 0 & 0 & 1 \end{bmatrix} \cdot \begin{bmatrix} c\dot{\theta}^2\cos\theta + \frac{1}{I_a}\left[X\left(\frac{I'_a}{m} - c^2\cos^2\theta\right) - Yc^2\cos\theta\sin\theta + Tc\sin\theta\right] \\ c\dot{\theta}^2\sin\theta + \frac{1}{I_a}\left[Y\left(\frac{I'_a}{m} - c^2\cos^2\theta\right) - Xc^2\cos\theta\sin\theta + Tc\sin\theta\right] \\ \frac{1}{I_a}(Xc\sin\theta - Yc\cos\theta + T) \end{bmatrix} + \begin{bmatrix} c\dot{\theta}^2\cos\theta \\ c\dot{\theta}^2\sin\theta \\ 0 \end{bmatrix} \cdot \tag{7.82}$$

7.2.2 Controller Design

The second-order nonholonomic constraint once again causes the vertical and horizontal actuation to be coupled in a singular fashion. Therefore, controller implementation must be appropriate for nonholonomic constraints. Particularly, the algorithm outlined in Reyhanoglu et al. (1999b) will be used here, and the reader is referred to the previous section and the original publication for elaboration. As such, the proposed controller, under the restrictions of $\frac{-\pi}{2} < \theta < \frac{\pi}{2}$ and $\theta_o \neq 0$, is proposed:

$$\ddot{\theta} = u_1 = -K(\dot{\theta} + k\theta) - k\dot{\theta}, \tag{7.83}$$

$$\ddot{y} = u_2 = -L\left(\dot{y} + l_1 y + l_2\frac{x}{\theta} + l_3\frac{\omega}{\theta}\right) - l_1\dot{y} - l_2\left(\frac{\dot{x}\theta - x\dot{\theta}}{\theta^2}\right) - l_3\left(\frac{\dot{\omega}\theta - \omega\dot{\theta}}{\theta^2}\right), \tag{7.84}$$

$$\ddot{x} = u_3 = -u_2\tan\theta + c\dot{\theta}^2\sec\theta, \tag{7.85}$$

where ω, L, K, k, l are identically defined as in the planar robot derivation. Reyhanoglu et al. (1999b) then proves the exponential convergence of the resulting closed-loop system to the origin.

7.2.3 Simulations

Confirmation of the modeling and control techniques provided is seen through the following benchmark system:

Table 7.2: Physical parameters of the PPR robot.

Parameter	Value
m	1.0 kg
c	1 m
I_a	2 kg m^2
k_s	200 N/m

The system starts at the initial conditions of

$$x_o = y_o = 0.25\,\text{m},\ \theta_o = \frac{\pi}{3}\,\text{rad},\ \dot{\text{x}}_o = \dot{\text{y}}_o = 0\,\text{m/s},\ \dot{\theta}_o = 0\,\text{rad/s},$$

and the chosen control gains for regulation to the origin are

$$k = 1,\ l = [3, -15, 11.5],\ K = L = 5.$$

The closed-loop system behavior is seen in the following plots.

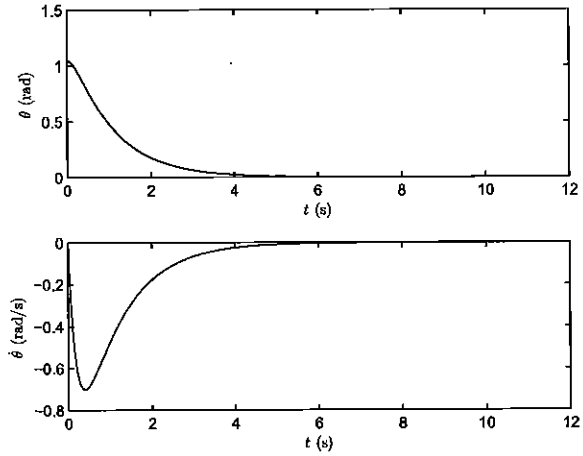

Figure 7.10: PPR angular behavior.

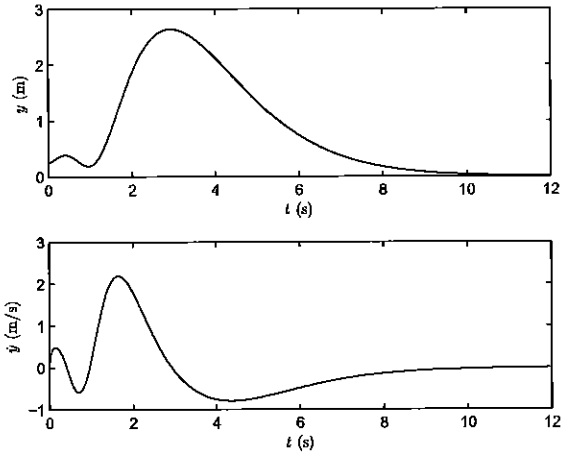

Figure 7.11: PPR vertical behavior.

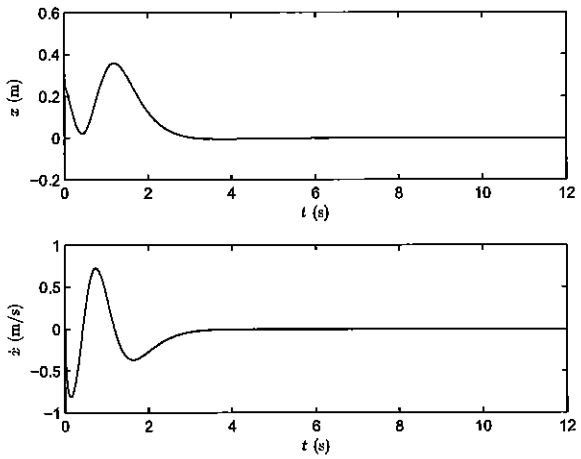

Figure 7.12: PPR horizontal behavior.

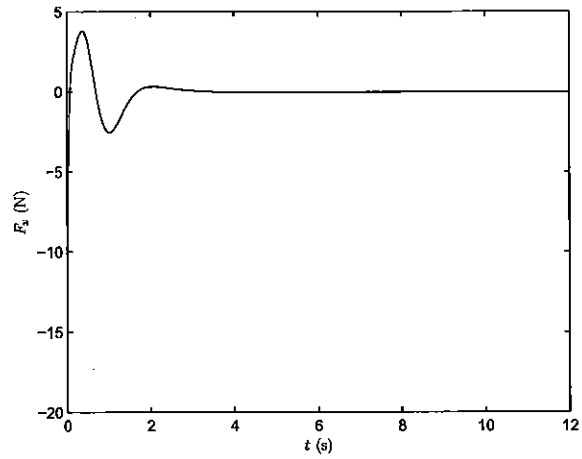

Figure 7.13: PPR horizontal actuation effort.

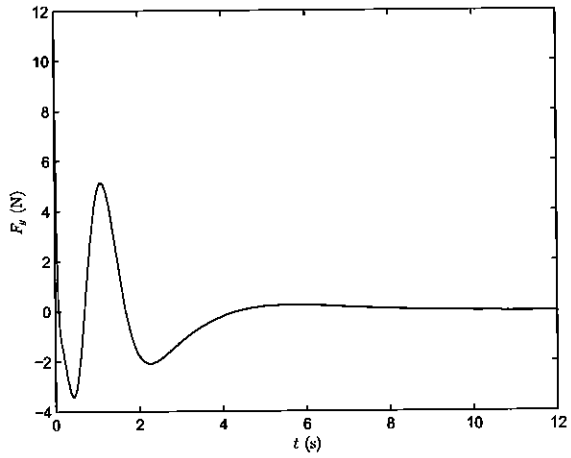

Figure 7.14: PPR vertical actuation effort.

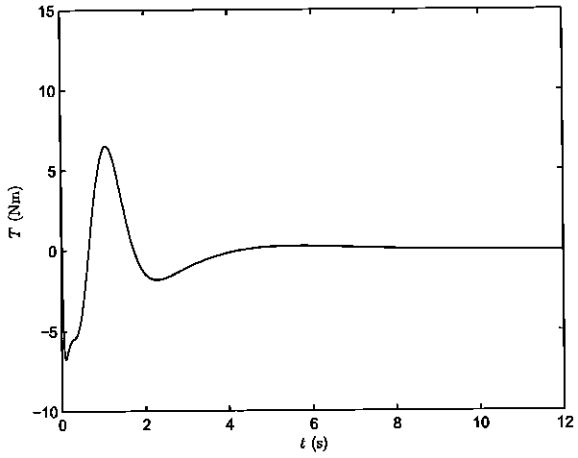

Figure 7.15: PPR torque actuation.

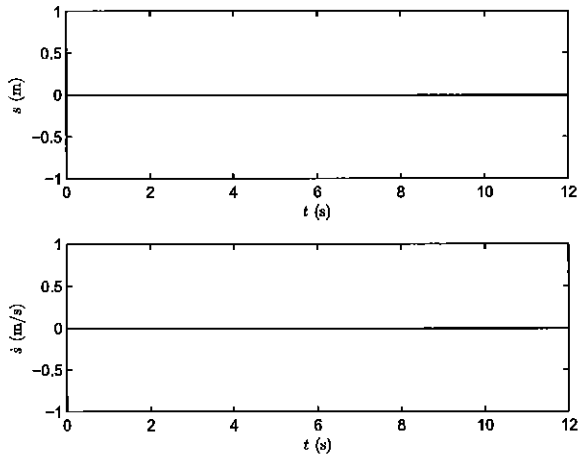

Figure 7.16: PPR end effector behavior.

The described control objective is reached within 10s, with the final graph demonstrating that the end effector is never perturbed.

Chapter 8

Conclusions and Future Research

The dynamical formulation of underactuated systems in local and global coordinate perspectives, as well as the modeling of unactuated degrees of freedom constraints, have been expanded on in the provided document. Through the application of robotics and aerospace systems, equations of motion are established that allow for in-depth analysis of dynamical coupling and ultimately an effective controller for the purpose of each provided control objective. Methods for such control design include traditional Lyapunov stability analysis, notch filter/nonlinear proportional-derivative algorithms, and discontinuous feedback. Two contributions to the state-of-the-art can be seen: 1) The establishment of a general procedure for deriving both equations of motion and control paradigms in terms of singularity-free manifold trajectories, and 2) The closed-form modeling of constraints due to unactuated degrees of freedom, also through the use of manifolds. The effectiveness of these methods has been clearly demonstrated in simulations and experiments, to include: hybrid robotic manipulators with one and two torques, a compliant base robotic manipulator, a 3D revolute robot, a Quanser quadrotor attitude test bed, a planar robot subjected to an internal sliding mass, and a planar PPR robot with an elastic end-effector.

Further potential may be gleaned from these concepts. Naturally, application to increasingly elaborate systems will yield more insight, as well as highlight further the advantage of manifold techniques to provide concise results. Moreover, fundamental extensions should also be considered in future research focuses, some examples of which are:

1. Application of the general global coordinate technique to previously simplified dynamics, or those never before derived: The examples given in this document were specifically chosen to compare to local coordinate counterparts, for the purpose of demonstrating their equivalency. Since this has now been determined, full potential of the process will be seen in addressing systems whose dynamics previously required simplifications that restricted modeling accuracy, or those that have yet to be fully derived in a closed-form manner.

2. Manifold-based physical limitation constraints: it must be stressed here that manifold definition is restricted only by the available states provided (ex: configuration spaces may only restrict configuration), and the form in which they are presented. Thus, researcher imagination becomes a critical resource in creating manifolds that incorporate constraints representing physical limitations. An interesting example of this is maximum energy or power available for control input. For such a case, optimality techniques will likely be required, necessitating care in the original action integral.

3. Extension of the constraint-embedding procedure to multiple unactuated degrees of freedom: The examples provided suffered only one constraint, in order to compare modeling and control results to previous literature. The derivation does not demand this special case, and can readily model more constrained dynamics. A noteworthy suggestion is the challenge of a cargo plane observing a

runaway cargo box. Control of such a setup would be especially difficult, as the already-underactuated cargo plane will face six degrees of freedom in addition to a planar constraint with only four control inputs.

Given the high practical utility of the presented ideas and these proposed extensions, it is the author's sincerest hope that the above be given the deserved attention and mathematical insight.

Bibliography

Ahmad, M. A., Mohamed, Z., and Hambali, N. (2008). Dynamic Modeling of a Two-Link Flexible Manipulator System Incorporating Payload. *Proceedings of IEEE Conference on Industrial Electronics and Applications*, pp. 96–101.

Anderson, P. L., Mahoney, A. W., and Webster, R. J. (2017). Continuum Reconfigurable Parallel Robots for Surgery: Shape Sensing and State Estimation with Uncertainty. *IEEE Robotics and Automation Letters*, Vol. 2, Issue 3, pp. 1617–1624.

Aoustin, Y., Chevallereau, C., Glumineau, A., and Moog, C.H. (1994). Experimental Results for the End-Effector Control of a Single Flexible Robotic Arm. *IEEE Transactions on Control Systems Technology*, Vol. 2, No. 4, pp. 371–381.

Azad, A. (1994). Analysis and Design of Control Mechanisms for Flexible Manipulator Systems. Master's Thesis, University of Sheffield.

Azimian, H., Naish, M. D. , Kiaii, B., and Patel, R. V. (2015). A Chance-Constrained Programming Approach to Preoperative Planning of Robotic Cardiac Surgery Under Task-Level Uncertainty. *IEEE Journal of Biomedical and Health Informatics*, Vol. 19, Issue 2, pp. 612–622.

Barbazza, L., Zanotto, D., Rosati, G., and Agrawal, S. K. (2017). Design and Optimal

Control of an Underactuated Cable-Driven Micro-Macro Robot. *IEEE Robotics and Automation Letters*, Vol. 2, Issue 2, pp. 896-903.

Bo, X., Fujimoto, K., and Hayakawa, Y. (2005). An Energy-Based Nonlinear Control for a Two-Link Flexible Manipulator. *Transactions of the Japan Society for Aeronautical and Space Sciences*, Vol. 48, No. 160, pp. 92–101.

Bullo, F. and Lewis, A. (2003). Geometric Control of Mechanical Systems. *ser. Texts in Applied Mathematics.* New York: Springer-Verlag, Vol. 24.

Casella, F., Locatelli, A., and Schiavoni, N. (2002). Modeling and Control for Vibration Suppression in a Large Flexible Structure with Jet Thrusters and Piezoactuators. *IEEE Transactions on Control Systems Technology*, Vol. 10, Issue 4, pp. 589–599.

Cavallo, A. and Natale, C. (2003). Output Feedback Control Based on a Higher-Order Sliding Manifold Approach. *IEEE Transactions on Automatic Control*, Vol. 48, Issue 3, pp. 469-472.

Chen, F., Jiang, R., Zhang, K, Jiang, B., and Tao, G. (2016). Robust Backstepping Sliding Mode-Control and Observer-Based Fault Estimation for a Quadrotor UAV. *IEEE Transactions on Industrial Electronics*, Vol. 63, Issue 8, pp. 5044-5056.

Cho, S., Reyhanoglu, M., and Kolmanovsky, I. (1998). Discontinuous Feedback Control of a Planar Rigid Body with an Unactuated Degree of Freedom. *Proceedings of the 37th IEEE Conference on Decision and Control.*

Choi, Y-C. and Ahn, H-S. (2015). Nonlinear Control of Quadrotor for Point Tracking: Actual Implementation and Experimental Tests. *IEEE/ASME Transactions on Mechatronics*, Vol. 20, Issue 3, pp. 1179-1192.

Chong, N. K., Yokoi, K., Oh, S. R., and Tanie, K. (1997). Position Control of Collision-Tolerant Passive Mobile Manipulator with Base Suspension Characteristics. *Proceedings of IEEE International Conference on Robotics and Automation*, pp. 594-599.

Crampin, M. and Pirani, F.A.E. (1986). Applicable Differential Geometry. *Lecture Notes Series, London Mathematical Society*, Cambridge University Press, Vol. 59.

Damen, R., Reyhanoglu, M., MacKunis, W., and Hervas, J.R. (2016). Passivity-Based Quaternion Feedback Control of a Hover System. *IEEE 16th International Conference on Control, Automation and Systems.*

Dawson, D., Bridges, M., and Qu, Z. (1995). Nonlinear Control of Robotic Systems for Environmental Waste and Restoration. *Englewood Cliffs, New Jersey: Prentice Hall PTR.*

Dogan, A. and Iftar, A. (1998) Modeling and Control of a Two-Link Flexible Robot Manipulator. *Proceedings of IEEE International Conference on Control Applications*, pp. 761-765.

Dong, W. and Kuhnert, K-D. (2005). Robust Adaptive Control of Nonholonomic Mobile Robot with Parameter and Nonparameter Uncertainties. *IEEE Transactions on Robotics*, Vol. 21, Issue 2, pp. 261-266.

Eckhart, J. (2005) Modeling and Slew-Maneuver Control of a Flexible Spacecraft. Master's Thesis, Embry-Riddle Aeronautical University.

Faessler, M., Falanga, D., and Scaramuzza, D. (2017). Thrust Mixing, Saturation, and Body-Rate Control for Accurate Aggressive Quadrotor Flight. *IEEE Robotics and Automation Letters*, Vol. 2, Issue 2, pp. 476-482.

Fanni, M. and Khalifa, A. (2017). A New 6-DOF Quadrotor Manipulation System: Design, Kinematics, Dynamics, and Control. *IEEE/ASME Transactions on Mechatronics*, Vol. 22, Issue 3, pp. 1315-1326.

Ghommam, J. and Saad, M. (2017). Autonomous Landing of a Quadrotor on a Moving Platform. *IEEE Transactions on Aerospace and Electronic Systems*, Vol. 53, Issue 3, pp. 1504-1519.

Goes, L.C.S., Costa, A., Grandinetti, F.J., and Soares, A.M.S. (2001). Nonlinear Dynamic Modeling and Control of an Underactuated Flexible Structure Mounted Micromanipulator System. *Proceedings of the IX DINAME*, pp. 225-230.

Goldstein, H., Poole, C. P., and Safko, J. (2011). Classical Mechanics, Third Edition. Pearson.

Haimo, V.T. (1986). Finite Time Controllers. *SIAM Journal on Control and Optimization*, Vol. 24, No. 4, pp. 760-770.

Hervas, J.R. and Reyhanoglu, M. (2015). Controllability and Stabilizability of a Class of Systems with Higher-Order Nonholonomic Constraints. *Automatica*, Vol. 54, pp. 229-234.

Hoffman, D., Rehan, M., MacKunis, W., and Reyhanoglu, M. (2017). Robust Quaternion-based Nonlinear Output Feedback Tracking Control of a Quadrotor Hover System. *Proceedings of IEEE Conference on Decision and Control*, pp. 4872-4877.

Hoffman, D., Rehan, M., MacKunis, W., and Reyhanoglu, M. (2018). Differential Geometric Tracking Approach to Input-Multiplicative Uncertainty of a Quadrotor Hover System. under review, *Mathematical Problems in Engineering.*

Hoffman, D. and Reyhanoglu, M. (2017a). Geometric Approach to Robust Control of Robotic Manipulators with Oscillatory Bases. under review, *Mathematical Problems in Engineering.*

Hoffman, D. and Reyhanoglu, M. (2017b). Geometric Tracking Control of a Three-Dimensional Revolute Joint Robot. *Proceedings of Asian Control Conference*, pp. 641-646.

Hoffman, D. and Reyhanoglu, M. (2018). Constraint Embedding Method for a Class of Underactuated Systems. under review, Chapter in *Nonlinear Systems*, InTech.

Huang, P., Wang, D., Meng, Z., Zhang, F., and Liu, Z. (2016). Impact Dynamic Modeling and Adaptive Target Capturing Control for Tethered Space Robots with Uncertainties. *IEEE/ASME Transactions on Mechatronics*, Vol. 21, Issue 5, pp. 2260-2271.

Huang, X. and Yan, Y. (2016). Output Feedback Control of Underactuated Spacecraft Hovering in Circular Orbit With Radial or In-Track Controller Failure. *IEEE Transactions on Industrial Electronics*, Vol. 63, Issue 9, pp. 5569-5581.

Hughes, P. (1994). Spacecraft Attitude Dynamics. Wiley, New York.

Hung, N.V.Q., Tuan, H.D., Narikiyo, T., and Apkarian, P. (2008). Adaptive Control for Nonlinearly Parametrized Uncertainties in Robot Manipulators. *IEEE Transactions on Control Systems Technology*, Vol. 16, Issue 3, pp. 458-468.

Islam, S., Liu, P., and Saddik, A.E. (2015). Robust Control of Four-Rotor Unmanned Aerial Vehicle With Disturbance Uncertainty. *IEEE Transactions on Industrial Electronics*, Vol. 62, Issue 3, pp. 1563-1571.

Junkins, J.L. and Kim, Y. (1993). *Introduction to Dynamics and Control of Flexible Structures.* AIAA Educational Series.

Kayacan, E. and Maslim, R. (2017) Type-2 Fuzzy Logic Trajectory Tracking Control of Quadrotor VTOL Aircraft with Elliptic Membership Functions. *IEEE/ASME Transactions on Mechatronics*, Vol. 22, Issue 1, pp. 339-348.

Khalil, H. (1996). Nonlinear Systems, 2nd Edition. Ed. Prentice Hall.

Lee, T. (2017). Geometric Control of Quadrotor UAVs Transporting a Cable-Suspended Rigid Body. *IEEE Transactions on Control Systems Technology*, Vol. PP, Issue 99, pp. 1-10.

Lee, T. (2015a). Geometric Controls for a Tethered Quadrotor UAV. *IEEE Annual Conference on Decision and Control.*

Lee, T. (2015b). Global Exponential Tracking Controls on SO(3). *IEEE Transactions on Automatic Control*, Vol. 60, Issue 10, pp. 2837-2842.

Lee, T. (2013). Robust Adaptive Attitude Tracking on SO(3) With an Application to a Quadrotor UAV. *IEEE Transactions on Control Systems Technology*, Vol. 21, Issue 5, pp. 1924-1930.

Lee, T., Leok, M., and McClamroch, N.H. (2017). Global Formulations of Lagrangian and Hamiltonian Dynamics on Manifolds: A Geometric Approach to Modeling and Analysis. *Springer.*

Lew, J.Y. and Moon, S-M. (1999). Acceleration Feedback Control of Compliant Base Manipulators. *Proceedings of American Control Conference*, pp. 1955-1959.

Lew, J.Y. and Moon, S-M. (2001). A Simple Active Damping Control for Compliant Base Manipulators. *IEEE/ASME Transactions on Mechatronics*, Vol 6, No. 3, pp. 305-310.

Lin, J., Huang, Z.Z., and Huang, P.H. (2007). An Active Damping Control of Robot Manipulators with Oscillatory Bases by Singular Perturbation Approach. *Journal of Sound and Vibration*, Vol. 304, pp. 345-360.

Lin, J. and Huang, Z.Z. (2007). A Hierarchical Fuzzy Approach to Supervisory Control of Robot Manipulators with Oscillatory Bases. *Mechatronics*, Vol. 17, pp. 589-600.

Liu, H., Xi, J.,and Y. Zhong, Y. (2017a). Robust Attitude Stabilization for Nonlinear Quadrotor Systems with Uncertainties and Delays. *IEEE Transactions on Industrial Electronics*, Vol. 64, Issue 7, pp. 5585-5594.

Liu, H., Zhao, W., Zuo, Z., and Zhong, Y. (2017b). Robust Control for Quadrotors with Multiple Time-Varying Uncertainties and Delays. *IEEE Transactions on Industrial Electronics*, Vol. 64, Issue 2, pp. 1303-1312.

Ma, D., Xia, Y., Li, T., and Chang, K. (2016). Active Disturbance Rejection and Predictive Control Strategy for a Quadrotor Helicopter. *IET Control Theory and Applications*, Vol. 10, Issue 17, pp. 2213-2222.

Martins, J.M., Mohamed, Z., Tokhi, M.O.,da Costa, J.S., and Botta, M.A. (2003). Approaches for Dynamic Modeling of Flexible Manipulator Systems. *IEEE Proceedings–Control Theory and Applications*, Vol. 150, No. 4, pp. 401-411.

Mayhew, C., Sanfelice, R., and Teel, A. (2011a). Quaternion-Based Hybrid Control for Robust Global Attitude Tracking. *IEEE Transactions on Automatic Control.*

Mayhew, C., Sanfelice, R., and Teel, A. (2011b). On The Non-Robustness of Inconsistent Quaternion-Based Attitude Control Systems Using Memory-Less Path-Lifting Schemes. *Proceedings of American Control Conference.*

Mebarki, R., Lippiello, V., and Siciliano, B. (2015). Nonlinear Visual Control of Unmanned Aerial Vehicles in GPS-Denied Environments. *IEEE Transactions on Robotics*, Vol. 31, Issue 4, pp. 1004-1017.

Mirzaei, M., Meskin, N., and Abdollahi, F. (2017). Robust Consensus of Autonomous Underactuated Surface Vessels. *IET Control Theory and Applications*, Vol. 11, Issue 4, pp. 486-494.

Morales, D.O. and de La Hera, P.X. (2012). Design of Energy Efficient Walking Gaits for a Three-Link Planar Biped Walker with Two Unactuated Degrees of Freedom. *Proceedings of IEEE International Conference on Robotics and Automation*, pp. 148-153.

Naldi, R., Furci, M., Sanfelice, R.G., and Marconi, L. (2017). Robust Global Trajectory Tracking for Underactuated VTOL Aerial Vehicles Using Inner-Outer Loop Control Paradigms. *IEEE Transactions on Automatic Control*, Vol. 62, Issue 1, pp. 97-112.

Nenchev, D.N., Yoshida, K., Vichitkulsawat, P., and Uchiyama, M. (1999). Reaction Null-Space Control of Flexible Structure Mounted Manipulator Systems. *IEEE Transactions on Robotics and Automation*, Vol. 15, No. 6, pp. 1011-1023.

Nijmeijer, H. and van der Schaft, A.J. (1990). Nonlinear Dynamical Control Systems. *New York: Springer-Verlag.*

Ortiz, J.P., Minchala, L.I., and Reinoso, M.J. (2016). Nonlinear Robust H-Infinity

PID Controller for The Multivariable System Quadrotor. *IEEE Latin America Transactions*, Vol. 14, Issue 3 pp. 1176-1183.

Ott, C., Albu-Schäffer, A., and Hirzinger, G. (2006). A Cartesian Compliance Controller for a Manipulator Mounted on a Flexible Structure. *IEEE Proceedings on International Conference on Intelligent Robots and Systems*, pp. 4502-4508.

Reinoso, M.J., Minchala, L.I., Ortiz, P., Astudillo, D.F., and Verdugo, D. (2016). Trajectory Tracking of a Quadrotor Using Sliding Mode Control. *IEEE Latin America Transactions*, Vol. 16, Issue 5, pp. 2157-2166.

Reyhanoglu, M. (2008). Slewing Maneuver of a Flexible Spacecraft Using Finite Time Control. *Proceedings of IEEE Conference on Industrial Electronics*, pp. 2667-2671.

Reyhanoglu, M. (2003). Maneuvering control problems for a spacecraft with unactuated fuel slosh dynamics. *Proceedings of IEEE Conference on Control Applications*, pp. 695-699.

Reyhanoglu, M., van der Schaft, A.J., McClamroch, N.H., and Kolmanovsky, I. (1999a). Dynamics and Control of a Class of Underactuated Mechanical Systems. *IEEE Transactions on Automatic Control*, Vol. 44, No. 9, pp. 1663-1671.

Reyhanoglu, M. and Hoffman, D. (2016). Modeling and Control of a Flexible-Structure-Mounted Manipulator. *Proceedings of IEEE International Conference on Advanced Intelligent Mechatronics*, pp. 953-957.

Reyhanoglu, M., Hoffman, D., and de Wit, J. (2016). Nonlinear Modeling and Control of a Two-Link Hybrid Manipulator. *Proceedings of International Conference on Control, Automation, Robotics and Vision*, pp.1-5.

Reyhanoglu, M. and Hoffman, D. (2017). Finite-Time Control of a Compliant Base Robot Manipulator. *Proceedings of Asian Control Conference*, pp. 1335-1340.

Reyhanoglu, M., Cho, S., and McClamroch, N.H. (1999b). Feedback Control of a Planar Manipulator with an Unactuated Elastically Mounted End Effector. *Proceedings of the IEEE International Conference on Robotics and Automation*, pp. 2805-2810.

Reyhanoglu, M., Cho, S., McClamroch, N.H., and Kolmanovsky, I. (1998). Discontinuous Feedback Control of a Planar Rigid Body with an Unactuated Degree of Freedom. *Proceedings of IEEE International Conference on Decision and Control*, pp. 433-438.

Reyhanoglu, M. and Hervas, J.R. (2012). Nonlinear Dynamics and Control of Space Vehicles with Multiple Fuel Slosh Modes. *IFAC Journal Control Engineering Practice*, Vol. 20, pp. 912-918.

Rigatos, G.G. (2009). Model-Based and Model-Free Control of Flexible-Link Robots: a Comparison Between Representative Methods. *Applied Mathematical Modeling*, Vol. 33, No. 10, pp. 3906-3925.

Roy, S., Kar, I.N., Lee, J., and Jin, M. (2017). Adaptive Robust Time-Delay Control for a Class of Uncertain Euler-Lagrange Systems. *IEEE Transactions on Industrial Electronics*, Vol. PP, Issue 99, pp. 1-10.

Ryan, T. and Kim, H.J. (2013). LMI-Based Gain Synthesis for Simple Robust Quadrotor Control. *IEEE Transactions on Automation Sciences and Engineering*, Vol. 10, Issue 4, pp. 1173-1178.

Satici, A.C., Poonawala, H., and Spong, M.W. (2013). Robust Optimal Control of Quadrotor UAVs. *IEEE Access*, Vol. 1, Issue 1, pp. 79-93.

Sharf, I. (1995). Active Damping of a Large Flexible Manipulator with a Short Reach Robot. *Proceedings of American Control Conference*, pp. 3329-3333.

Sharkey, P. and O'Reilly, J. (2003). Exact Design Manifold Control of a Class of Nonlinear Singularly Perturbed Systems. *IEEE Transactions on Automatic Control*, Vol. 32, Issue 10, pp. 933-935.

Shi, Y., Zhao, J., and Liu, Y. (2017). Switching Control for Aero-Engines Based on Switched Equilibrium Manifold Expansion Model. *IEEE Transactions on Industrial Electronics*, Vol. 64, Issue 4, pp. 3156-3165.

Takeda, H., Facchinetti, C., and Latombe, J-C. (1994). Planning the Motions of a Mobile Robot in a Sensory Uncertainty Field. *IEEE Transactions on Pattern Analysis and Machine Intelligence*, Vol. 16, Issue 10, pp. 1002-1017.

Tedrake, R. (2009). Underactuated Robots: Learning, Planning, and Control for Efficient and Agile Machines. *MIT, Course Notes for 6.832.*

Tilley, S. and Cannon, R. (1986). End-Point Control of a Very Flexible Manipulator with a Fast End-Effector. *ASME Journal of Dynamic Systems, Measurement and Control*, Vol. 3, pp. 1-9.

Tokhi, M.O., Mohamed, Z., and Shaheed, M.H. (2001). Dynamic Characterization of a Flexible Manipulator System. *Robotica*, Vol. 19, No. 5, pp. 571-580.

Torres, M.A. and Dubowsky, S. (1993). Path-Planning for Elastically Constrained Space Manipulator Systems. *Proceedings of IEEE International Conference on Robotics and Automation*, pp. 812-817.

Tso, S.K., Yang, T.W., Xu, W.L., and Sun, Z.Q. (2003). Vibration Control for

a Flexible-Link Robot Arm with Deflection Feedback. *International Journal of Nonlinear Mechanics*, Vol. 38, No. 1, pp. 51-62.

Usoro, P.B., Nadira, R., and Mahil, S.S. (1986). A Finite Element/Lagrange Approach to Modeling Lightweight Flexible Manipulators. *ASME Journal of Dynamic Systems, Measurement, and Control*, Vol. 108, No. 3, pp. 198-205.

Weng, S., Yue, D., and Yang, T. (2013). Coordinated Attitude Motion Control of Multiple Rigid Bodies on Manifold SO(3). *IET Control Theory and Applications*, Vol. 7, Issue 16, pp. 1984-1991.

Wie, B. (1998). Space Vehicle Dynamics and Control. *AIAA Educational Series.*

Wongratanaphisan, T. and Cole, M.O.T. (2009). Robust Impedance Control of a Flexible Structure Mounted Manipulator Performing Contact Tasks. *IEEE Transactions on Robotics*, Vol. 25, No. 2, pp. 445-451.

Xian, B., Dawson, D.M., de Queiroz, M.S., and Chen, J. (2004). A Continuous Asymptotic Tracking Control Strategy for Uncertain Nonlinear Systems. *IEEE Transactions on Automatic Control*, Vol. 49, No. 7, pp. 1206-1211.

Yang, B-J., Calise, A.J., and Craig, J.I. (2007). Adaptive Output Feedback Control of a Flexible Base Manipulator. *Journal of Guidance, Control, and Dynamics*, Vol. 30, No. 4, pp. 1068-1080.

Yang, C., Li, Z., Cui, R., and Xu, B. (2014). Neural Network -Based Motion Control of an Underactuated Wheeled Inverted Pendulum Model. *IEEE Transactions on Neural Networks and Learning Systems*, Vol. 25, Issue 11, pp. 2004 - 2016.

Yang, Z. and Sadler, J.P. (1990). Large-Displacement Finite Element Analysis of Flexible Linkages. *Journal of Mechanical Design*, Vol. 112, No. 2, pp. 175-182.

Yoshikawa, T., Harada, K., and Atsushi, M. (1996). Hybrid Position/Force Control of Flexible-Macro/Rigid-Micro Manipulator Systems. *IEEE Transactions on Robotics and Automation*, Vol. 12, No. 4, pp. 633-640.

Yu, X., Chen, G., Xia, Y., Song, Y., and Cao, Z. (2001). An Invariant-Manifold-Based Method for Chaos Control. *IEEE Transactions on Circuits and Systems I: Fundamental Theory and Applications*, Vol. 48, Issue 8, pp. 930-937.

Yu, Y. and Ding, X. (2016). A Global Tracking Controller for Underactuated Aerial Vehicles: Design, Analysis, and Experimental Tests on Quadrotor. *IEEE/ASME Transactions on Mechatronics*, Vol. 21, Issue 5, pp. 2499-2511.

Zhao, B., Xian, B., Zhang, Y., and Zhang, X. (2015). Nonlinear Robust Adaptive Tracking Control of a Quadrotor UAV Via Immersion and Invariance Methodology. *IEEE Transactions on Industrial Electronics*, Vol. 62, Issue 5, pp. 2891-2902.

Zhao, D., Li, S., Zhu, Q., and Gao, F. (2010). Robust Finite-Time Control Approach for Robotic Manipulators. *IET Control Theory and Applications*, Vol. 4, Issue 1, pp. 1-15.

Zuo, Y. (2017). Trajectory Tracking Controller for Quadrotors Without Velocity and Angular Velocity Measurements. *IET Control Theory and Applications*, Vol. 11, Issue 1, pp. 101-109.

Zuo, Z. (2010). Trajectory Tracking Control Design with Command-Filtered Compensation for a Quadrotor. *IET Control Theory and Applications*, Vol. 4, Issue 11, pp. 2343-2355.